Point-Contact Tunneling Study of High Temperature Superconductors

A Dissertation
Presented to the Faculty of the Graduate School
of
Yale University
in Candidacy for the Degree of
Doctor of Philosophy

by
June Chen-Todt

Dissertation Director: Dr. Daniel E. Prober
Co-Advisors: Dr. John F. Zasadzinski
Dr. Kenneth E. Gray

November, 1995

TABLE OF CONTENTS

ACKNOWLEDGMENT v

LIST OF FIGURES vi

LIST OF TABLES xi

LIST OF SYMBOLS xii

I. INTRODUCTION 1

1.1 Conventional Superconductors 1
1.2 High-Temperature Superconductors 3
1.3 Tunneling Measurements 4

II. THEORY OF SUPERCONDUCTIVITY 11

2.1 BCS Theory 11
2.2 Strong Coupling Theory 16
2.3 High-Temperature Superconductor Theory 21

III. TUNNELING SPECTROSCOPY 24

3.1 Superconductive Tunneling 24
3.1.1 Superconductor-Insulator-Normal Metal (SIN) Tunneling 26
3.1.2 Superconductor-Insulator-Superconductor (SIS) Tunneling 29
3.2 Tunneling Methods. 30

IV. EXPERIMENTAL SETUP 35

4.1 Point-Contact Tunneling Apparatus. 35
4.2 Data Acquisition System 40

V. TUNNELING STUDY OF $HgBa_2CuO_{4+x}$ 44

5.1 Modeling Studies of SIS' Junctions 44
5.2 Point-Contact Tunneling Study of $HgBa_2CuO_{4+x}$ by SIN Junctions 50
5.2.1 Introduction. 50
5.2.2 Experimental 51
5.2.3 Results and Discussion 55

5.3 SIS Junctions and Device Potential 62
5.3.1 Introduction 63
5.3.2 Results and Discussion 64

VI. TUNNELING STUDY OF THE INFINITE LAYER COMPOUND
$Sr_{1-x}Nd_xCuO_2$ 71

6.1 Introduction 71
6.2 Sample Preparation and Experimental Procedure . . . 74
6.3 Experimental Results. 76

VII. PROXIMITY EFFECT TUNNEL JUNCTIONS 98

7.1 Introduction 98
7.2 Proximity Effect Models 101
7.3. Experimental Result and Discussions 107

VIII. CONCLUSIONS 114

REFERENCES 117

ACKNOWLEDGMENT

This thesis would not be here without the help of many people. First of all, I thank my advisor at Yale University, Prof. Dan Prober, who made it possible for me to carry out my dissertation research at Argonne National Laboratory and who was always there when I needed him. I thank him for setting a high standard not only for my research but also for my education in general. I am especially grateful to Prof. John Zasadzinski and Dr. Ken Gray for their guidance, support, and encouragements during the course of this study at Argonne. I have learned many things from them, not only their scientific knowledge, but also their way of thinking and problem solving. It is beyond words to say how much I appreciate what they have done for me while working in their group.

I am grateful to all my instructors, colleagues, classmates, and friends who helped me in various ways. In particular, I am indebted to Dr. Qiang Huang for showing me many experimental techniques, to Dr. Paola Romano for her contribution to the tunneling measurements, and to Dr. Nilesh Tralshawala who taught me laser ablation techniques. I also enjoyed working with Mr. Bob Kampwirth on the development and implementation of a computer controlled system for laser ablation. I would like to acknowledge Prof. John Wagner and Dr. Dave Hinks for providing $HgBa_2CuO_{4+x}$ samples, and Prof. John Markert for providing $Sr_{1-x}Nd_xCuO_2$ samples.

I also owe many thanks to Prof. Sean Barrett, Prof. Subir Sachdev, and Prof. Jack Sandweiss for going through this thesis in detail and suggesting changes to improve its clarity and focus. For making all the arrangements for my thesis defense, I thank Ms. Jean Belfonti. I am grateful to Prof. Laszlo Mihaly of SUNY-Stony Brook for being the outside reader of my thesis.

For my graduate study and thesis research, I acknowledge the financial support from Yale University, the NSF Science and Technology Center for Superconductivity, and the Division of Educational Programs at Argonne National Laboratory.

For their love and dedication, I thank my family, especially my parents and grandma. Finally and most importantly, I thank my husband, Volker, for his support, understanding, and love. I will always appreciate his presence in my life.

LIST OF FIGURES

Figure — Page

2.1. Feynman diagram of the electron-electron interaction via phonon exchange 11

2.2. Electron-phonon coupling strength λ plotted versus coupling strength parameter $2\Delta_0/k_BT_c$ 22

3.1. a) Schematic view of a tunneling junction. b) Energy diagram of the tunneling junction under bias 25

4.1. Tunneling apparatus 36

4.2. Sample can and tip assembly 37

4.3. Schematics of the bridge circuit for tunneling measurements. Normally, R1 = R2 42

5.1. Normalized conductances calculated from Eqs. (5.1) and (5.2) for a tunnel junction between a HTS (Δ = 16 meV, Γ/Δ = 0.1%) and a Nb counterelectrode (Δ_{Nb} = 1.5 meV, Γ_{Nb}/Δ_{Nb} = 1%). The inset shows the expanded gap region data displaying a weak feature at the Nb gap voltage . . . 47

5.2. Normalized conductances calculated from Eqs. (5.1) and (5.2) for a tunnel junction between a HTS (Δ = 16 meV, Γ/Δ = 1%) and a Nb counterelectrode (Δ_{Nb} = 1.5 meV, Γ_{Nb}/Δ_{Nb} = 1%) 48

5.3. Same as Fig. 5.2 but with Γ/Δ = 5, 10, 50%. Note that curves are shifted vertically by 0.1 for clarity 49

5.4. Schematic representation of the unit cell $HgBa_2CuO_{4+x}$. The positions indicated as O(3) in the figure are partially occupied, about 6% full and 94% empty (From Chmaissem *et al.*, 1993) 52

5.5. AC susceptibilities for two samples of $HgBa_2CuO_{4+x}$ with T_c(onset) = 97 K and 95 K. Curve A (corresponds to

tunneling sample A) is for a bulk sample, which was powdered before susceptibility measurements. Curve B corresponds to the bulk tunneling sample B 53

5.6. (a through c): Experimental conductances (dots) with the fitted normal state conductances (solid lines) for junctions #1, #2 of sample B and junction #1 of sample A, respectively; (d through f): The dots are the corresponding normalized conductances, while the solid lines are the smeared BCS fits including thermal smearing. Experimental I(V) curve for junction #1 of sample B is shown in Fig. 5.6a as an inset. All tunneling curves here were measured at T = 4.2 K 56

5.7. Experimental conductances (measured at 4.2 K) of junction #3 of sample B showing a smaller gap value . . . 59

5.8. The dots are normalized conductances for junctions #4 and #5 of sample B, shown in (a) and (b) respectively. The solid lines are the smeared BCS fits including thermal smearing. Measurements were taken at T = 4.2 K 60

5.9. (a through c): Experimental conductances (dots) with the fitted normal state conductances (solid lines) for junctions #1, #2 of sample C and junction #1 of sample D, respectively; (d through f): The dots are the corresponding normalized conductances, while the solid lines are the smeared BCS fits including thermal smearing. Experimental I(V) curve for junction #1 of sample D is shown in Fig. 5.9c as an inset. All tunneling curves here were measured at T = 4.2 K 65

5.10. Scanning electron microscope (SEM) picture of $HgBa_2CuO_{4+x}$ surface. Note that the grain size can be as large as 20 μm 68

6.1. Crystal structure of the infinite layer compound $Sr_{1-x}Nd_xCuO_2$. The small and large circles represent the Cu and O atoms, respectively. The solid circles indicate the Sr sites with Nd doping. 72

6.2. Experimental I vs. V (solid line) and dI/dV vs. V (dots)

for a typical point-contact SIN junction on $Sr_{1-x}Nd_xCuO_2$ using a Au tip. The normal state curve (dashed line) is obtained using a polynomial fit (4th order) to the high-bias data, $|V| > 20$ mV 77

6.3. Normalized tunneling conductance (dots), σ_S/σ_n, for the junction shown in Fig. 6.2. The fit (solid line) utilizes the smeared BCS DOS as discussed in the text with Δ and Γ values as indicated 79

6.4. Experimental superconducting tunneling conductances for four different junctions made on the same $Sr_{1-x}Nd_xCuO_2$ sample. Numbering of the junction sequence corresponds to raising and lowering of the temperature between 4.2 K and 6.0 K. The topmost curve is the same junction as shown in Fig. 6.2. 81

6.5. (a) Superconducting tunneling conductances of the junctions shown in Fig. 6.4 normalized by the value of the conductance at V = 6 mV. The data are numbered according to the junction sequence shown in Fig. 6.4. (b) Expanded voltage scale demonstrating that the normalized conductances in the gap region lie on top of each other. 83

6.6. Solid line is the superconducting tunneling conductance of a thin-film Al-Al_2O_3-Cr_2O_3-Pb junction (from Kirtley *et al.*, 1992) showing the strong linear background conductance coming from spin fluctuations in the Cr oxide. The temperature is 0.5 K. The dotted curve is with a field of 1 T applied normal to the plane of the film to suppress the Pb superconductivity. The dashed curve is the inelastic component of the total conductance as inferred from a model based on a broad, flat continuum of states. The dot-dashed curve is the inferred elastic conductance obtained by subtraction of the inelastic term from the data 84

6.7. Tunneling conductances of four point-contact junctions on $Nd_{1.85}Ce_{0.15}CuO_4$ taken by Huang *et al.* (1990a). Note the similarity in magnitude and shape of the asymmetric

linear background to that of the $Sr_{1-x}Nd_xCuO_2$ shown in Figs. 6.4 and 6.5. The straight lines inside the gap are due to lock-in overload, because the junctions are balanced to maximize the sensitivity for phonon structures at high-bias voltage. 86

6.8. Tunneling conductances of six different point-contact junctions on $Pr_{1.85}Th_{0.15}CuO_4$ from the unpublished data of Huang *et al.* (1992) 87

6.9. Tunneling conductances of three point-contact junctions on $Pr_{1.85}Th_{0.15}CuO_4$ (after Huang *et al.*, 1992) taken out to higher bias voltages demonstrating the asymmetric linear background conductance 88

6.10. Normalized tunneling conductance (dots) of $Pr_{1.85}Th_{0.15}CuO_4$ obtained from the top curve of Fig. 6.8. The solid line is a fit using the smeared BCS DOS as discussed in the text with parameters Δ and Γ as indicated. 89

6.11. (a) Conductance curves at temperatures from 4.2 K to 7.0 K for a SIS' tunnel junction on $Sr_{1-x}Nd_xCuO_2$ using a Nb tip. (b) Expanded x and y scale plot of the SIS' conductances at the following temperatures: a) 4.2 K, b) 4.8 K, c) 6.1 K, d) 7.0 K 92

6.12. Model calculation of the SIS' junction conductances. Curve A is at 4.2 K (solid line) and curve B is at 7.0 K (dashed line). In both calculations the $Sr_{1-x}Nd_xCuO_2$ parameters are fixed at Δ = 6.0 meV and Γ/Δ = 0.2. The values of the parameters for the Nb electrode are discussed in detail in the text 94

7.1. Experimental conductance peak positions (solid diamonds) versus gold film thickness. The fit shown as solid lines (open circles) is from Arnold (McMillan) model of proximity effect tunneling (after Huang *et al.*, unpublished) 100

7.2. Schematic view of a proximity tunneling junction 102

7.3. Normalized conductances for a N-I-NS junction using the

McMillan model density of states for the normal metal of the NS sandwich, with $\Delta_{Nph} = 0$ and $\Delta_{Sph} = 22.5$ meV. Thermal smearing at T = 4.2 K is accounted for by introducing a smearing parameter $\Gamma = k_BT = 0.36$ meV. . . 105

7.4. (a) Experimental I(V) characteristics (solid line) and conductances (dots) for a proximity effect junction on all-thin-film $Bi_2Sr_2CaCu_2O_8$/Au bilayer with an In tip. Au thickness ~ 400 Å. (b) Expanded x-scale plot of the junction in (a), showing the gap region data. (c) Experimental conductances for a proximity effect junction on single crystal $Bi_2Sr_2CaCu_2O_8$/Au with an In tip. Au thickness ~ 400 Å (after Zasadzinski *et al.*, 1994). Notice the similarity of (b) and (c). 109

7.5. (a) Experimental I(V) characteristics and conductances for a proximity effect junction on all-thin-film $Bi_2Sr_2CaCu_2O_8$/Au bilayer with an In tip. Measurement is taken at T = 2.5 K. (b) Solid line is a fit to the experimental conductance (dots), using BCS gaps, $\Delta = 0.85$ meV and $\Delta_{In} = 0.35$ meV 111

7.6. (a) Comparison of a McMillan density of states (Δ_S = 22.5 meV, $\Gamma_N = 0.85$ meV, and $\Gamma/\Gamma_N = 7\%$), shown as dots, with a BCS density of states ($\Delta = 0.85$ meV and $\Gamma/\Delta = 7\%$), shown as solid lines. (b) Same density of states taken out to high bias voltage, showing the weak feature at $\Delta_S = 22.5$ meV for the McMillan model 113

LIST OF TABLES

Table Page

2.1. Comparison of BCS to Strong-Coupling Theory 18

2.2. Superconductivity Parameters of the Materials 22

LIST OF SYMBOLS

$N(E)$	Electron density of states
$N(0)$	Electron density of states of one spin index at the Fermi level in the normal state
$N_T(E)$	Quasiparticle density of states measured by tunneling experiments
σ_s	Superconducting conductance
σ_n	Normal state conductance
σ_s/σ_n	Normalized conductance
ω	Frequency or energy parameter
ω_{pl}	The electron plasma frequency
ω_D	The lattice Debye frequency
$F(\omega)$	Phonon density of states
$\alpha^2(\omega)$	A measure of the coupling strength of electrons to phonons of frequency ω
$\alpha^2F(\omega)$	The Eliashberg function
$\Delta_S(E)$	The pair potential or the gap parameter of the superconductor, also denoted as $\Delta(E)$
$\Delta_N(E)$	Induced pair potential in the normal metal
Γ	A smearing parameter, introduced in the smeared BCS density of states
λ	Strength of the electron-phonon coupling, given by $\lambda = 2\int_0^\infty \frac{\alpha^2(\omega)F(\omega)}{\omega} d\omega$
μ^*	Coulomb pseudopotential

$Z(E)$	Renormalization function
$Z(0)$	Describes the renormalization of the electron mass by the electron-phonon coupling. $Z(0) = 1+\lambda$
Ω_N	Induced proximity energy gap in the normal metal by the underlying superconductor (in the McMillan model)

CHAPTER I
INTRODUCTION

In this thesis, the point-contact tunneling results on high-temperature superconductors (HTS) are reported. In order to better understand superconductivity and the role tunneling measurements play, a brief history of conventional superconductors is presented, followed by recent developments of HTS. Then we focus on tunneling measurements and try to provide the background information and put the work in this thesis into perspective.

1.1. Conventional Superconductors

It was the interests of many scientists to study what would happen to the resistivity of pure metals as the temperature approached absolute zero. In the pursuit of reaching this low temperature limit, Professor H. Kamerlingh Onnes was the first to liquify helium. Three years later in 1911, he observed that the electrical resistivity of mercury suddenly vanished (Onnes, 1911) as it was cooled down to 4.2 K. The phenomenon, called superconductivity, was observed for many other metals and alloys when the specimen is cooled to a sufficiently low temperature, often a temperature in the liquid helium range. At a critical temperature T_c the specimen undergoes a second order phase transition from a state of normal electrical resistivity to a superconducting state.

What happens in a superconductor is that electrons form Cooper pairs. All Cooper pairs in a superconductor move coherently, as one single particle. Disturbance of one pair would affect many

more electron pairs (located within the Ginzburg-Landau coherence length) and the largest number of allowed scattering events is obtained by pairing electrons with equal and opposite momenta. Thus, the total momentum will be conserved and it seems any pair can travel without hindrance. This fact gives rise to superconductivity. The pairing mechanism can be described by a successful quantum theory of superconductivity -- the BCS theory (Bardeen *et al.*, 1957) given by Bardeen, Cooper, and Schrieffer in 1957. The phonon induced attraction proceeds when one electron interacts with the lattice and deforms it; a second electron sees the deformed lattice and adjusts itself to take advantage of the deformation to lower its energy. Thus, the second electron interacts with the first electron via the lattice deformation. This attractive interaction between electrons leads to a ground state separated from excited states by an energy gap. The critical field, the thermal properties, and most of the electromagnetic properties are consequences of the energy gap (Kittel, 1986).

The early experiments of Giaever and Megerle (1961) showed that the tunneling technique provides a direct measure of the energy gap and the quasiparticle density of states (DOS). This work gave strong experimental confirmation to the BCS theory. However, it was not until the tunneling experiments of McMillan and Rowell (1969) on Pb that tunneling was established as a quantitative spectroscopic tool. They presented a method of inverting tunneling data to obtain the energy dependent gap parameter $\Delta(E)$, which is the strong-coupling analog of the BCS gap. More importantly, they were able to

determine the electron-phonon coupling strength λ and the screened Coulomb pseudopotential μ^* in metals. The prediction of the transition temperature, T_c, for Pb within experimental error gave strong support to both the validity of the method and to the Eliashberg (1960a) strong-coupling theory of superconductivity.

1.2. High-Temperature Superconductors

A new era in the field of superconductivity started with the discovery of HTS. The first HTS, $La_{2-x}Ba_xCuO_4$, was discovered by Bednorz and Müller (1986) in the search of a material with metallic-like conductance properties but with the highest possible electron-phonon coupling. According to the BCS theory, a stronger electron-phonon interaction would promote a larger energy gap and thereby a higher T_c. There are now quite a number of ceramic compounds that are superconducting above the temperature of liquid nitrogen (77 K). The record high T_c of 135 K holds for $HgBa_2Ca_2Cu_3O_{8+\delta}$ (Huang *et al.*, 1993). Further enhancements of T_c up to 150 K are reported in an applied pressure of 150 kbar for this material (Chu *et al.*, 1993).

Before the discovery of HTS, one pairing mechanism, phonon-induced attraction, could explain almost all of the superconducting materials. Now various mechanisms including phonons, plasmons, excitons, the resonating valence bond (RVB), correlated charge fluctuations (exchange of charged bosons), interband pairing, etc., are suggested to explain just a few high T_c superconductors. Yet none of them is accepted generally (Ginsberg, 1994). New and more accurate

experimental measurements are needed to decide on the validity of the various proposed models.

1.3. Tunneling Measurements

Tunneling measurement is one of the most important techniques in obtaining the fundamental physical properties of superconductors such as the gap parameter Δ and DOS. Direct information about novel mechanisms and pairing in HTS can be revealed by measuring the magnitude of Δ, anisotropy of Δ, temperature and magnetic field dependence of Δ, and DOS. The Eliashberg function $\alpha^2F(\omega)$ can also be obtained through the inversion of tunneling data and compared with the phonon density of states $F(\omega)$ obtained from neutron scattering experiments. Here $\alpha^2(\omega)$ is a measure of the coupling strength of electrons to phonons of energy $\hbar\omega$. Thus, tunneling spectroscopy provides a direct measure of the strength of the electron-phonon interaction and gives insight into the pairing mechanism of HTS. In the event that pairing in HTS is mediated by some other boson, e.g., spin fluctuations, then a more general spectral function must be considered. If an Eliashberg type of model applies, then it is assumed that tunneling spectroscopy will still provide $\alpha^2F(\omega)$, but that $F(\omega)$ is now a general boson density of states.

Point-contact tunneling studies on HTS are presented in this thesis. This work is part of the collaborative effort of many people. A number of questions need to be addressed. Why do we use the point-contact tunneling as opposed to other tunneling methods?

Does it have the same sensitivity as found in thin-film tunneling spectroscopy? What are our objectives when studying the HTS? In order to answer these questions, a brief review of what has been done previously is given here, followed by questions we would like to address in this thesis.

The first generation of our tunneling apparatus is a variation of the vacuum-tunneling devices in common use for scanning tunneling microscopy. It was designed and built by M. E. Hawley and K. E. Gray to study organic superconductors and a detailed description is given (Hawley *et al.*, 1986). An electrochemically polished Au tip is moved along a direction perpendicular to the sample surface by the combined action of a differential micrometer and a stack of piezoelectric crystals. The exponential dependence of the current on the tip movement demonstrated vacuum tunneling on chemically inert samples of Au with a Au tip. Spectrum analysis of such junctions indicated that vibrations could be virtually eliminated by use of a sandbox mounted on an air-suspension system. As the first test for the system, single crystals of $ErRh_4B_4$ were studied in vacuum tunneling mode and energy gap measurements showed the expected superconducting gap of 1.15 meV at $\approx$ 2 K. This apparatus was also used successfully to provide the first direct measurement of a superconducting energy gap in an organic superconductor (Hawley *et al.*, 1986) and into the HTS $La_{1.85}Sr_{0.15}CuO_{4-y}$ (Hawley *et al.*, 1987). For samples exhibiting an insulating surface layer, however, the surface layer resistance can easily exceed the preset shut off tunneling resistance of 5 MΩ, preventing the tip from stopping

before burrowing into the sample. These samples require mechanical touching and can be analyzed as the point-contact tunneling (Blonder and Tinkham, 1983).

Q. Huang and J. F. Zasadzinski further modified the tunneling system in 1988 in order to study then newly discovered HTS. For most HTS, the insulating surface layer prevents vacuum tunneling and the point-contact tunneling becomes necessary. Thus, the piezoelectric stacks and the feedback circuit were not necessary and removed from the system to further reduce noise. A bridge circuit with the junction as one arm was added to the system. dI/dV and d^2I/dV^2 can be taken with much improved sensitivity by using a combination of the bridge circuit and lock-in amplifier techniques (Huang *et al.*, 1990b). As a test for the tunneling apparatus as well as the point-contact tunneling method, tunneling spectroscopy measurements were made on single crystals of Nb using the point-contact technique with a Au tip. Niobium has been studied extensively by conventional and proximity-effect tunneling methods so its phonon spectrum is well established. Also, the phonon structures in Nb junctions are rather small, about a 1% change in dI/dV, and therefore present a challenging test for the point-contact method. It was found (Huang *et al.*, 1990b) that the current-voltage characteristics, I(V) and dI/dV, reproduce the results obtained from conventional, thin-film planar junctions. The tunneling conductance displays the characteristic structures (Wolf *et al.*, 1980; Khim *et al.*, 1981; Geerk *et al.*, 1982) associated with the phonon density of states for Nb. These results demonstrate that the point-contact tunneling

method can be used to measure the electron-phonon interaction in superconductors with the same sensitivity as found in thin-film tunneling spectroscopy.

This point-contact tunneling apparatus was then used by Zasadzinski et al (1992) to study a variety of HTS. Ideal BCS quasiparticle characteristics of $Ba_{1-x}K_xBiO_3$ were first discovered using the point-contact tunneling method at Argonne (Huang *et al.*, 1990c). The highest quality tunneling results on cuprate superconductors $Bi_2Sr_2CaCu_2O_8$ (Bi-2212) (Huang *et al.*, 1990b) and $Nd_{2-x}Ce_xCuO_{4-y}$ (Huang *et al.*, 1990a) with a normalized zero-bias conductance $\sigma_s/\sigma_n(0) \sim 15\%$ were also obtained using this point-contact method and still remain the best until this day. The results on Bi-2212 are also consistent with those obtained with break junctions (Mandrus *et al.*, 1991). Generally the point-contact tunneling method has provided the best quasiparticle junction characteristics of most HTS materials and has also preceded the development of thin-film junctions (Zasadzinski *et al.*, 1992). But the results on cuprate HTS do not exhibit ideal BCS behavior. Prior to the tunneling study on $HgBa_2CuO_{4+x}$ presented in this thesis, all cuprate superconductors exhibit broadened characteristics (Hasegawa et al, 1992a) typified by $\sigma_s/\sigma_n(0) \sim 15 - 60\%$ and a monotonic increase of the conductance about zero-bias. The question is whether these tunneling characteristics are intrinsic to the cuprates (i.e. arising from novel pairing states, gaplessness or anisotropy) or are a manifestation of poor junction quality due to damaged or reconstructed surfaces, proximity effects, bad tunnel barriers, etc.

With the above question in mind, we have studied $HgBa_2CuO_{4+x}$ using the point-contact tunneling method. $HgBa_2CuO_{4+x}$ is of particular interest because of its unusual high T_c of 97 K for a compound with only one CuO_2 layer per unit cell. The distance between CuO_2 layers (Putilin *et al.*, 1993; Wagner *et al.*, 1993) is only 9.5 Å. Such a small spacing between CuO_2 layers may lead to better intrinsic superconducting properties in a magnetic field (Welp *et al.*, 1993; Umezawa *et al.*, 1993; Kim *et al.*, 1991). Both superconductor-insulator-normal metal (SIN) and superconductor-insulator-superconductor (SIS) junctions have been studied using Au and Nb tips, respectively and consistent results are obtained. The data exhibit significantly lower and flatter subgap conductance values than any other cuprate and they can be reproducibly obtained. By fitting the data to a smeared BCS density of states, the energy gap has been determined and the smearing parameter is so small that it is comparable to thermal smearing. The data are compatible with an s-wave pairing state, but d-wave cannot be ruled out due to the possibility of directional tunneling.

Another interesting system is the infinite-layer compound $Sr_{1-x}Nd_xCuO_2$ with T_c = 35 K. Unlike other cuprates which have non-superconducting oxide layers between superconducting layers of CuO_2, the infinite-layer compound consists of CuO_2 planes separated only by alkaline elements. The lattice parameters vary with dopant concentration x, but in general we have a ~ 3.9 Å and c ~ 3.4 Å (Smith *et al.*, 1991). Thus, structurally $Sr_{1-x}Nd_xCuO_2$ is much closer to the cubic oxide $Ba_{1-x}K_xBiO_3$ than any other cuprates. The question we

wish to answer is whether this cuprate would reproduce the anomalies found in other cuprates or behave like the cubic oxides such as $Ba_{1-x}K_xBiO_3$ which show ideal BCS tunneling characteristics. We performed quasiparticle tunneling measurements at 4.2 K. Both SIN and SIS' tunnel junctions have been fabricated using a mechanical point-contact technique with Au and Nb tips, respectively. All junctions exhibit a strong, asymmetric linear background conductance indicative of inelastic tunneling contributions from a broad continuum of states. We found that the magnitude and shape of this background conductance are very similar to that found in two other electron-doped cuprates, $Nd_{2-x}Ce_xCuO_{4-y}$ and $Pr_{2-x}Th_xCuO_{4-y}$. The energy gap of $Sr_{1-x}Nd_xCuO_2$ is found consistently to be 6 meV, leading to $2\Delta/k_BT_c = 4.0$. The reproducibility of the measured gap values is similar to that found in other electron-doped cuprates and is consistent with the apparent s-wave symmetry found in $Nd_{2-x}Ce_xCuO_{4-y}$. The gap region tunneling data of the $Sr_{1-x}Nd_xCuO_2$ junctions all display subgap conductances, but there is no evidence of the Nb gap in the SIS' junctions, suggesting that the subgap conductance is of extrinsic origin.

This thesis begins with an overview of the theory of superconductivity in Chapter II. Chapter III applies the theory to superconductive tunneling. Different tunneling methods will be discussed and the advantage and validity of point-contact tunneling on HTS will be addressed. Chapter IV gives a detailed description of the tunneling apparatus and experimental procedure. In Chapter V, experimental data on $HgBa_2CuO_{4+x}$ are presented and results are

discussed. Modeling studies for tunneling between two superconductors are carried out in order to better understand the superconducting tunneling data for SIS' junctions. We used a much smeared DOS for one electrode to account for the usual broadening in HTS DOS. In Chapter VI, data on the electron-doped infinite-layer compound $Sr_{1-x}Nd_xCuO_2$ are presented and compared with other electron-doped systems. As an extension of the above method, proximity-effect tunneling was utilized to study interface properties on *in-situ* deposited metal/superconductor bilayers. Some preliminary results and corresponding theory are presented in Chapter VII. Conclusions and discussions are made in Chapter VIII.

CHAPTER II
THEORY OF SUPERCONDUCTIVITY

In order to better understand superconductive tunneling, this chapter is devoted to a brief review of superconductivity. The Bardeen-Cooper-Schrieffer (BCS) theory (Bardeen *et al.*, 1957) and its extension-strong coupling theory (Eliashberg, 1960a) will be presented, followed by theoretical progress on high temperature superconductors (HTS).

2.1. BCS Theory

The normal-to-superconducting transition occurs due to the formation of Cooper pairs which are bound states formed from an electron in the band state ($\mathbf{k}\uparrow$) and an electron in the band state ($-\mathbf{k}\downarrow$) by electron-electron interaction via phonon exchange. This process can be described by the diagram in Fig. 2.1. This is because

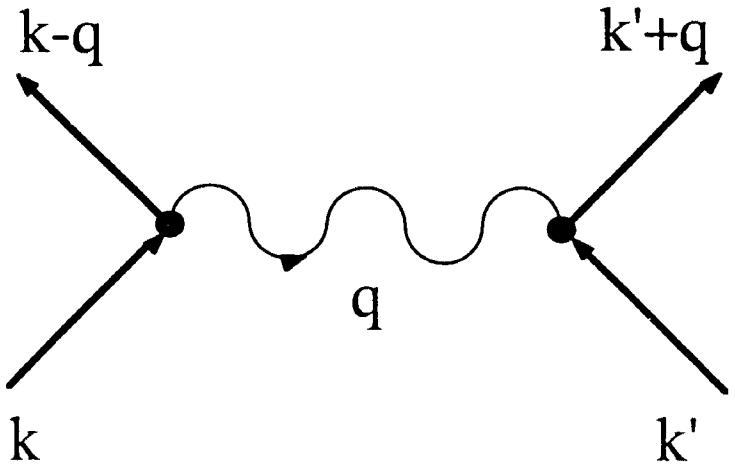

Fig. 2.1. Feynman diagram of the electron-electron interaction via phonon exchange.

only the terms of the electron-phonon matrix elements which couple the states ($\mathbf{k}\uparrow$, $-\mathbf{k}\downarrow$) are most important for superconductivity because of the allowed phase space for scattering processes shown in Fig. 2.1. This results in the total energy of the pair being less than the sum of the energies of the states from which it was formed ($E_p < \varepsilon_{k\uparrow} + \varepsilon_{-k\downarrow} = 2\varepsilon_k$). This reduction in the total energy can be described by the BCS theory.

The BCS theory (Bardeen *et al.*, 1957) of superconductivity uses a very simple model of electron dynamics in metals. Electrons in an electron gas attractively interact with each other and form electron pairs near the Fermi surface resulting from the virtual exchange of phonons. The basic physical idea of an effective, attractive electron–electron interaction is that one conducting electron attracts positive ions of the lattice and deforms the lattice. This lattice deformation lowers the local energy of the second conducting electron appearing nearby. In a quantum mechanical picture, the first electron occupying state $\mathbf{k}$ emits a phonon of wave vector $\mathbf{q}$ and energy $\hbar\omega_q$ which is absorbed by the second electron occupying state $\mathbf{k'}$ and the resulting new electronic states are $\mathbf{k-q}$ and $\mathbf{k'+q}$. The BCS theory assumes a nonlocal and instantaneous interaction, attractive for any pair of electrons both within Debye energy $\hbar\omega_D$ of the Fermi surface. The excited states of the normal metal are long-lived quasiparticles whose "effective" mass contains the interaction between phonons and electrons. The superconducting wave function will contain configurations involving normal state excitations near the Fermi surface and it is just these configurations which are best described

by the Landau theory (Schrieffer, 1964). One therefore imagines the system as composed of quasi-electrons which interact via a shielded Coulomb interaction, dressed phonons whose frequencies have been renormalized by interactions with the electrons, and finally a residual electron-electron interaction which is a formulation of the coupling of the quasi-electrons to the dressed phonons. The Hamiltonian of the electron-phonon system can be written as

$$H = H_{electron}^{quasi} + H_{int} \tag{2.1}$$

where the effective interaction is

$$H_{int} = H_{Coulomb}^{screened} + H_{phonon}^{dressed} + H_{phonon}^{electron} = \sum_{k,k',q} V_{kq} c_{k'-q}^{+} c_{k'} c_{k-q}^{+} c_{k} \tag{2.2}$$

The c^+ and c are quasi-electron creation and annihilation operators, and

$$V_{kq} = \frac{4\pi e^2}{q^2 + \lambda_F^2} + \frac{2\hbar\omega_q |M_q|^2}{(\varepsilon_k - \varepsilon_{k+q})^2 - \hbar\omega_q^2} = V_c + V_{BP} \ , \tag{2.3}$$

where λ_F is the screened Fermi wave length and ω_q is the phonon frequency. The second term, V_{BP}, is known as the Bardeen-Pines interaction and was first derived by Frohlich (1952). M_q is proportional to the shielded electron-phonon coupling. When $|\varepsilon_k - \varepsilon_{k+q}|$ is sufficiently small, V_{BP} is negative (this occurs for $|\varepsilon_k|$ and $|\varepsilon_{k+q}|$ less than a typical phonon energy, for example Debye energy ω_D). If M_q is large enough, V_{BP} dominates V_c, and the net interaction is attractive. Cooper (1956) showed that two electrons above a filled Fermi surface with an attractive interaction would form a bound

state. Therefore the Fermi sea was unstable and it was energetically favorable for the system to form a correlated state in which every electron, $\mathbf{k}\uparrow$, was paired off with its mate in $-\mathbf{k}\downarrow$. It is this assumption as to the nature of the ground state wave function that leads to superconducting effects. The results of the BCS model are that the ground state is lowered in energy with respect to the normal state and that excitations are long-lived quasiparticles, whose energy, E_k, is related to the long-lived normal state quasiparticles by

$$E_k = \sqrt{\varepsilon_k^2 + \Delta_k^2} \quad , \tag{2.4}$$

where

$$\varepsilon_k = \frac{h^2 k^2}{2m^*}, \quad \Delta_k = -\sum_{k'} V_{k\,k'} \frac{\Delta_{k'}}{2E_{k'}} \tanh \frac{E_{k'}}{2k_B T}, \quad \mathbf{k'} = \mathbf{k} - \mathbf{q}, \tag{2.5}$$

for temperature $T < T_c$. By Eq. (2.4), a minimum value for the excitation energy, a energy gap Δ_k, exists. The superconducting density of states $N_S(E)$ can be found

$$N_S(E) = N_N(E)\ \mathrm{Re}\left(\frac{E}{\sqrt{E^2 - \Delta_k^2}} \right) \quad . \tag{2.6}$$

To simplify the problem even further, BCS replaced V_{BP} with a square-well model interaction,

$$V_{BCS}(k, k') = -V_{BCS}\,\theta(\omega_D - |\varepsilon_k|)\,\theta(\omega_D - |\varepsilon_{k'}|) \, . \tag{2.7}$$

where

$$\theta(x) = \begin{cases} 1 & \text{for } x > 0 \\ 0 & \text{for } x \leq 0 \end{cases} \qquad (2.8)$$

and ω_D is the lattice Debye frequency.

Similarly, the Coulomb part of V_{kq} was included by Bogoliubov *et al.* (1959), using a square-well model with a high energy cutoff equal to the electron plasma frequency, ω_{pl}, such that

$$V_c(k, k') = - V_c \, \theta(\omega_{pl} - |\varepsilon_k|) \, \theta(\omega_{pl} - |\varepsilon_{k'}|) \, . \qquad (2.9)$$

Within these approximations, the transition temperature, T_c, of the superconductor is found to be

$$T_c = \frac{\omega_D}{k_B} \exp\left(\frac{-1}{\lambda - \mu^*}\right) , \qquad (2.10)$$

where μ^* is the Coulomb pseudopotential

$$\mu^* = \frac{\mu}{1 + \mu \ln \frac{\omega_{pl}}{\omega_D}} \quad \text{and} \quad \begin{matrix} \mu = N(0) V_c \\ \lambda = N(0) V_{BCS} \end{matrix} , \qquad (2.11)$$

It is important to notice that the Coulomb repulsion term enters the T_c equation reduced from μ (a number of order 1.0) to μ^* (a number of order 0.1). This reduction arises from the increased spacing between paired electrons that results from the relatively slow response of the ions to the electronic motion. The summation on k introduces the term N(0), which is the density of electron states of one spin index at the Fermi surface.

It should be noted that under the assumptions of Eqs. (2.7) and (2.9), the BCS energy gap Δ_k in Eq. (2.6) is isotropic in k-space which corresponds to s-wave symmetry. In a more generalized approach (Anderson, 1961), the pair potential Δ_k is allowed to be **k**-dependent to treat gap anisotropy, or position dependent as in the important cases of inhomogeneous superconductivity. Anderson employed Hartree and Hartree-Fock treatments of many electrons interacting via a two-body potential in a metal and interprets Δ as a mean potential for pair formation. It is showed that this leads to the usual BCS results. Anisotropy in Δ_k can enter either through the interaction $V_{kk'}$ itself or through the sum on states k' over an anisotropic Fermi surface. Anderson (1959) also generalized the pairing to time-reversed states to include "dirty superconductors" of short mean free path. The states which now interact via $V_{kk'}$ are the true scattered states in the sample. All results of the BCS theory come out as before, with matrix elements now averaged over the Fermi surface. Hence, dirty superconductors are those most accurately fitting the BCS model, for all anisotropies are averaged out in the limit of rapid scattering.

2.2. Strong Coupling Theory

The BCS assumption of weak coupling between the electrons and phonons greatly simplifies the calculations. This assumption requires only the use of a single average matrix element, V_{BCS}, for the electron-phonon interaction. Though this approximation may work in most cases, it fails to explain certain experimental findings such as the critical field curves of soft metals deviating from a

parabolic dependence (Decker *et al.*, 1958; Finnemore *et al.*, 1960), or the dependence of the tunneling density of states of Pb deviating from predictions near peaks in the phonon spectrum (Rowell and Kopf, 1965). It was found that in some metals, the electron-phonon interaction is quite strong and needs to be considered in greater detail in the calculations. Eliashberg theory (Eliashberg, 1960b), sometimes referred to as strong-coupling theory, incorporates these corrections.

In contrast to the nonlocal instantaneous nature of the BCS model interaction, attractive for any pair of electrons both within $\hbar\omega_D$ of the Fermi surface, Eliashberg theory considers that the electron-electron coupling is local in space and retarded in time, reflecting the delay $\tau \approx 1/\omega_{ph}$ in the development of lattice overscreening. The Eliashberg electron-phonon function is given as

$$V_{k,k-q} \propto \frac{E_{k-q} + \hbar\omega_q}{(E_{k-q} + \hbar\omega_q)^2 - E_k^2} \qquad (2.12)$$

and is energy dependent. A rigorous derivation of the details of Eliashberg or strong-coupling theory is not needed for a complete understanding of this thesis. However, a comparison of the results of both BCS and strong-coupling theory is informative. This comparison is made in Table 2.1. Its contents can be derived from the following relations. The BCS results can be calculated from the self-consistent BCS equation

$$\frac{1}{V_{BCS} N_S(E_f)} = \int_0^{\omega_D} d\xi (\xi^2 + \Delta^2)^{-1/2} \tanh\left[\frac{1}{2k_B T}(\xi^2 + \Delta^2)^{1/2}\right] \qquad (2.13)$$

Table 2.1. Comparison of BCS to Strong-Coupling Theory

BCS Theory	Strong-Coupling Theory
Δ	$\tilde{\Delta}(E) = \Delta_1(E) + i\Delta_2(E)$
$T_c = \frac{\omega_c}{k_B} \exp\left(\frac{-1}{\lambda - \mu^*}\right)$	$T_c = \frac{\omega_{log}}{1.2 k_B} \exp\left[\frac{-1.04(1+\lambda)}{\lambda - \mu^*(1+.62\lambda)}\right]$ where $\omega_{log} \equiv \exp\left\{\frac{2}{\lambda}\int_0^\infty \frac{\alpha^2 F(\omega) \ln \omega d\omega}{\omega}\right\}$
$N_s(E) = N(0)\frac{\lvert E\rvert}{\sqrt{E^2 - \Delta^2}}$	$N_s(E) = N(0)\mathrm{Re}\left\{\frac{\lvert E\rvert}{\sqrt{E^2 - \tilde{\Delta}^2(E)}}\right\}$
$\lambda = N(0)V_{BCS}$	$\lambda = 2\int_0^\infty \frac{\alpha^2(\omega)F(\omega)}{\omega} d\omega$
$Z = 1 + \lambda$	$Z(0) = 1 + \lambda$

where V_{BCS}, the attractive potential, and Δ, the energy gap are considered constant. The strong-coupling analog to these BCS equations are the Eliashberg equations. Averaged over the Fermi surface, as is appropriate for dirty superconductors, at T = 0, and neglecting the weak k dependence (on the scale of k_F) of Δ and Z, these equations become

$$\Delta(\omega) = [Z(\omega)]^{-1} \int_{\Delta_0}^{\omega_c} \mathrm{Re}\left\{ \frac{\Delta(\omega')}{\left[\omega'^2 - \Delta^2(\omega)\right]^{1/2}} \right\} \left[K_+(\omega,\omega') - \mu^*\right] d\omega' \qquad (2.14)$$

$$[1 - Z(\omega)]\omega = \int_{\Delta_0}^{\omega_c} \mathrm{Re}\left\{ \frac{|\omega'|}{\left[\omega'^2 - \Delta^2(\omega)\right]^{1/2}} \right\} K_-(\omega,\omega') d\omega' \qquad (2.15)$$

where the kernel in these equations is given by

$$K_{\pm}(\omega,\omega') = \int_0^{\infty} \alpha^2 F(\Omega) \left[\frac{1}{\omega + \omega' + \Omega + i\delta} \pm \frac{1}{\omega - \omega' + \Omega - i\delta} \right] d\Omega \qquad (2.16)$$

Here, ω_c is a cutoff frequency taken as five or ten times the maximum phonon frequency. A useful measure of the strength of electron-phonon coupling is the electron-phonon coupling function λ expressed as

$$\lambda = 2 \int_0^{\infty} \frac{\alpha^2(\omega) F(\omega)}{\omega} d\omega \qquad (2.17)$$

The renormalization function Z at E = 0, describes the renormalization of the electron mass by the electron-phonon coupling and is defined as $Z(0) = 1 + \lambda$.

In contrast to the constant gap parameter Δ in the BCS model, the Eliashberg theory gives an energy-dependent pair potential $\Delta(E)$, which is complex, leading to energy-dependent structures which are observed in many experiments including tunneling. It should be noted that the imaginary (lifetime) part of $\Delta(E)$ becomes nonzero as sufficient energy becomes available for real phonon emission. The stronger the coupling, the larger the imaginary part becomes. Thus, the Eliashberg theory is often called the strong coupling theory. As the coupling becomes weaker, the imaginary term vanishes and $\Delta(E)$ reduces to a constant, leading back to the BCS theory.

The Eliashberg equations relate the superconducting parameters to the normal state quantities μ^* and $\alpha^2F(\omega)$. The function, $\alpha^2F(\omega)$, counts the number of phonons of frequency ω and weights each phonon by the strength and number of electron transitions in which it participates. The terms $\alpha^2F(\omega)$ and μ^* are both dependent only on the intrinsic properties of the material they are describing.

The tunneling process is a powerful way of probing the superconducting state to measure $\Delta(E)$, and thus determining $\alpha^2F(\omega)$ and μ^* from an inversion of Eqs. (2.14) and (2.15). The electron-phonon coupling strength λ can be then calculated, adding quantitatively to the understanding of the electron-phonon and Coulomb interactions. By using the temperature dependent form of these equations, one can find the temperature, T_c, at which the pair potential goes to zero. The prediction of T_c for Pb within experimental error (McMillan and Rowell, 1969) gave strong support

to both the validity of the tunneling spectroscopy and the Eliashberg strong coupling theory.

It is worth noting that there is a direct correlation between the coupling strength parameter $2\Delta_0/k_BT_c$ and λ. See Table 2.2 (Wolf, 1985) for values of conventional superconductors. Thus, $2\Delta_0/k_BT_c$ is a crucial parameter to distinguish between weak and strong coupling and may give insight into the electron-phonon coupling strength. We fit the data in Table 2.2 to a smooth curve as in Fig. 2.2. For most HTS, the maximum value is $2\Delta_0/k_BT_c \approx 6$ and $\lambda \approx 2.8$ is predicted. Based on this correlation, most HTS are in the strong coupling regime.

2.3. High Temperature Superconductor Theory

Various pairing mechanisms are proposed to explain HTS. However, none of them is widely accepted. Some theoretical models may be broadly classified as phonon-mediated, others are based on purely electronic mechanisms.

The phononic mechanisms include BCS coupling, Eliashberg strong coupling, bipolaronic negative-U and Jahn-Teller mechanisms.

The various electronic mechanisms include Little-Ginzburg exciton exchange, charge transfer excitation exchange, charge fluctuation, acoustic plasmon exchange, Hubbard-U induced formation of polarons, antiferromagnetic spin fluctuations, resonating valence bonds, and correlated charge fluctuations (exchange of charged bosons). Although these theoretical models appear to differ greatly from each other, the general agreement is that electron

Table 2.2. Superconductivity Parameters of the Materials

Material	T_c (K)	λ	$2\Delta_0/k_BT_c$
Al	1.18	0.38	3.5
In	3.41	0.805	3.68
Pb	7.2	1.55	4.49
Hg(α)	4.15	1.6	4.61
$Pb_{0.7}Bi_{0.3}$	8.45	2.01	4.86
Nb	9.2	1.04	3.9
V	5.4	0.82	3.51

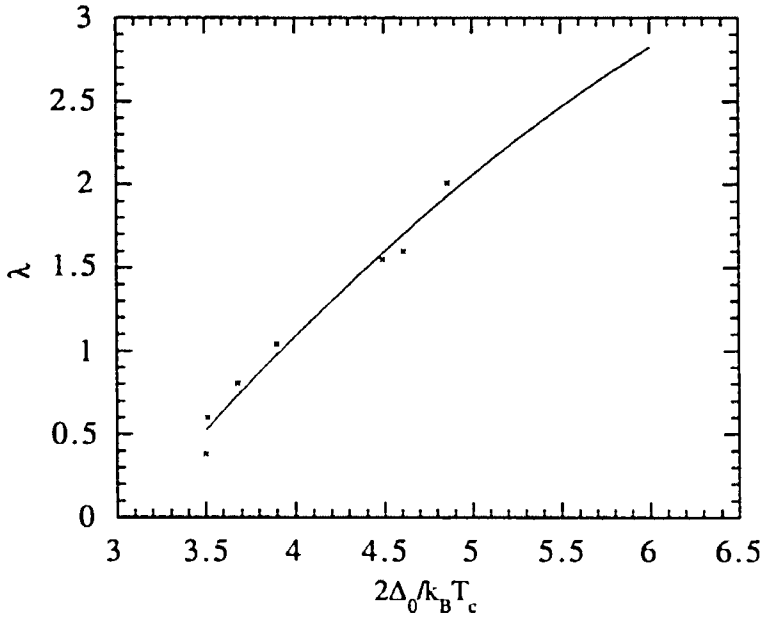

Fig. 2.2. Electron-phonon coupling strength λ plotted versus coupling strength parameter $2\Delta_0/k_BT_c$.

correlations play an important role in these newly discovered high-T_c systems.

Josephson tunneling (Esteve *et al.*, 1987) and flux quantization (Gough *et al.*, 1987) experiments have shown early that the superconductive charge quantum is 2e and that superconductivity involves electron (or hole) carriers making Cooper pairs. Nuclear magnetic resonance studies show fairly clearly the existence of a Knight shift which disappears below the critical temperature and the total electron spin S = 0 in the non-conductive phases (Mendels and Alloul, 1988; Takigawa *et al.*, 1989; Wzietek *et al.*, 1989). Also, Knight shift measurement in $YBa_2Cu_3O_{7-y}$ (Barrett *et al.*, 1990) shows that, within a BCS framework, the pairing is spin singlet (i.e. $\uparrow\downarrow$ as opposed to $\uparrow\uparrow$ for Cooper pairs). The main problem is to identify the origin of the strong binding energy of the pairing interaction for the high T_c superconductivity in these systems. Isotope effect (Hinks *et al.*, 1988; Schwarz *et al.*, 1991) and tunneling experiments (Zasadzinski *et al.*, 1989; Huang *et al.*, 1990b; Tralshawala *et al.*, 1995) have shown evidence of phonon-mediated mechanism of pairing in $Ba_{1-x}K_xBiO_3$ and $Nd_{2-x}Ce_xCuO_{4-y}$ systems.

CHAPTER III
TUNNELING SPECTROSCOPY

The theory of superconductive tunneling, which will be applied to our experimental data later, is presented in this chapter. Different tunneling methods will be discussed and the advantage and validity of point-contact tunneling on high temperature superconductors (HTS) will be addressed.

3.1. Superconductive Tunneling

It is well known from quantum mechanics that a particle with an energy E has a finite probability of tunneling through an energy barrier having a width W and a height U > E. This tunnel probability decreases exponentially with W, and for typical U, a thickness W of the order of a few nanometers is necessary to have significant transmission coefficient. A typical tunnel junction is formed by two metals (normal or superconducting) separated by a thin insulating layer as shown in Fig. 3.1a. The two metals M_l, M_r at temperature T = 0 K have the conduction band completely filled up to the Fermi energy (E_{Fl}, E_{Fr}), while the insulator forms a barrier, the height of which is determined by the lowest level of the conduction band of the insulator, as shown in the energy diagram of Fig. 3.1b. In the case of different metals with different Fermi levels, contact potentials localized on the insulator arise, giving rise to asymmetric barriers. Moreover, the presence of image forces leads to a rounding of the barrier.

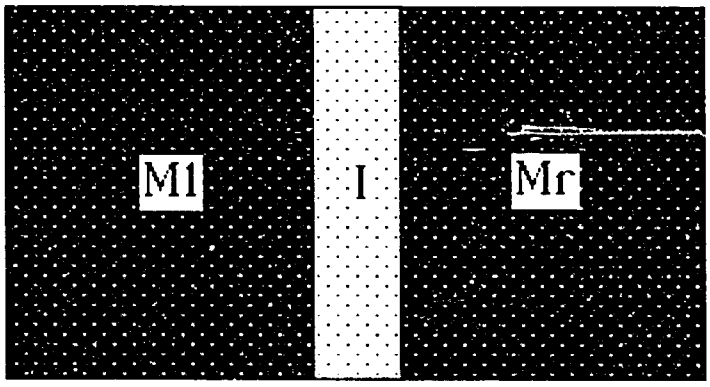

(a)

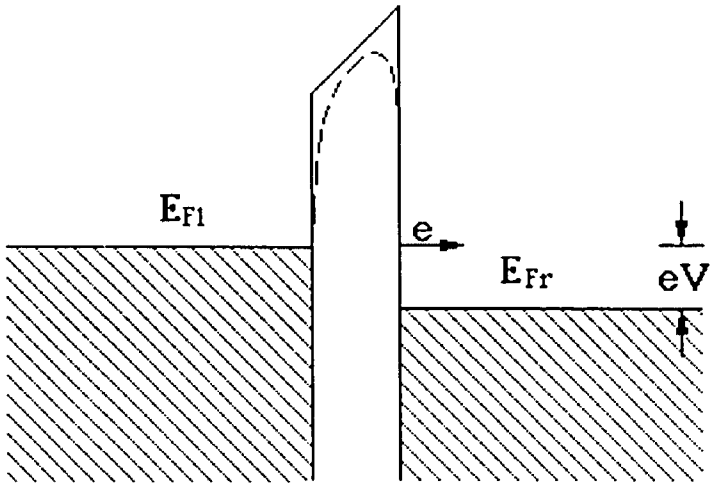

(b)

Fig. 3.1. a) Schematic view of a tunneling junction. b) Energy diagram of the tunneling junction under bias.

Upon application of a potential, V, across the junction, a tunneling current, I, will flow. The total tunneling current, I, can be determined by the independent-particle approximation (Tinkham, 1975),

$$I = A\int N_1(E)N_2(E+eV)[f(E)-f(E+eV)]dE \qquad (3.1)$$

where A is proportional to an assumed energy independent tunneling matrix element, $N_1(E)$ and $N_2(E)$ are the electron density of states of the two electrodes, and f(E) is the Fermi function

$$f(E)=\frac{1}{1+\exp(E/k_BT)} \qquad (3.2)$$

3.1.1. Superconductor-Insulator-Normal Metal (SIN) Tunneling

Equation 3.1 can be simplified by assuming that one of the metals (right) is always normal and has a constant density of states $N_r(E) \approx N_r(0)$ near the Fermi surface. The other (left) metal is in the superconducting state and the density of states is energy dependent given by equation 2.6 for weak coupling superconductors. Differentiating current with respect to voltage, then one has

$$\frac{dI(V)}{dV} \equiv \sigma_s(V) = A\,N_r(0)\int N_{1S}(E)\left(-\frac{c}{k_BT}\frac{\exp\left(\frac{E+eV}{k_BT}\right)}{\left[1+\exp\left(\frac{E+eV}{k_BT}\right)\right]^2}\right)dE. \qquad (3.3)$$

The dI/dV in the normal state, $\sigma_n(V)$, for the superconductor can be measured by applying a large magnetic field above the critical field

or raising the temperature above T_c. By dividing the results of the two measurements one obtains,

$$\frac{\sigma_s}{\sigma_n} \equiv \sigma = N_T(eV) \equiv \int \frac{N_{1S}(E)}{N_{1N}(0)} \left(\frac{1}{k_B T} \frac{\exp\left(\frac{E+eV}{k_B T}\right)}{\left[1+\exp\left(\frac{E+eV}{k_B T}\right)\right]^2} \right) dE , \quad (3.4)$$

where the quantity σ is called the normalized conductance which is equivalent to the tunneling density of states of a superconductor $N_T(E)$ for the ideal conditions shown above. The term in brackets is a bell-shaped curve, centered at E = -eV, having width at half maximum of approximately 3.5 $k_B T$ and unit area under the curve. At very low temperature, this curve is approximately a delta function. As temperature approaches zero, this gives

$$\sigma(V) = N_T(eV) = \frac{N_{1S}(eV)}{N_{1N}(0)} . \quad (3.5)$$

For a weak coupling superconductor (BCS theory), the density of states is given by equation 2.6 and the tunneling density of states is then

$$N_T(E) = Re \left(\frac{E}{\sqrt{E^2 - \Delta^2}} \right) , \quad (3.6)$$

where Δ is a constant gap parameter. A measurement of $N_T(E)$ therefore gives a direct energy gap measurement.

For a strong coupled superconductor, it can be shown that the observed density of states is (Schrieffer, 1964)

$$N_S(E) = N_N(E)\,\mathrm{Re}\left\{\frac{E}{\sqrt{E^2 - \Delta^2(E)}}\right\}, \qquad (3.7)$$

where $\Delta(E)$ is a complex pair potential given by equation 2.13. The tunneling density of states is then

$$N_T(E) = \mathrm{Re}\left\{\frac{E}{\sqrt{E^2 - \Delta^2(E)}}\right\}. \qquad (3.8)$$

For $E \gg \Delta$, one has

$$N_T(E) = 1 + \frac{1}{2}\,\mathrm{Re}\left\{\frac{\Delta^2(E)}{E^2}\right\}. \qquad (3.9)$$

The observed phonon effects are due to the energy dependence of the pair potential, $\Delta(E)$, which affects the tunneling density of states $N_T(E)$. Therefore, the tunneling experiment gives an implicit measure of the phonon effects.

Superconductive tunneling is a very sensitive probe of the superconducting state and gives a detailed picture of a superconductor. The normalized conductance σ is almost an exact measure of the density of excitations of the superconductor, $N_T(E)$, because any variations in the particular junction normal state conductance, σ_n, is almost completely cancelled by the normalization (Eq. 3.5). The full power of this tunneling method was first demonstrated by McMillan and Rowell (1965) in getting a detailed

picture of the strong coupling superconductivity of Pb by working from spectra earlier recorded by Giaever. By this method, it is possible to obtain the electron-phonon spectral function $\alpha^2F(\omega)$, the coupling parameter λ, and the Coulomb pseudopotential parameter μ^*, and then the complex energy dependent pair potential $\Delta(\omega)$ and the renormalization function $Z(\omega)$ via Eqs. (2.14) and (2.15). The critical temperature T_c can be estimated from the Allen-Dynes-McMillan formula given in Table 2.1. Comparison of these values with the observed T_c then gives a test of the consistency of the resulting picture of the superconductor. Evidently the key to this analysis is the Eliashberg function $\alpha^2F(\omega)$, which is almost directly measured by Giaever-McMillan-Rowell tunneling spectroscopy.

3.1.2. Superconductor-Insulator-Superconductor (SIS) Tunneling

If both materials are superconducting and the density of states is given by Eq. 2.6, Eq. 3.1 becomes

$$I_{SS} = AN_{LN}(0)N_{rN}(0)\int \frac{|E|}{\sqrt{E^2-\Delta_l^2}} \frac{|E+eV|}{\sqrt{(E+eV)^2-\Delta_r^2}} [f(E)-f(E+eV)]dE \quad (3.10)$$

where the range of integration excludes values of E such that $|E| < |\Delta_l|$ and $|E+eV| < |\Delta_r|$.

When temperature T = 0, no current can flow until $V = (\Delta_l+\Delta_r)/e$. Above this point the current can be expressed in terms of complete elliptic integrals (Douglass and Falicov, 1964). There is a discontinuous jump in current at $V = (\Delta_l+\Delta_r)/e$ since the density of states is infinity. For temperature $T \neq 0$, numerical integration is required to compute the current. The tunneling current can also flow

at lower voltages because of the availability of thermally excited quasiparticles. This current rises sharply to a peak when $V = |\Delta_l - \Delta_r|/e$ because this voltage provides just the energy to allow thermally excited quasiparticles in the peak of the density of states Δ_l, say, to tunnel into the peaked density of available states at Δ_r. It subsequently decreases because the density of states decreases. This leads to a "negative-resistance region" for $|\Delta_l - \Delta_r|/e \leq V \leq (\Delta_l + \Delta_r)/e$. At $V = (\Delta_l + \Delta_r)/e$, there is again a large increase in tunneling current as the great increase of the densities of states. The existence of sharp features at both $|\Delta_l - \Delta_r|$ and $\Delta_l + \Delta_r$ allows very convenient determination of Δ_l and Δ_r from the tunneling data. The SIS tunneling junction is superior to the SIN tunneling junction in this regard because the existence of very sharply peaked densities of states at the gap edges of both materials helps to counteract the effects of thermal smearing. This feature is of appreciable practical importance.

3.2. Tunneling Methods

It is much more difficult to conduct the tunneling measurement in high temperature superconductors (HTS) than in conventional superconductors. First, the HTS coherence lengths are almost an order of magnitude smaller than those in conventional superconductors and comparable to the crystal cell dimensions. The short coherence length of HTS makes superconductive tunneling much more difficult because of the requirement of preparing well ordered superconducting phase to within a distance of the coherence length from the tunneling barrier. Second, these materials may be

intrinsically insulating at their surface. This "dead layer" may be too thick to form suitable barriers for superconductive tunneling. Third, these materials are quite complex, with properties that depend sensitively on their composition and lattice structure.

Despite such difficulties, a variety of junction configurations has been explored for tunneling studies of the HTS. Among them are planar junction, break junction, vacuum and point-contact tunnel junctions.

Planar tunneling junctions are fabricated by using a thin film for one or both electrodes. Here a thin insulating region separates the sample from a second normal or superconducting metal. This technique has been very successfully used to study conventional superconductors. Planar junctions are very stable and can be cycled in temperature and magnetic field without changing their characteristics. But it is nontrivial to prepare planar tunneling junctions for HTS because of their short coherence lengths and potentially the thick dead layers. The barrier layer not only must be thin and pinhole free but also must not leech oxygen out of the HTS or interdiffuse into it during the various processing steps. This technique is also incompatible with small specimens such as single crystals. Consequently there have only been a few published reports of planar junctions on HTS, that exhibit gap features.

The break junction technique, pioneered by Moreland and Ekin (Moreland and Ekin, 1985) and also applied to HTS (Mandrus *et al.*, 1991), is one way to solve such surface problems. In this case, a

bulk sample is glued to a flexible substrate and broken in the cryogenic environment into two pieces by flexing the substrate. The pieces are then formed into a junction in the fractured region by flexing back the substrate, thereby avoiding any contamination of the junction surface. The drawbacks of this method are that only SIS type junctions can be formed and junctions are unstable during the cycling in temperature and magnetic field.

The technique of forming a junction by mechanically bringing the pointed tip of an electrode near the surface of a specimen has emerged as a powerful spatial and spectroscopic probe. With vacuum tunneling, as occured in the scanning tunneling microscope, a tip is held a few Angstroms above the sample surface and current tunnels through a vacuum barrier. Since in the scanning tunneling microscope the tip can be scanned laterally relative to the sample, spatially resolved information on the gap can be obtained. The powerful combination of spatial and spectral resolution in the scanning tunneling microscope has been demonstrated in the mapping of the Abrikosov flux lattice in the anisotropic superconductor $NbSe_2$ (Hess *et al.*, 1989 and 1991). Use of the scanning tunneling microscope for HTS has proved more difficult. First, the separation between the tip and sample results in a high tunneling resistance (10^7-$10^9\Omega$) and a relatively poor signal to noise ratio compared to thin film junctions. Another difficulty results from dead surface layer because metallic surface properties are necessary for vacuum tunneling. Even so, vacuum tunneling was reported on $Bi_2Sr_2CaCu_2O_x$ (Hasegawa *et al.*, 1989; Tanaka *et al.*, 1989) and on

$Bi_2Sr_2CaCu_2O_x$/Au and $HgBa_2CuO_{4+x}$/Ag proximity bilayers (R. Zasadzinski *et al.*, unpublished).

Because of the above problems, most tunneling measurements for HTS have been of the point-contact type. A junction is formed by mechanically bringing the pointed tip of an electrode near the surface of a specimen and actually touching the sample surface. This method relies on the sample to provide a native, insulating surface layer that serves as the tunnel barrier. The tip can be used to mechanically scrape and clean the sample surface. Compared to the vacuum tunneling, where the vacuum between the tip and sample forms the barrier, the point-contact junction is mechanically more stable. It has a lower resistance with a better signal to noise ratio. A drawback of the point-contact tunneling and STM is the difficulty in measuring the junction characteristics continuously through the transition temperature for $T_c > 30$ K due to different thermal expansions of the mechanical apparatus. For quantitative tunneling spectroscopy, a normal state measurement is required.

The point-contact apparatus used in this thesis was tested on single crystals of Nb with a Au tip (Huang *et al.*, 1990b). Niobium has been studied extensively by conventional and proximity-effect methods (Wolf *et al.*, 1980; Khim *et al.*, 1981; Geerk *et al.*, 1982) so its phonon spectrum is well established. Also, the phonon structures in Nb junctions are rather small, about a 1% change in dI/dV, and therefore present a challenging test for the point-contact method. The point-contact tunneling data, I(V) and dI/dV, reproduce the results obtained from conventional, thin-film planar junctions

including the characteristic structures associated with the Nb phonon density of states. These results demonstrate that the point-contact tunneling method can be used to measure the electron-phonon interaction in superconductors with a similar degree of sensitivity as found in thin-film tunneling spectroscopy. The point-contact method was also the first to demonstrate the ideal tunneling characteristics of $Ba_{1-x}K_xBaO_3$ (Huang *et al.*, 1990a). This result, together with the Josephson tunneling results (Pargellis *et al.*, 1991), has stimulated all-thin-film junction development of this material (Hou *et al.*, 1992; Kussmaul *et al.*, 1993).

CHAPTER IV
EXPERIMENTAL SET-UP

This chapter gives a detailed description of the tunneling apparatus and data acquisition system used in this thesis.

4.1. Point-Contact Tunneling Apparatus

The point-contact apparatus used for tunneling is essentially a variation of the vacuum tunneling devices in common use for scanning tunneling microscopy. The whole set up (Fig. 4.1) and the data acquisition system is housed in an electromagnetically and acoustically screened room. The cryostat is supported by a vibration isolation and damping system (NRC pneumatic isolation mounts type XL-A). Approximately 2000 lbs of lead brick are piled uniformly around the perimeter of the upper plate of the platform to damp any oscillations of the air table. The dewar sits inside a sand-filled plastic drum on the lower plate of the platform.

The tunneling junction assembly is inside a stainless steel can which is sealed by indium, see Fig. 4.2. The can is pumped to rough vacuum and then filled with approximately 200 millitorr of helium as an exchange gas, and finally inserted into the dewar. The helium dewar is an aluminium superinsulated vessel (International Cryogenics) without liquid nitrogen jacket. The dewar is precooled by filling the inner space with liquid nitrogen. The nitrogen is blown out of the dewar prior to filling with liquid helium. The tunneling assembly is cooled by the exchange gas inside the can, which is immersed in liquid N_2 (77 K) or ^4He (4.2 K). The temperature can be

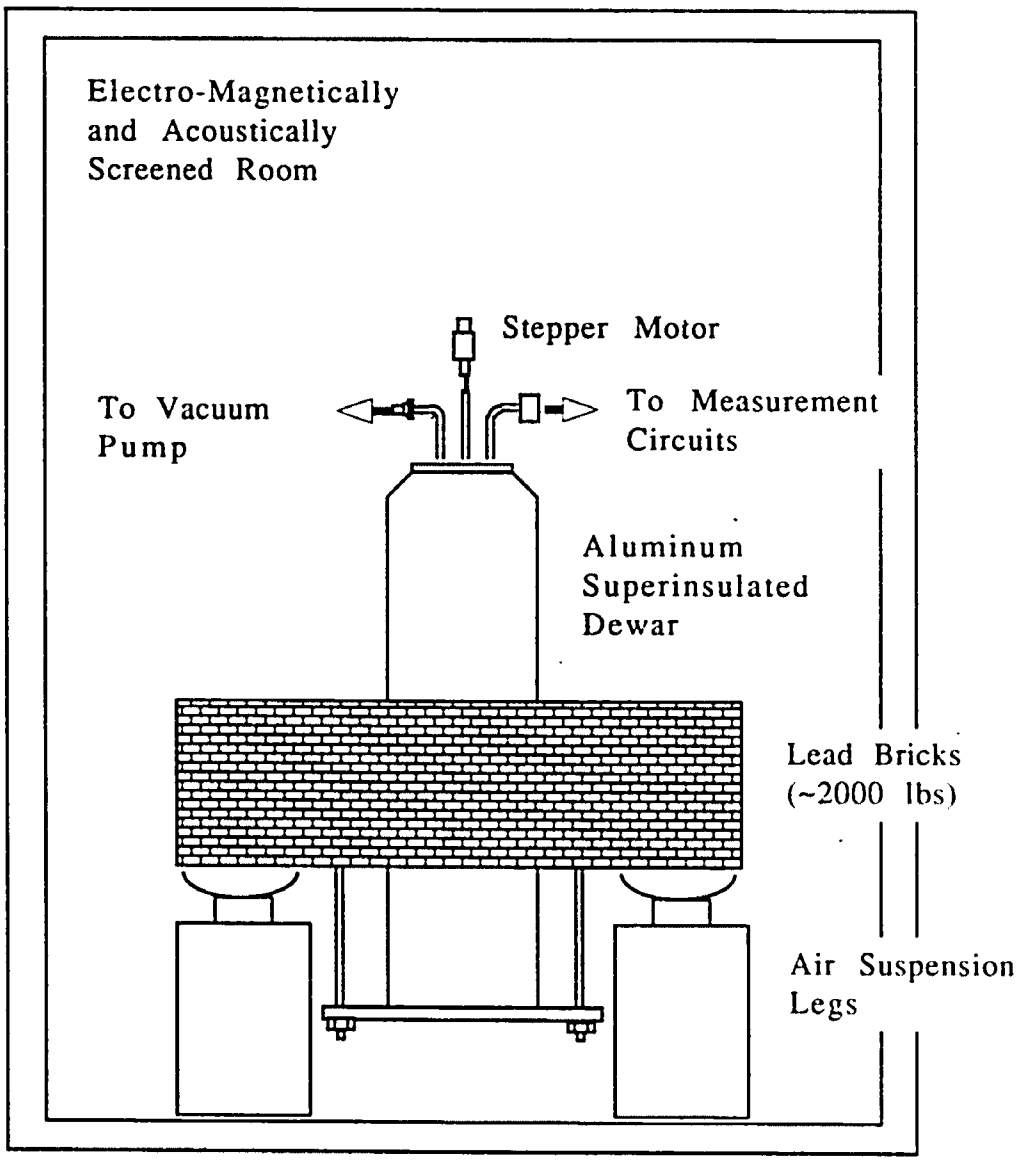

Fig. 4.1. Tunneling apparatus.

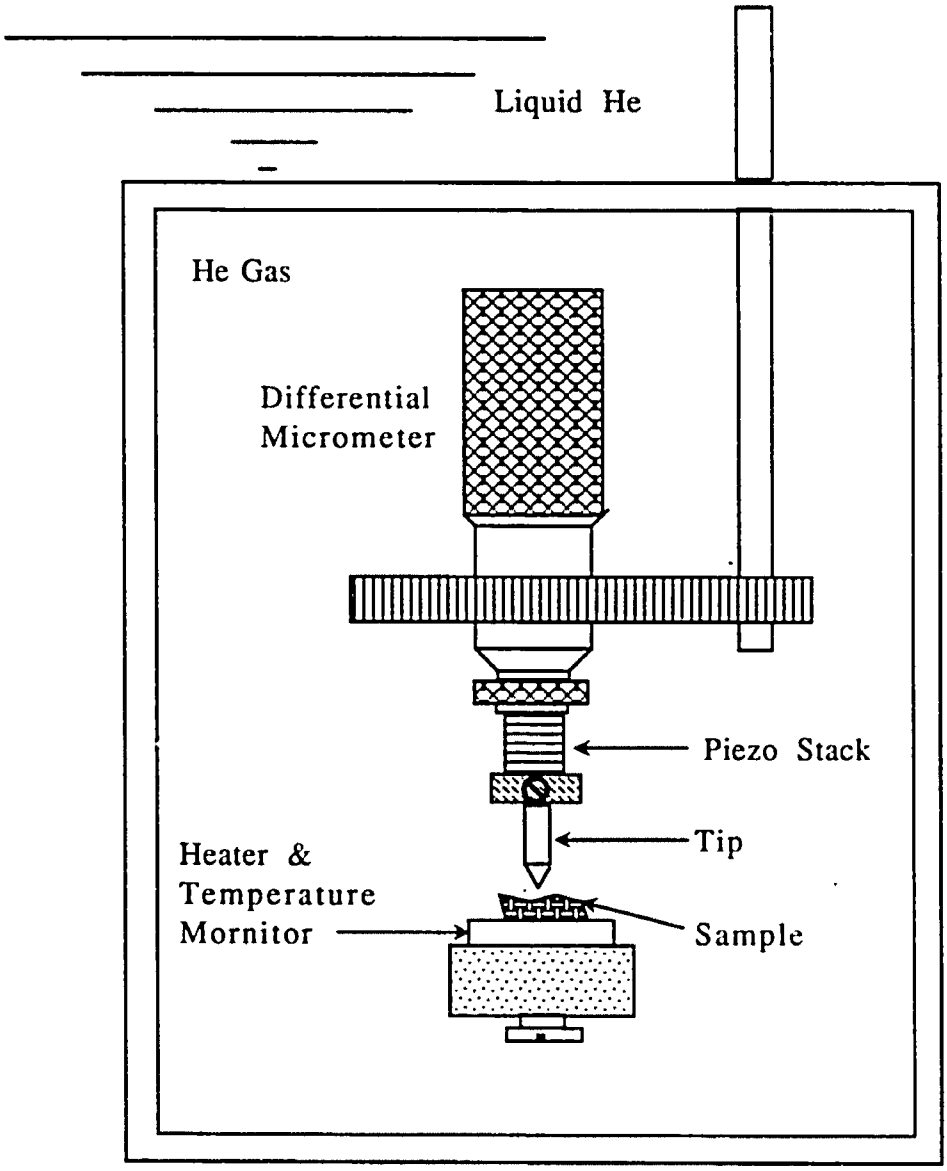

Fig. 4.2. Sample can and tip assembly.

further lowered by pumping out the ^{4}He bath. Usually, it is necessary to wait more than five hours after filling the appropriate cryogen for thermal stability before a stable point-contact junction can be formed and reproducible data can be taken.

The sample is mounted on a 0.5" x 0.25" x 0.015" sapphire substrate which in turn is securely held down on the sample platform by the heads of two screws. The sapphire substrate serves to provide the sample with electrical insulation from the platform while still maintaining good thermal contact. Electrical connections to a sample can be made in two ways: 1) Two Ag strips are evaporated onto the substrate, and the sample is glued down to these Ag pads with Ag filled conductive paint, then electrical connections to the Ag strips are made with indium solder; 2) The sample is glued to the substrate by fast drying epoxy (5 Minute Epoxy by Devcon Corporation), then electrical connections to the sample are made with Ag filled conductive paint. After the contacts are applied, the assembly is stored in dry N_2 while the Ag paint dries. The assembly is then mounted in the can and put in the cryostat for making a tunneling junction. At room temperature, the final resistance of the contact leads plus the sample is typically about 5–50 Ω depending on the sample material and the size. This is much lower than the resistance of the point-contact tunnel junction which is usually a few kΩ.

The electrode tip is moved up and down by a differential micrometer. These are placed in a suitably rigid assembly mounted in the can. The differential micrometer (Lansing) possesses very fine

differential threads with a total translational motion of its spindle of only 0.01" and resolution of about 250 Å. One degree rotation of the micrometer corresponds to an average of 176 Å tip movement. A stainless steel gear is brazed onto the handle of the micrometer for controlling its rotation from outside the cryostat and is mated with a pinion rod resulting in an 8:1 reduction ratio. The micrometer pinion rod is turned manually, or by a small dc stepper motor mounted outside the dewar.

The tip can be chosen from a wide variety of materials depending on the study of interest. In this study, a Au tip is chosen for most experiments to form SIN tunneling junctions. Sometimes, an In or W tip is chosen for very soft or very hard materials, respectively. Niobium or even HTS materials are used for making SIS junctions. Gold has a low oxidation rate and is very malleable. It also has both good electrical and thermal conductivity. The Au tips are made from 1 mm pure gold wire (99.999%) and annealed at ~ 900 °C for three days. The In tips are fabricated from 1 mm indium wire (99.99%) and annealed at ~100 °C for one day. The Nb tips come from single crystal niobium foil, which is also used as the sample in making point-contact junctions with a Au tip (Huang *et al.*, 1990b). The tips are formed by knife and polished with various grades of diamond paper (the final one containing 3 μm diameter grit), and then the tips are etched (in aqua regia for Au, in hydrofluoric acid for Nb, in nitric acid for In) before being mounted in the tunneling apparatus for each low-temperature run.

An SR-4 strain gauge (FAE-25-35 S6 EC from BLH Electronics) is mounted on the sample platform and used as a heater to increase the temperature of the sample. The temperature is monitored by a calibrated germanium resistance thermometer (C2295 from Cryo Cal, Inc.) inserted inside the sample platform. Usually it is difficult to keep the same junction configuration while raising the temperature above the T_c due to the differential thermal expansions in the tip assembly materials. For those relatively low T_c (less than 30 K) materials like $Ba_{1-x}K_xBiO_3$ and $Nd_{2-x}Ce_xCuO_{4-y}$ (Huang *et al.*, 1990b&c), it is occasionally possible to measure the normal state conductance σ_n by increasing the temperature for some stable junctions with relatively low junction resistance.

4.2. Data Acquisition System

The tunneling measurements of I(V) and dI/dV are measured using quasi-four probe technique, with two leads at the tip and two at the ends of the sample. Direct measure of dV/dI and d^2V/dI^2 can be made by applying a small ac signal, $Ae^{i\omega t}$, on the tunnel junction. This can be understood by expanding the voltage V across the junction in terms of the Taylor series,

$$V(I) = V(I_0) + (dV/dI)_{I_0} Ae^{i\omega t} + 1/2\ (d^2V/dI^2)_{I_0} A^2 e^{i2\omega t} + \cdots \quad (4.1)$$

where $V(I_0)$ is the dc bias of the tunnel junction and ω is the modulating frequency. It follows that if A is constant then the component of voltage across the junction at frequency ω is proportional to $(dV/dI)_{I_0}$ and the component at 2ω is proportional to $(d^2V/dI^2)_{I_0}$. In order to display small variations in dI/dV and

provide the required high resolution by lock-in amplifier (lock-in), we need to balance most of the signal across the junction prior to amplification. This can be done by a combination of harmonic detection and a double-Kelvin bridge circuit (Adler and Jackson, 1966), as shown in Fig. 4.3. The junction impedance is balanced by decade resistor R_S and capacitor C_S at a point of interest in the bias region. Assuming that the junction capacitance is balanced out, the bridge output for R1 = R2 is (Rogers, 1970),

$$V_\omega = A\ [R_S - (dV/dI)_{Io}]\ e^{i\omega t} \qquad (4.2)$$

$$V_{2\omega} = 1/2\ A^2\ (d^2V/dI^2)_{Io}\ e^{i2\omega t} \qquad (4.3)$$

Proper choice of R_S enables one to use the full scale of the lock-in to display a small variation in dV/dI of the tunnel junction rather than dV/dI itself. The near balance condition also provides a near null of the first derivative, which is very helpful in measuring the second derivative. Since different capacitive and inductive influences in the circuit introduce a phase shift in the bridge output relative to the oscillator signal, the correct phase of the phase sensitive detector in the lock-in needs to be found. This is done by first balancing the bridge, then changing the R_S by a small amount and adjusting the detector phase to maximize the detector response. This procedure locks the phase of the lock-in to the resistive component of the junction impedance.

The bridge efficiency is further improved by using large values for the bridge resistances R1 and R2. Their resistances are much larger than those of the junctions. The large values of R1 and R2 are

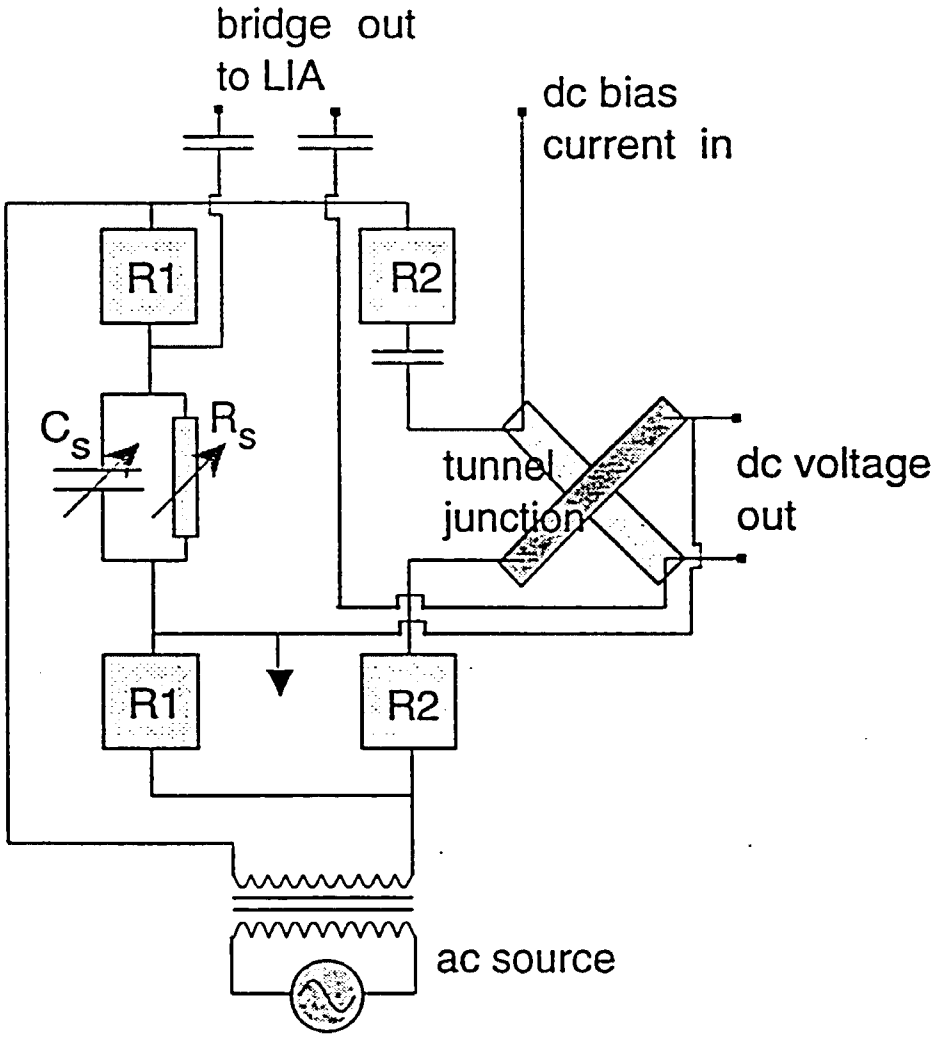

Fig. 4.3. Schematics of the bridge circuit for tunneling measurements. Normally, R1 = R2.

to make the measurement insensitive to changes in the junction lead resistances at different temperatures. The dc biasing circuitry is battery operated and the ac signal generator is isolated from the bridge by a step-down transformer, to eliminate any extraneous source of noise. Proper care is taken to eliminate all the ground-loop signals.

The junction I-V is highly non-linear in the gap region and the dynamic conductance varies over a wide range, so the bridge is usually balanced near the gap edges of the curve to resolve fine details found there. Because the zero-bias resistance of a good tunnel junction is very high and may be beyond the capability of the bridge to balance out accurately, the lock-in output data set is combined with numerical derivative of the I-V characteristics to obtain an accurate zero-bias conductance.

CHAPTER V

TUNNELING STUDY OF $HgBa_2CuO_{4+x}$

In this chapter, experimental data on $HgBa_2CuO_{4+x}$ (Hg-1201) are presented and results are discussed. Superconductor-insulator-nomal metal (SIN) junctions with a Au tip and superconductor-insulator-superconductor (SIS') junctions with a Nb tip are examined. In order to better understand the measured conductances of SIS' junctions, modeling studies for tunneling between a HTS and a conventional superconductor are presented first.

5.1. Modeling Studies of SIS' Junctions

The tunneling characteristics between a HTS and a conventional superconductor are likely to be quite different from those of the usual SIS tunnel junctions between two conventional superconductors. This is due to the experimentally observed broadening of SIN tunneling characteristics of HTS and the large gap voltages of HTS compared to that of a conventional superconductor (Hasegawa *et al.*, 1992a). Usually, the broadening of tunneling characteristics of HTS are fit to the smeared BCS density of states, first proposed by Dynes *et al.* (1978) in which

$$N_T(E) = \mathrm{Re}\frac{E - i\Gamma}{\sqrt{(E - i\Gamma)^2 - \Delta^2(E)}} \qquad (5.1)$$

Compared to the BCS DOS in Eq. (3.6), the addition of a smearing parameter Γ accounts for lifetime effects, such as inelastic scattering. It should be emphasized that the choice of Eq. (5.1) to account for broadening is mainly one of convenience and while the value of Γ

may not have any intrinsic, physical meaning for HTS, it nevertheless is a useful way to compare materials and junctions. From Eq. 3.1, the normalized conductance is then given by (Wolf, 1985)

$$\sigma_s / \sigma_n = \frac{d}{dV} \int_{-\infty}^{\infty} \frac{N_1(E)}{N_1(0)} \frac{N_2(E+eV)}{N_2(0)} [f(E) - f(E+eV)] dE \qquad (5.2)$$

where $N_1(E)$ and $N_2(E)$ are the quasiparticle DOS for the two electrodes and f(E) is the Fermi function which accounts for thermal smearing.

In this modeling study, the literature values for Nb DOS were used for one electrode since Nb tips were used in the tunneling study of $HgBa_2CuO_{4+x}$ and the infinite-layer compound $Sr_{1-x}Nd_xCuO_2$. The Nb gap is assumed to be the bulk value, Δ = 1.5 meV. Since Γ/Δ = 1% is found for conventional, strong-coupled superconductors $Pb_{0.9}Bi_{0.1}$ at 3.5 K (Dynes *et al.*, 1978) and the measurement temperature of 4.2 K for Nb with T_c = 9.2 K is equivalent to a temperature of 3.5 K for $Pb_{0.9}Bi_{0.1}$ with T_c = 7.65 K (Dynes and Rowell, 1975), a small value of Γ/Δ = 1% is assumed to account for weak quasiparticle damping that occurs at finite temperatures for Nb. This is possibly a gap smearing instead of lifetime effects in Nb. A gap value of Δ = 16 meV is assumed for the HTS electrode, since this is a typical gap value for the best Hg-1201 junctions (Chen *et al.*, 1995). Modeling studies were carried out using Eq. (5.2) for different smearing parameters Γ of the HTS materials and thermal smearing is included. The temperature is set at the liquid helium temperature T = 4.2 K

because most of the data presented in this chapter were taken at this temperature.

The results are shown in Figs. 5.1-5.3 with only the Γ values indicated in terms of Γ/Δ for the HTS electrode. In Fig. 5.1 with Γ/Δ = 0.1%, gap difference peaks are clear as expected and there exists a extremely weak Nb gap feature as shown in the inset. In Fig. 5.2 with Γ/Δ = 1%, gap difference peaks are much more smeared out and the Nb feature becomes visible without expanding the vertical scale. But these are not realistic situations because the smearing is much higher for HTS, usually the zero-bias conductance N(E=0) is larger than 15%, and the lowest value is $\approx$ 5% as found in Hg-1201 (Chen *et al.*, 1995). It should be pointed out that N(E=0) $\approx \Gamma/\Delta$ when $\Gamma/\Delta << 1$ and increases with Γ/Δ monotonically. So modeling studies were carried out for Γ/Δ = 5%, 10% and 50% (see Fig. 5.3). The large Γ value and the large gap voltages compared to the Nb energy gap result in a missing gap difference $(\Delta_2 - \Delta_1)$ feature in these cases. The difference feature lies on the sharply rising part of the conductance and can be easily washed out by smearing of any kind. A weak feature near the Nb gap is developed and it becomes more obvious as Γ/Δ increases. This Nb feature arises from the finite DOS at E = 0 in Eq. (5.1) when $\Gamma > 0$.

Two important points emerge from this modeling study. The first is that the gap difference feature at $(\Delta_2 - \Delta_1)$ is very sensitive to broadening of the HTS DOS. Values of Γ/Δ for HTS which appear in the literature are typically $\geq$ 15% (Hasegawa *et al.*, 1992a). Thus,

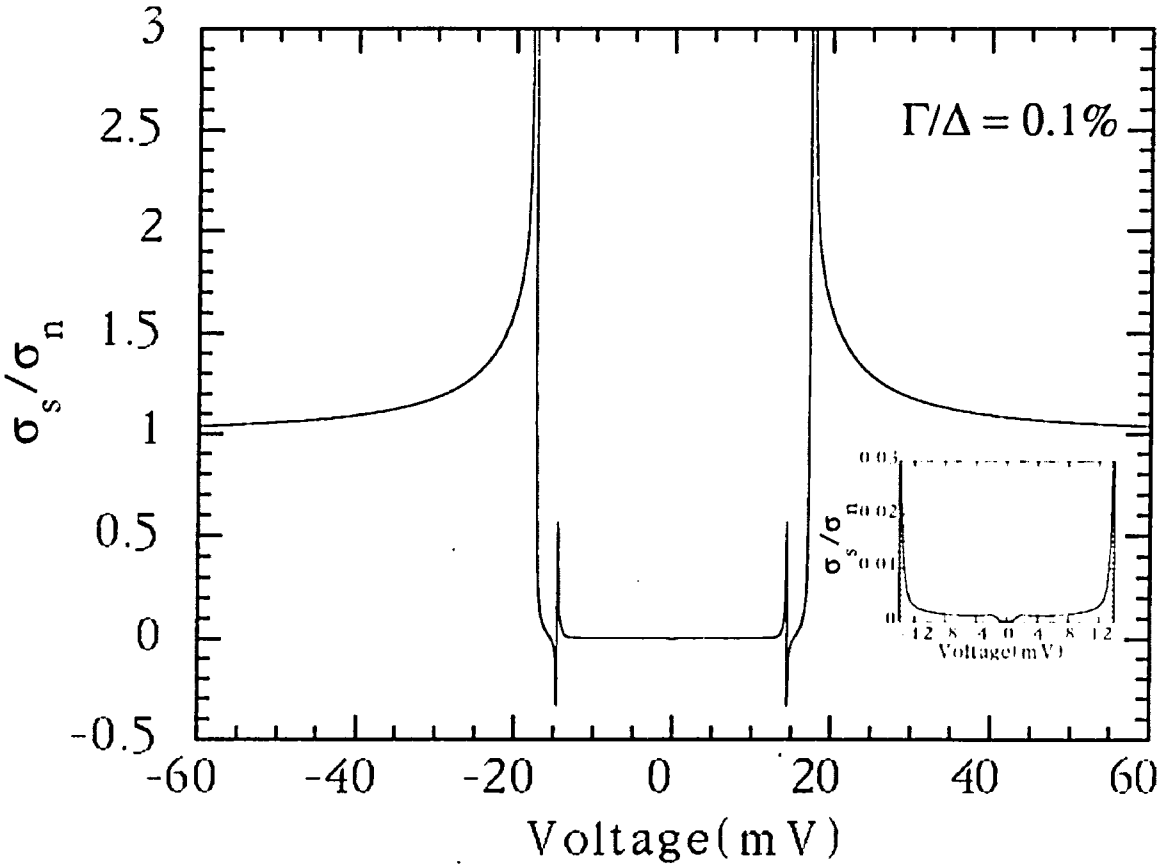

Fig. 5.1. Normalized conductances calculated from Eqs. (5.1) and (5.2) for a tunnel junction between a HTS (Δ = 16 meV, Γ/Δ = 0.1%) and a Nb counterelectrode (Δ_{Nb} = 1.5 meV, Γ_{Nb}/Δ_{Nb} = 1%). The inset shows the expanded gap region data displaying a weak feature at the Nb gap voltage.

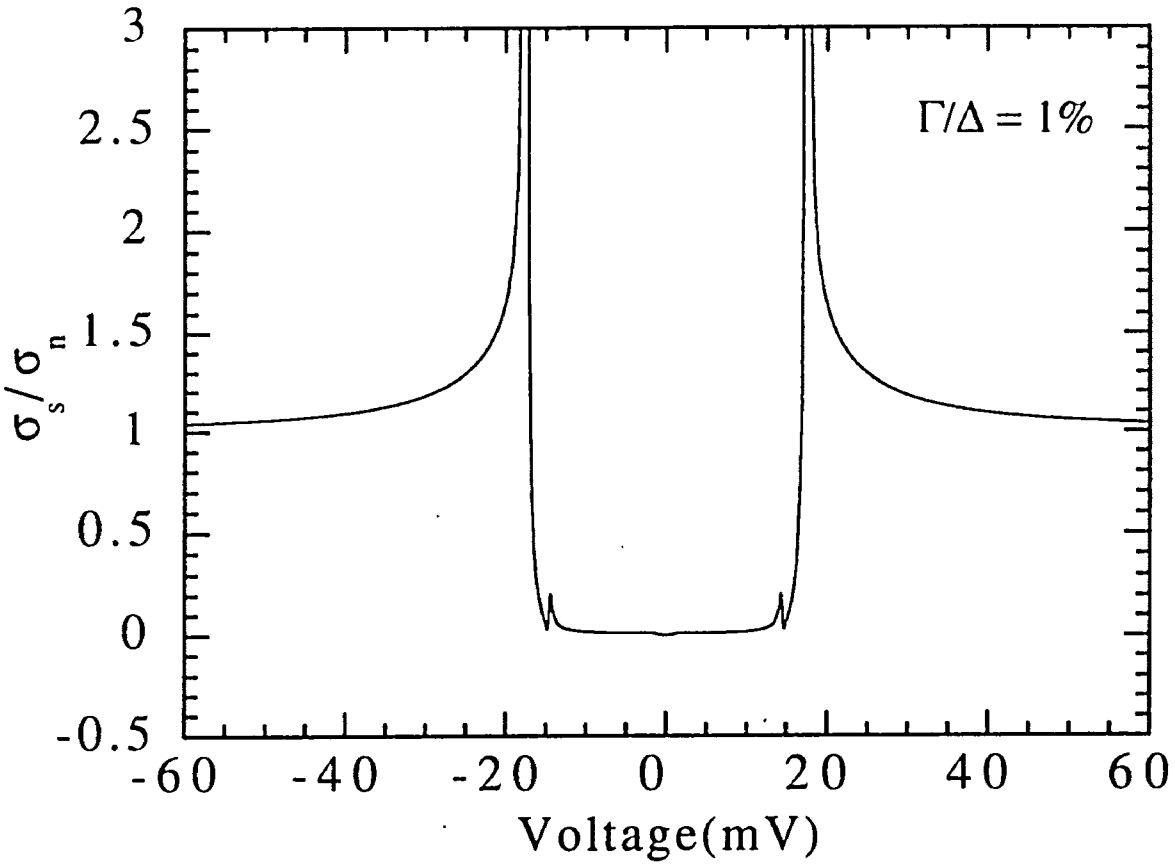

Fig. 5.2. Normalized conductances calculated from Eqs. (5.1) and (5.2) for a tunnel junction between a HTS (Δ = 16 meV, Γ/Δ = 1%) and a Nb counterelectrode (Δ_{Nb} = 1.5 meV, Γ_{Nb}/Δ_{Nb} = 1%).

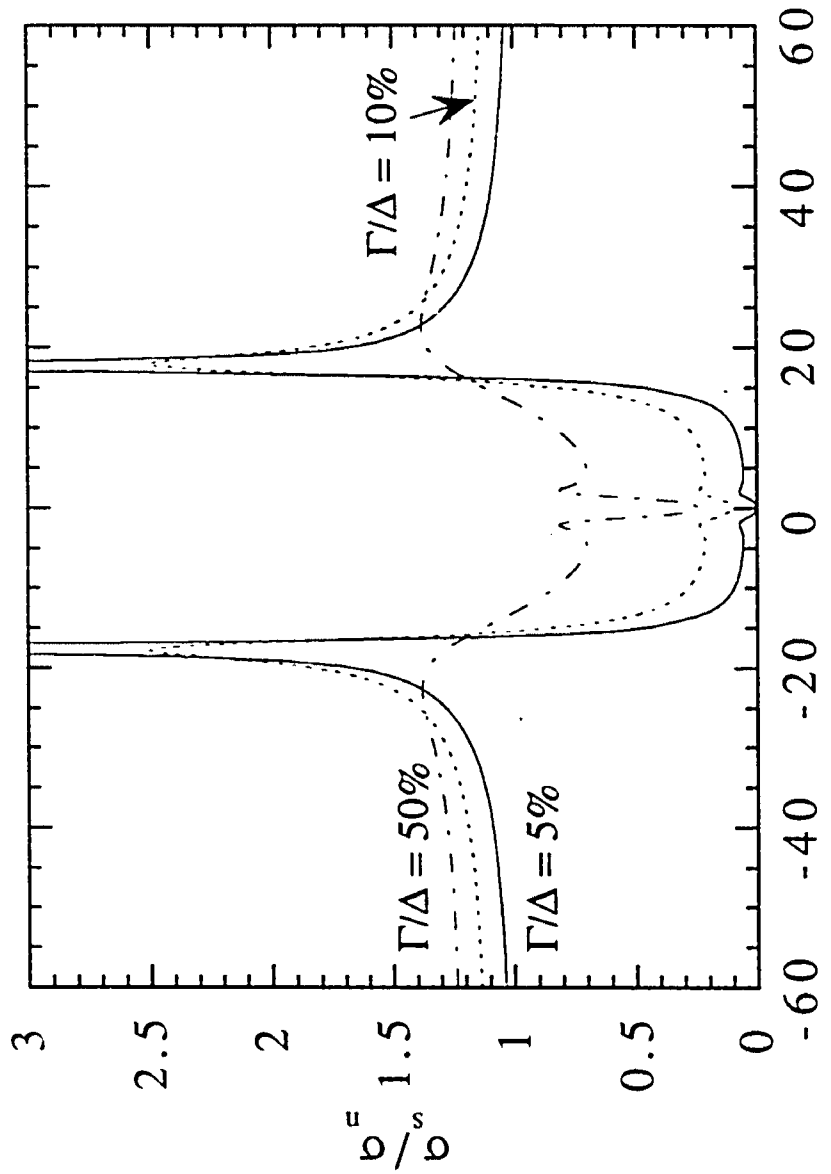

Fig. 5.3. Same as Fig. 5.2 but with Γ/Δ = 5, 10, 50%. Note that curves are shifted vertically by 0.1 for clarity.

the gap difference feature would easily be smear out completely. It might be conjectured that broadening of any type, e.g. from gap anisotropy, gap averaging, proximity effects, etc., would wash out this feature as well. However, we have not investigated the effects of other types of smearing in the gap difference feature. The second point is that if indeed the broadening found in SIN junctions is due to broadening of the HTS DOS as described by Γ, then this should result in an easily observable feature at the Nb gap voltage in SIS' junctions. For example, such a feature at Pb gap voltages is observed in $YBa_2Cu_3O_7$/Pb junctions (Sun *et al.*, 1994) and is consistent with states inside the gap.

In the following sections, experimental results will be presented and compared to fits using Eq. (5.2). This procedure provides values of Δ and Γ for the HTS materials and gives insight into the origin of the broadening.

5.2. Point-Contact Tunneling Study of $HgBa_2CuO_{4+x}$ by SIN Junctions

5.2.1. Introduction

In this section, the point-contact tunneling results on recently discovered $HgBa_2CuO_{4+x}$ (Hg-1201) compound (Putilin *et al.*, 1993) are reported using a Au tip. The two polycrystalline samples (Wagner *et al.*, 1993) have T_c (onsets) of 97 K and 95 K. In comparison with previous tunneling into HTS cuprates (Hasegawa *et al.*, 1992a), the conductances are unusually symmetrical, display well-defined peaks and have *lower* and *flatter* subgap ($V < \Delta/e$)

values. The zero-bias conductance is typically 6 - 8% of the normal-state and can be reproducibly obtained.

The above T_c is unusually high for a compound with only one CuO_2 layer per unit cell. The simple crystal structure of $HgBa_2CuO_{4+x}$ (see Fig. 5.4) consists of single CuO_2 layers separated by BaO-Hg-BaO insulating regions: the distance between CuO_2 layers (Putilin *et al.*, 1993; Wagner *et al.*, 1993) is only 9.5 Å. Such a small spacing between CuO_2 layers may lead to better intrinsic superconducting properties in a magnetic field (Welp *et al.*, 1993; Umezawa *et al.*, 1993; Kim *et al.*, 1991). This compound is the first member of the homologous series $HgBa_2R_{n-1}Cu_nO_{2(n+1)+x}$, similar to the single-thallium-layer series $TlBa_2Ca_{n-1}Cu_nO_{2n+3}$. The Hg-1223 phase was first synthesized as a multiphase component with T_c above 130 K (Schilling *et al.*, 1993; Gao *et al.*, 1993) and subsequently as a single phase with a record high T_c of 135 K (Huang *et al.*, 1993). Further enhancements of T_c up to 150 K are reported (Chu *et al.*, 1993) in an applied pressure of 150 kbar.

5.2.2. Experimental

Samples of Hg-1201, obtained from J. L. Wagner and D. G. Hinks at Argonne National Laboratory, were synthesized from stoichiometric mixtures of HgO and Ba_2CuO_3 (Wagner *et al.*, 1993), and then annealed at 300 °C in oxygen. X-ray diffraction studies confirmed all samples to be single-phase without any detectable impurities. AC susceptibility was measured in a 1 G, 100 Hz field using a Lake Shore Cryotronic susceptometer. Curve A in Fig. 5.5

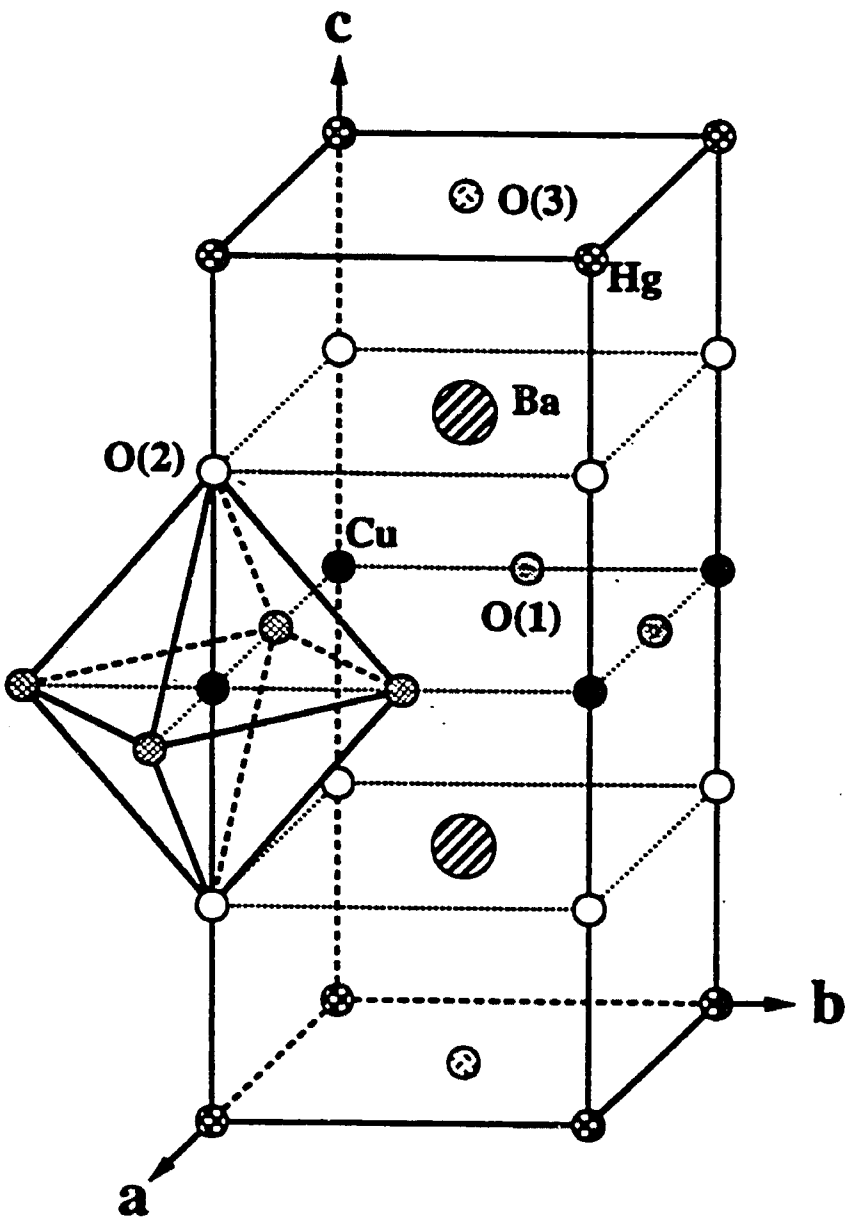

Fig. 5.4. Schematic representation of the unit cell $HgBa_2CuO_{4+x}$. The positions indicated as O(3) in the figure are partially occupied, about 6% full and 94% empty (From Chmaissem et al., 1993).

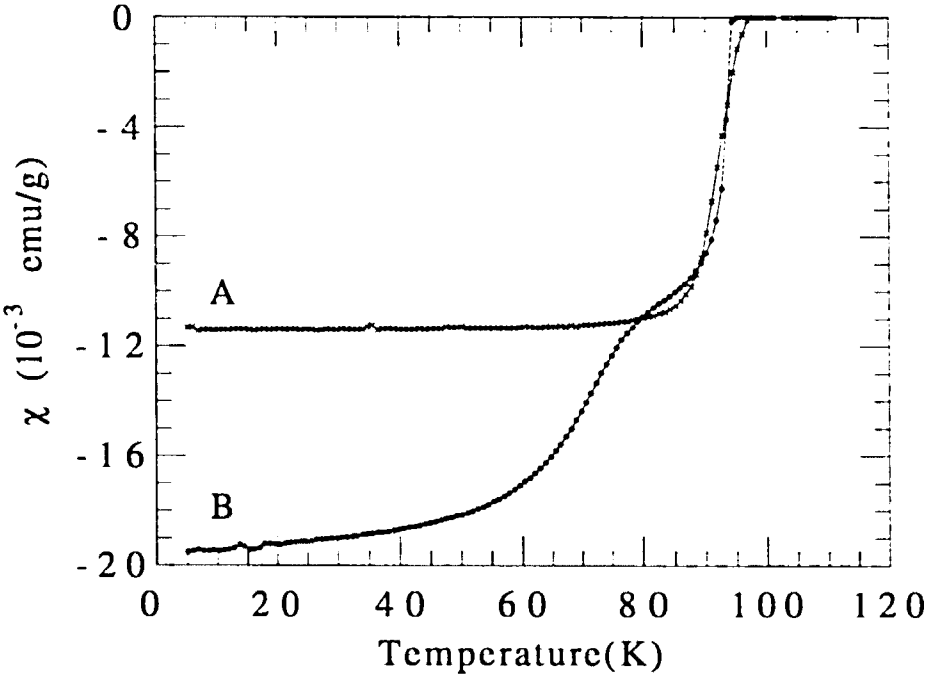

Fig. 5.5. AC susceptibilities for two samples of $HgBa_2CuO_{4+x}$ with T_c(onset) = 97 K and 95 K. Curve A (corresponds to tunneling sample A) is for a bulk sample, which was powdered before susceptibility measurements. Curve B corresponds to the bulk tunneling sample B.

shows the susceptibility of a bulk sample (tunneling sample A) which was powdered before susceptibility measurements. It exhibits a sharp transition with an onset T_c of 97 K and a full shielding fraction, consistent with the isolated grains of the polycrystalline material being uniform and fully superconducting. Susceptibility data (Fig. 5.5, curve B) on the bulk tunneling sample B (i.e., not ground into a powder before measuring), exhibits two transitions typical of that found in polycrystalline materials with weak coupling between grains (Paranthaman *et al.*, 1993). It is suggested that the first transition reflects the intragranular superconductivity of the decoupled grains in the polycrystalline sample, followed by a broader transition resulting from the intergranular coupling across the sample.

All low-temperature measurements were done with the apparatus cooled by exchange gas to liquid ^{4}He. After transfering liquid ^{4}He, we waited about 5 h for thermal stability so that stable junctions could be maintained. Raising the temperature above the cryogen boiling point with a heater was possible, but resulted in much poorer stability of the tunneling contact. As in previous cases (Gray *et al.*, 1988; Hawley *et al.*, 1986 & 1987; Huang *et al.*, 1989a&b), an insulating surface prevented vacuum tunneling and the Au tunneling tip was also used to mechanically cleave and/or scrape the surfaces at low temperatures, leaving a thin barrier for elastic tunneling. The resistance of resulting junctions could be varied by adjusting the force of the tip on the sample. The current-voltage characteristic, I(V), was monitored while the tip was

maneuvered to obtain an acceptable junction. First derivative data, dI/dV, were obtained using a Kelvin bridge (Adler and Jackson, 1966) with the usual lock-in techniques.

5.2.3. Results and Discussion

Typical experimental conductances (σ_s = dI/dV) are shown in Fig. 5.6a through c. Experimentally, similar trends were observed for the two samples. The high degree of symmetry is unusual for tunneling between asymmetrical electrodes of a normal metal and a cuprate HTS, although it is almost always found for conventional superconductors. For all such stable SIN junctions, the high voltage (background) conductance usually increases with voltage (see Fig. 5.6a) as is commonly found in HTS, and can be attributed (Huang *et al.*, 1989a&b) to the ordinary parabolic tunneling conductance (Wolf, 1985). Several junctions showed a flat background conductance (see Fig. 5.6b) and one junction showed a decreasing background conductance (see Fig. 5.6c). Such a decreasing background has also been observed previously in other cuprates (Hasegawa *et al.*, 1992a). Here in all plots, positive voltage means that the Au tip is at a positive voltage relative to the Hg-1201 sample.

In order to proceed, the conductances need to be normalized (i.e., divided by the normal-state value, σ_n). Direct measurements of σ_n can be made at $T > T_c$, but for HTS this is difficult due to the different thermal expansions in the tip assembly materials. However, σ_s is expected to approximate σ_n at high voltages, so we fit the high-voltage data ($|V| > 50$ meV) to a 4th-order polynomial to

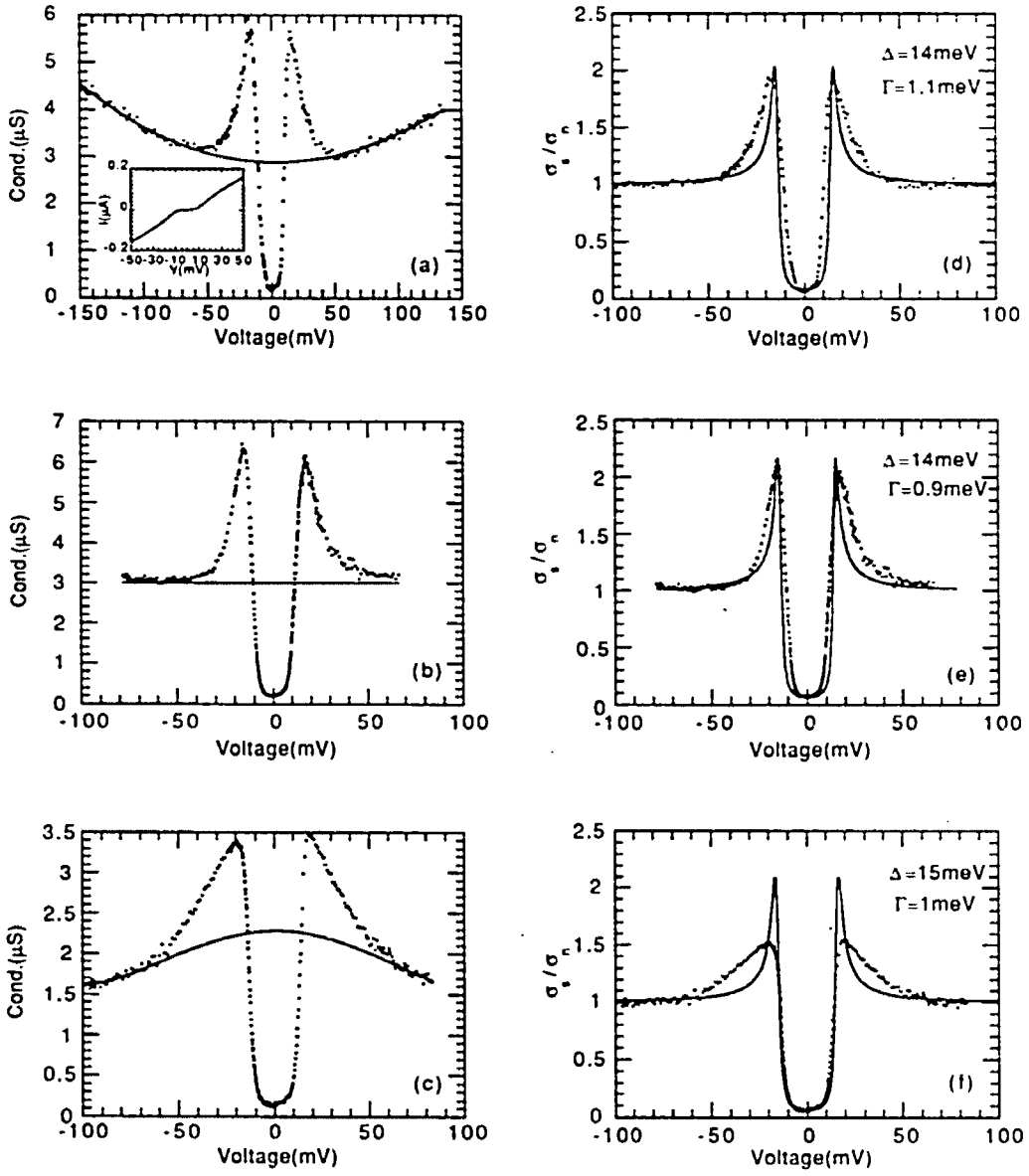

Fig. 5.6. (a through c): Experimental conductances (dots) with the fitted normal state conductances (solid lines) for junctions #1, #2 of sample B and junction #1 of sample A, respectively; (d through f): The dots are the corresponding normalized conductances, while the solid lines are the smeared BCS fits including thermal smearing. Experimental I(V) curve for junction #1 of sample B is shown in Fig. 5.6a as an inset. All tunneling curves here were measured at T = 4.2 K.

obtain an estimate of σ_n (solid lines in Fig. 5.6a through c). The tunneling data shown in Fig. 5.6b are interesting because of the very flat background and the data can be normalized by a constant (over the narrow voltage range), which ensures that no additional structure is introduced by this procedure.

When σ_s is normalized by σ_n, estimated in this way, we arrive at the normalized conductances (dots in Fig. 5.6d through f), which can be compared to theory. Usually, HTS tunneling results are compared to Eq. (5.1). The normalized conductance is then given by Eq. (5.2) and for a SIN junction this reduces to

$$\sigma_s / \sigma_n = \int_{-\infty}^{\infty} N_T(E)\left[-\frac{\partial f(E+eV)}{\partial(eV)}\right]dE \qquad (5.3)$$

The fits using Eq. 5.3, shown as solid lines in Fig. 5.6d through f, provide values of Δ and Γ. All tunneling curves here were measured at T ~ 4.2 K. Note that all subgap conductances (Fig. 5.6d through f) are very low and flat, resulting in small values of Γ. The small Γ (~ 1 meV) means that thermal smearing (k_BT = 0.36 meV) cannot be ignored in the above procedure. In previous work (Huang *et al.*, 1989a&b) on other cuprate HTS as well as other tunneling studies (Hasegawa *et al.*, 1992a), the normalized conductance was fit to Eq. 5.1 directly because Γ was much larger than k_BT.

Note that all the junctions of Fig. 5.6 are fit with Γ/Δ = 6% - 8%, making this the *lowest reproducible* value of all cuprate HTS. The subgap conductance in Fig. 5.6f is quite flat and agrees extremely well with the BCS expression (Eq. 5.3) with only small smearing. It is

thus much closer to what would be expected for s-wave superconductivity than is typically found in other cuprates (Zasadzinski *et al.*, 1992). A flat subgap conductance was also reported by Hasegawa (Hasegawa *et al.*, 1992b) using an STM on a single junction of $YBa_2Cu_3O_{7-x}$, but the preponderance of data on $YBa_2Cu_3O_{7-x}$ suggests more parabolic-like subgap conductances (Edwards *et al.*, 1992).

Figure 5.7 is an example of σ_s (measured at 4.2 K) showing well-defined conductance peaks with an energy gap, $\Delta \sim 5 - 6$ meV. The tunneling characteristics of this junction showed changes when the temperature was raised from 4.2 K to ~ 11 K using a heater. This indicates that the gap-like features are indeed due to the superconducting density of states and not a charging effect which would be less sensitive to this temperature change.

Figure 5.8 shows unpublished results for two other junctions. Normalized conductances are shown as dots, while smeared BCS fits as solid lines. Figure 5.8a is noisy but nevertheless can be fit very well with a smeared BCS expression using Eq. 5.3. Energy gap value $\Delta = 16$ meV is consistent with previous results for our best junctions. Similarly, the fit to Fig. 5.8b also provides values of Δ and Γ. Notice the gap region data is v-shaped and seems to resemble tunneling into a d-wave superconductor, in which the order parameter has nodes and a continuous subgap excitation spectrum is expected. However, this is the only junction that has v-shaped subgap conductances.

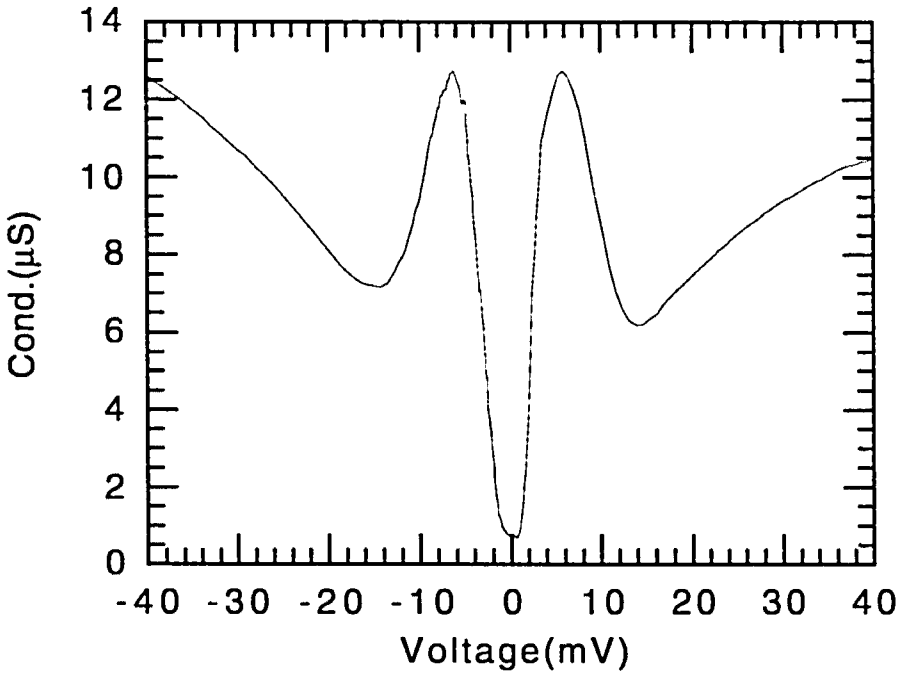

Fig. 5.7. Experimental conductances (measured at 4.2 K) of junction #3 of sample B showing a smaller gap value.

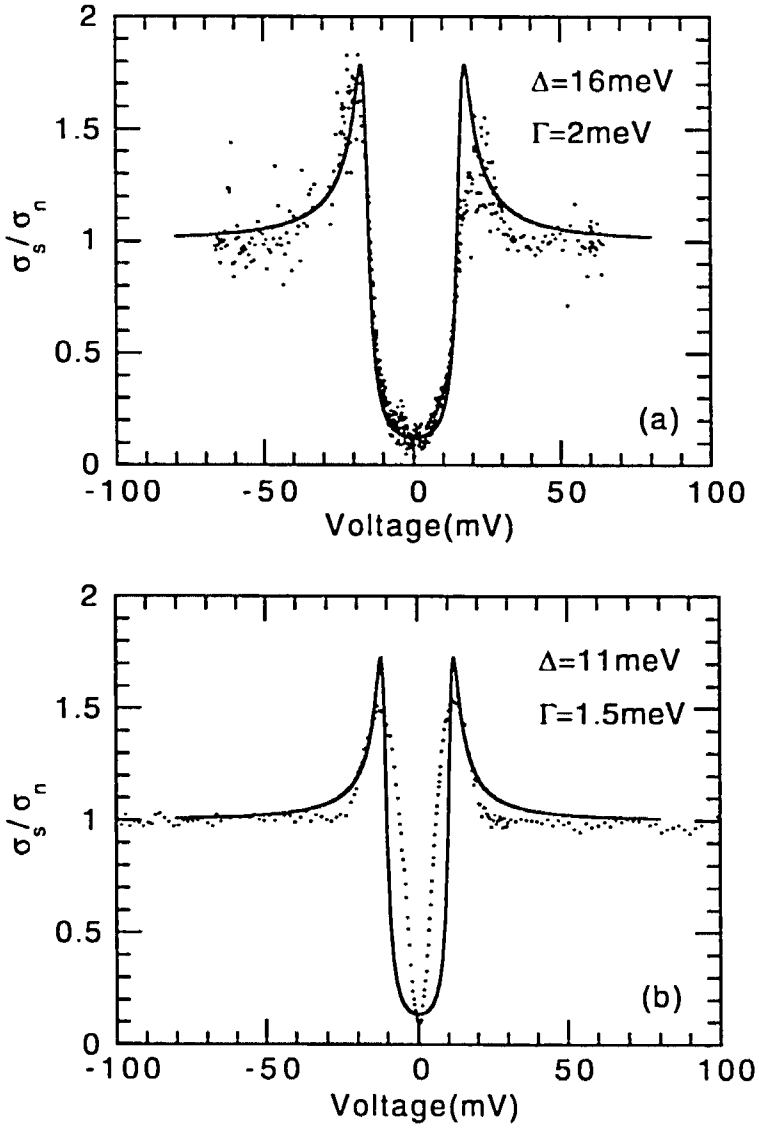

Fig. 5.8. The dots are normalized conductances for junctions #4 and #5 of sample B, shown in (a) and (b) respectively. The solid lines are the smeared BCS fits including thermal smearing. Measurements were taken at T = 4.2 K.

The energy gaps, Δ, determined according to the above procedure for 24 junctions range from ~ 5 meV to 20 meV. The origin of the spread in Δ is unknown. It could be due to an anisotropic gap, like in the conventional anisotropic layered superconductor $NbSe_2$ where the anisotropic gap is due to the sum on states k over an anisotropic Fermi surface. Extensive upper critical field studies (Prober *et al.*, 1977; Dalrymple and Prober, 1984) and scanning tunneling microscopy study of flux lattice structures (Hess *et al.*, 1992) of $NbSe_2$ have greatly enhanced our understanding of the anisotropic nature of this layered superconductor. Similar studies on Hg-1201 would shed light on the gap anisotropy issue. The variation of Hg-1201 gap values could also be an indication that there is a considerable variation in T_c, which possibly results from variations in oxygen content of $HgBa_2CuO_{4+x}$ near the sample surface. It is known (Wagner *et al.*, 1993) that T_c can be increased up to 97 K for x ~ 0.06 on annealing in oxygen at 300°C for 24 h. On annealing in argon at 500°C for 24 h, the T_c drops to 59 K for x ~ 0.01. Further reduction decreases the T_c to ~ 44 K, after which the compound decomposes. Also the Hg-1201 samples are found to be electromagnetically granular (Umezawa *et al.*, 1993). Thus, it is quite possible that we are probing local properties of individual grains with different x values and hence different T_c. Therefore it is suspected that the small gaps (~ 5 - 6 meV) observed in some cases are associated with this minimum value of T_c that can be obtained before decomposition. Although surface deterioration upon exposure to moisture causes no observed change in the bulk T_c (with only

minor changes in X-ray pattern) (Paranthaman *et al.*, unpublished), it may reduce the T_c of some grains on the surface which are probed by the tunneling tip.

Broadened conductance peaks (e.g., see Fig. 5.6c) suggest a distribution of gap values, and our fitted value of Δ is within this distribution. It is difficult to obtain an accurate value of $2\Delta/k_BT_c$ due to the spread of the energy gaps and the imprecisely known T_c associated with each junction. Using Δ for our best junctions (~ 15 meV) together with the onset T_c of 97 K, implies a lower limit of $2\Delta/k_BT_c$ ~ 3.6. This is significantly lower than the usual tunneling results for HTS cuprates, but is certainly consistent with the BCS value. An upper bound estimate would be to use the largest Δ value of 20 meV, leading to $2\Delta/k_BT_c$ = 4.5 consistent with the value found in strong-coupled conventional superconductors.

In summary, the SIN tunneling data of polycrystalline Hg-1201 are quite symmetrical and follow the general trend of the best curves seen in cuprate HTS, but with the *lowest* and *flattest* subgap conductances compared to other cuprates, and both features are obtained reproducibly. Energy gaps, Δ, are determined using a smeared BCS expression *including* thermal smearing.

5.3. SIS' Junctions and Device Potential

In order to check consistency and gain insights into the device potential, the point-contact tunneling was carried out on polycrystalline Hg-1201 superconductors using a superconducting Nb counterelectrode. These SIS' tunnel junctions are of unusually high

quality for cuprate superconductors, exhibiting low and flat subgap conductances and sharp conductance peaks as expected from a BCS-like density of states. These features are obtained reproducibly and are consistent with earlier SIN results using a Au counterelectrode. Use of experimental data to simulate the performance of a quasiparticle mixer indicates that Hg-1201 may be suitable for use in low noise heterodyne receivers operating at a few THz.

5.3.1. Introduction

Low subgap conductance and sharp gap-edge structure are required for SIS and SIN tunnel junction devices such as mixers (Hu and Richards, 1990). Such tunneling characteristics result from the BCS quasiparticle density of states found in conventional superconductors. The tunneling characteristics of high T_c cuprates have in general been non-ideal (Hasegawa *et al.*, 1992a), displaying strong subgap conductances which monotonically increase about the minimum value at zero-bias. In general, mechanical point-contact junctions display the optimum characteristics that can be obtained on HTS with a native surface tunnel barrier (Zasadzinski *et al.*, 1992). In this section, the point-contact tunneling results on two polycrystalline $HgBa_2CuO_{4+x}$ (Hg-1201) samples with a T_c onset of 97 K are reported using a superconducting Nb counterelectrode. These SIS' tunneling junctions exhibit the low, flat subgap conductances and sharp conductance peaks as expected from a BCS density of states. These features are obtained reproducibly and are consistent with earlier results with SIN junctions (Chen *et al.*, 1994).

The data were fit by introducing a small smearing parameter Γ into the BCS expression. The ratio Γ/Δ was typically 5 - 7%, making this the lowest reproducible value found on any HTS cuprate. Typical gap parameter values were Δ = 13-16 meV but one junction had Δ = 24 meV. Experimental data along with the Tucker theory (Tucker and Feldman, 1985) of quantum mixing were used to simulate the performance of a heterodyne photon detector (Kouznetsov *et al.*, 1994). It is demonstrated that noise temperature approaching the quantum limit are possible for SIS and SIN quasiparticle mixers in the range of 1-4 THz. Thus, Hg-1201 may be suitable for use in low noise heterodyne receivers operating at a few THz.

5.3.2. Results and Discussion

The experimental procedures are described in section 5.2.2; a Nb tip is used instead of a Au tip. Typical experimental conductances (σ_S = dI/dV) obtained on two Hg-1201 samples are shown in Fig. 5.9(a)-(c). For all such stable junctions, the high voltage (background) conductance usually increases with voltage and can be attributed to ordinary tunnel barrier transmission (Wolf, 1985). Compared to the point-contact tunneling in HTS single crystals (Hasegawa *et al.*, 1992a), the Hg-1201 data exhibit larger noise levels at above-gap voltages. This may be due to the weakly coupled grains (Paranthaman *et al.*, unpublished) of the polycrystalline samples which would have microshorts or Josephson contacts with low critical currents. Here in all plots, positive voltage means that the Nb tip is at a positive voltage relative to the Hg-1201 sample.

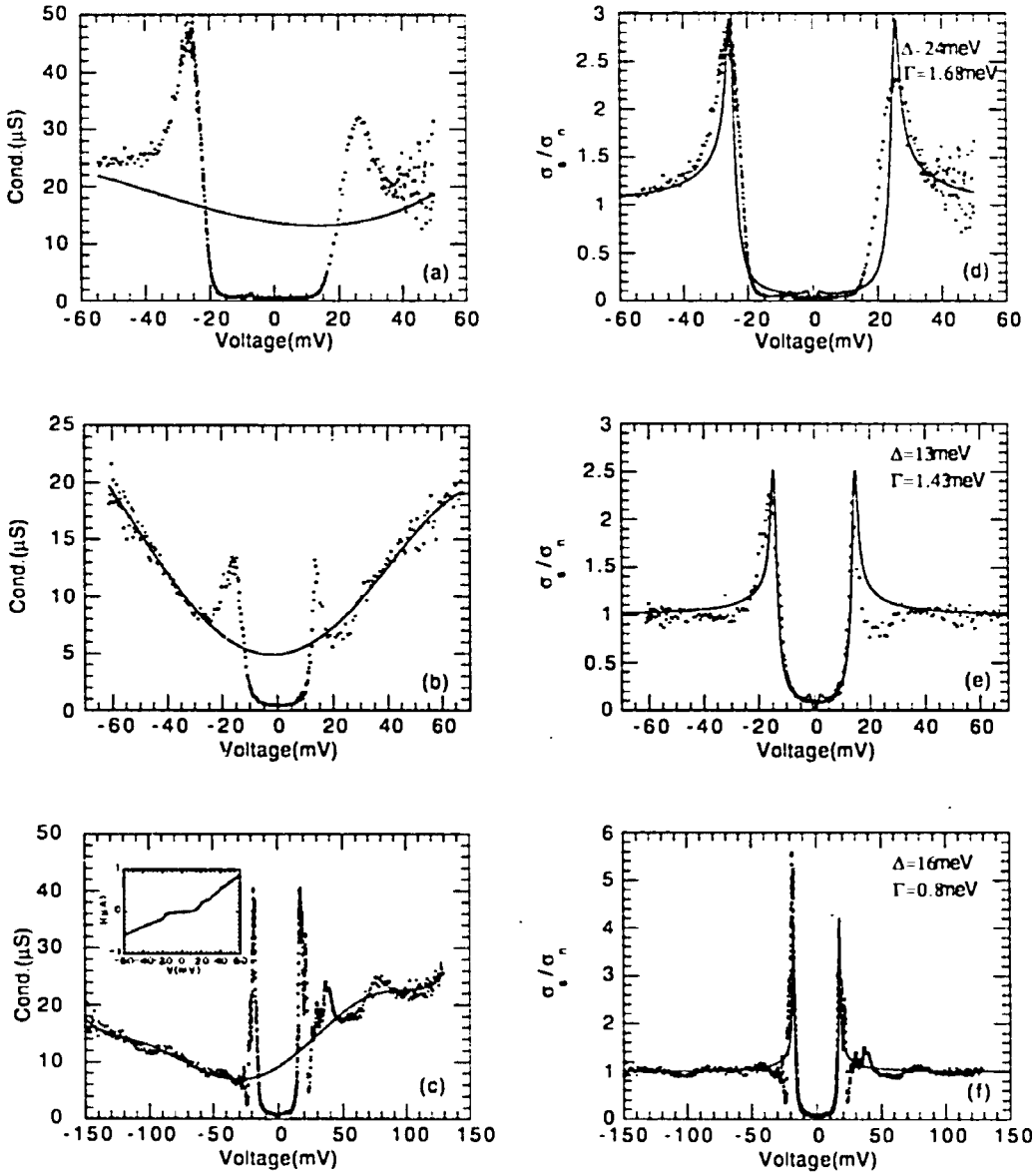

Fig. 5.9. (a through c): Experimental conductances (dots) with the fitted normal state conductances (solid lines) for junctions #1, #2 of sample C and junction #1 of sample D, respectively; (d through f): The dots are the corresponding normalized conductances, while the solid lines are the smeared BCS fits including thermal smearing. Experimental I(V) curve for junction #1 of sample D is shown in Fig. 5.9c as an inset. All tunneling curves here were measured at T = 4.2 K.

Using the same normalization procedure as in Section 5.2.3, we use the high-voltage data to generate a 4th-order polynomial as an estimate of σ_n [solid lines in Fig. 5.9(a)-(c)]. The smooth curve of σ_n ensures that no additional structure is introduced by this procedure. When σ_s is normalized by σ_n, estimated in this way, we arrive at the normalized conductances [dots in Figs. 5.9(d)-(f)], which can be compared to theory. Usually, HTS tunneling results are compared to the smeared BCS density of states, as in Eq. (5.1). The normalized conductance is then given by Eq. (5.2).

The Nb gap is assumed to be the bulk value, Δ = 1.5 meV and a small value of Γ/Δ = 1% is assumed to account for weak quasiparticle damping that occurs at finite temperatures in conventional, strong-coupled superconductors (Dynes *et al.*, 1978). The fits using Eq. (5.2), shown as solid lines in Fig. 5.9(d)-(f), provide values of Δ and Γ for Hg-1201. All tunneling curves here were measured at T ~ 4.2 K. There is good agreement with the weakly-smeared BCS model, especially in the magnitude of the conductance peaks and the subgap conductance values. Subgap conductances in Fig. 5.9(d) and (f) are very low and flat, resulting in ratios Γ/Δ = 5%-7%, consistent with those found for the SIN junctions. These are the lowest reproducible values found on any cuprate.

The non-zero Γ values and the large gap voltages (13-24 meV) of Hg-1201 compared to the Nb energy gap result in a missing gap difference ($\Delta_2 - \Delta_1$) feature. Our fitting of the data indicated that the difference feature lies on the sharply rising part of the conductance and can be easily washed out by smearing of any kind. This is also

demonstrated by the SIS' modeling study shown in Fig. 5.3. The junction shown in Fig. 5.9(f) is particularly noteworthy as it displays the highest conductance peaks ever observed for a HTS. It is fit with Δ = 16 meV and Γ = 0.8 meV. The ratio Γ/Δ = 5% is slightly improved over values obtained from SIN data (Chen *et al.*, 1994) on Hg-1201. The dip in conductance just above the peak [see Fig. 5.9(f)] is evidence of a proximity effect, as is often found (Huang *et al.*, 1990) in junctions using natural oxides of Nb.

Typical energy gaps were Δ = 13-16 meV, in excellent agreement with previous SIN results (Chen *et al.*, 1994), but one junction had Δ = 24 meV. The origin of the spread in Δ is unknown. It could be due to an anisotropic gap as discussed earlier in section 5.2.3. Or it could be an indication that there is a variation in T_c along the surface of the sample which possibly results from variations in oxygen content of $HgBa_2CuO_{4+x}$. Scanning electron microscopy in Fig. 5.10 showed that grain sizes of Hg-1201 surface can be as large as ~ 20 μm, while the radius of the Nb tip is below 1 μm. Thus, it is quite possible that we are probing local properties of individual grains with different x values and hence different T_c.

A final point to be made is that the fit curves of Fig. 5.9(d)-(f) display a weak feature near the Nb gap which arises from the finite density of states at E = 0 in Eq. (5.1) when $\Gamma > 0$. The fact that the experimental data display a much weaker Nb gap structure (if any) and lower conductance values suggests that Eq. (5.1) may not be the correct way to account for the weak broadening observed in the tunneling data. The subgap conductance indicates that Γ is closer to

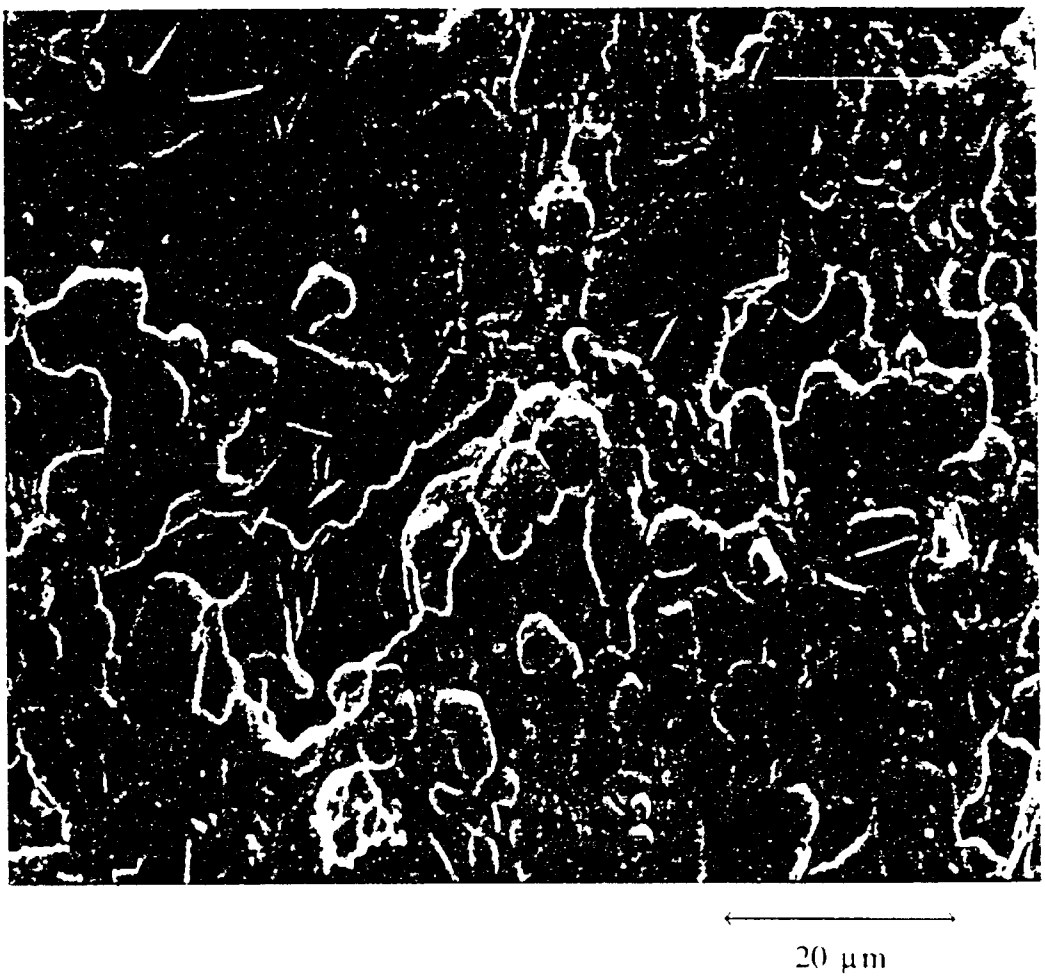

Fig. 5.10. Scanning electron microscope (SEM) picture of $HgBa_2CuO_{4+x}$ surface. Note that the grain size can be as large as 20 μm.

zero, whereas the conductance peaks are broader than the fit. These two facts suggest that the true origin of broadening may be that a small distribution of gap values is being probed, i.e., due to spatial distribution. We have not pursued this approach for data analysis as it would not change the basic conclusion which is that the tunneling data are approximately BCS-like.

The low subgap conductances and sharp conductance peaks indicate that Hg-1201 has potential as a sensitive photon detector. A typical current-voltage characteristic I(V) was shown in Figs. 5.6a and 5.9c for SIN and SIS' junctions, respectively. The large energy gaps are ideal for exploring the THz frequency regime. It should also be noted that since $k_B T << \Delta$ even at 12 K, thermal smearing of junction characteristics is small and operating at a temperature accessible with close-cycle refrigeration can be expected. To test these ideas, experimental data along with the Tucker theory (Tucker and Feldman, 1985) of quantum mixing were used (Kouznetsov *et al.*, 1994) to simulate the performance of a heterodyne receiver based on Hg-1201. This modeling study was carried out by Kouznetsov and Coffey at Illinois Institute of Technology. The fully general, three-port Tucker model, both single and double side band regimes (SSB and DSB), was combined with a numerical optimization routine to predict the gain and noise of the HTS mixer. At a given mixer operating temperature (T_{OP}), this model allows us to find the values of source, image and load impedances, bias voltage, operating frequency (f) and local oscillator voltage (V_{LO}) that either maximize the conversion efficiency (1/L) or minimize the mixer noise

temperature (T_M). Details of the modelling study are given by Kouznetsov et al (1994). In the case of T_{OP} = 4.2 K, experimentally determined values Δ = 20 meV and Γ = 0.07 Δ were used. At higher temperatures (T_{OP} > 4.2 K), Δ and Γ values were appropriately adjusted (Kouznetsov *et al.*, 1994). It is demonstrated that minimum SSB values of mixer noise temperatures may approach the quantum limit for SIS and SIN quasiparticle mixers in the range of 1-4 THz.

In summary, the SIS' tunneling data of Hg-1201 show the lowest and flattest subgap conductances and highest conductance peaks of all cuprates. Energy gap parameters are determined and consistent with earlier published SIN data. Modeling studies (Kouznetsov *et al.*, 1994) indicate that mixer noise temperatures approaching the quantum limit are possible for SIS and SIN quasiparticle mixers based on Hg-1201 in the THz regime.

CHAPTER VI

TUNNELING STUDY OF THE INFINITE LAYER COMPOUND $Sr_{1-x}Nd_xCuO_2$

In this chapter, we report on point-contact tunneling into the infinite-layer compound $Sr_{1-x}Nd_xCuO_2$ (SNCO) with a T_c of 35 K, using both Au and Nb tips. Comparisons are made to other electron-doped cuprate superconductors.

6.1. Introduction

The infinite-layer compound is of particular interest because of its simplest structure among cuprates. Unlike other cuprates which have non-superconducting oxide layers between superconducting layers of CuO_2, the infinite-layer compound consists of CuO_2 planes separated only by alkaline earth elements (Fig. 6.1). The 'infinite-layer' parent compound of the copper oxide superconductors, $Ca_{1-x}Sr_xCuO_2$, was first reported by Siegrist et al (1988). But the compound they obtained at ambient pressure, $Ca_{0.86}Sr_{0.14}CuO_2$, was non-superconducting. The isostructural compound $Sr_{1-x}Nd_xCuO_2$, in which the substitution of Nd for Sr adds electrons to the CuO_2 planes, is found to superconduct at T_c onset ~ 40 K (Smith *et al.*, 1991). Both the screening and Meissner fraction increased with decreasing amount of impurity phases. Furthermore, no superconductivity was observed down to 2 K in the undoped parent compound $SrCuO_2$ prepared under identical conditions. These observations demonstrate that the observed bulk superconductivity is due to the electron-doped SNCO and not due to any impurity phase. While the

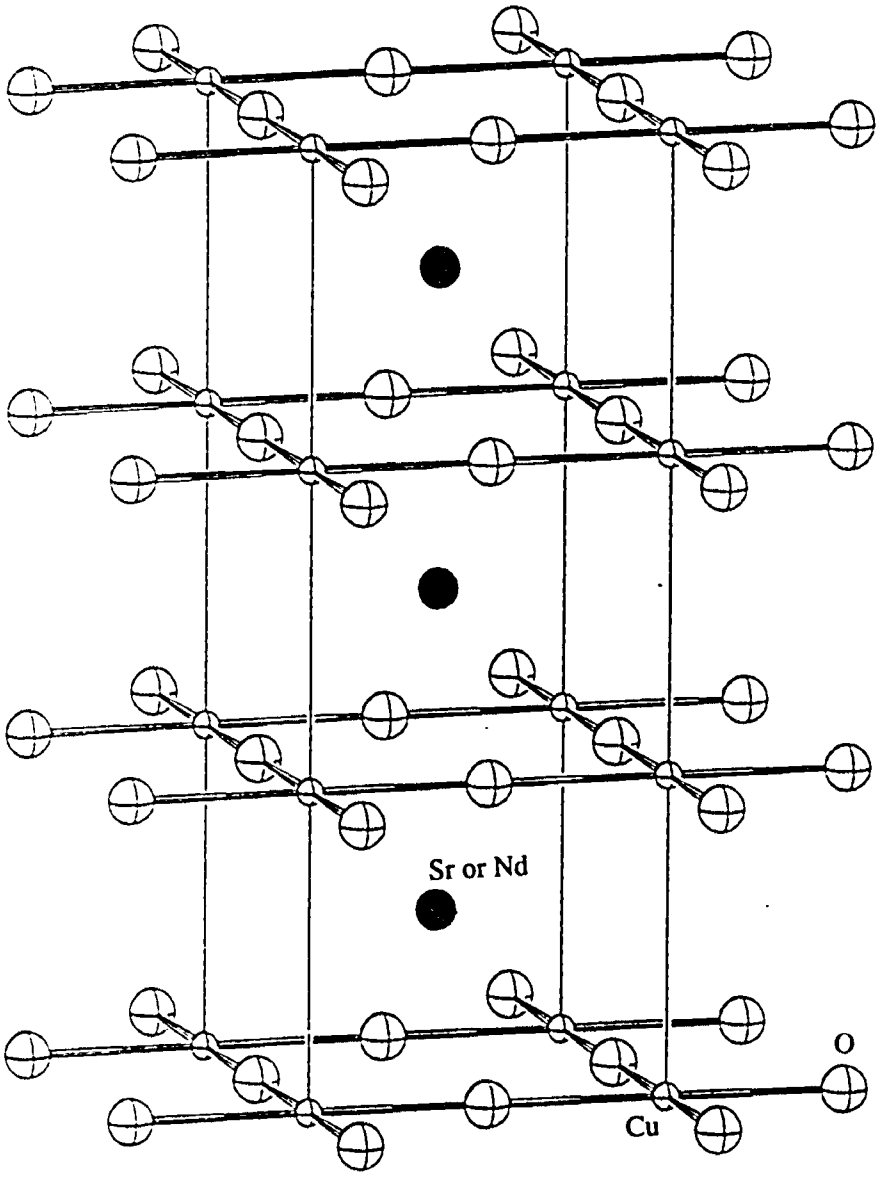

Fig. 6.1. Crystal structure of the infinite-layer compound $Sr_{1-x}Nd_xCuO_2$. The small and large circles represent the Cu and O atoms, respectively. The solid circles indicate the Sr sites with Nd doping.

lattice parameters vary with dopant concentration x, in general we have a ~ 3.9 Å and c ~ 3.4 Å (Smith *et al.*, 1991). Thus, structurally SNCO is much closer to the cubic oxide $Ba_{1-x}K_xBiO_3$ than any other cuprates. The question we addressed was whether this cuprate, which has lower structural anisotropy, would reproduce the anomalies found in other cuprates or behave like the cubic oxides such as $Ba_{1-x}K_xBiO_3$ which show ideal BCS tunneling characteristics (Huang *et al.*, 1990a).

Quasiparticle tunneling measurements are reported here for the infinite-layer, high T_c superconductor SNCO with T_c (midpoint) ~ 35 K. Both superconductor-insulator-nomal metal (SIN) and superconductor-insulator-superconductor (SIS') tunnel junctions have been fabricated using a mechanical point-contact technique with Au and Nb tips, respectively. All junctions exhibit a strong, asymmetric linear background conductance indicative of inelastic tunneling contributions from a broad continuum of states. Surprisingly, the magnitude and shape of this background conductance are very similar to that found in two other electron-doped cuprates, $Nd_{2-x}Ce_xCuO_{4-y}$ (NCCO) and $Pr_{2-x}Th_xCuO_{4-y}$ (PTCO) where comparisons are made to published data as well as new results. The energy gap of SNCO is found consistently to be 6 meV leading to $2\Delta/k_BT_c = 4.0$. The reproducibility of the measured gap values is similar to that found in the other electron-doped cuprates and is consistent with the apparent s-wave symmetry found in NCCO. The gap region tunneling data of the SNCO junctions all display subgap conductances, but there is no evidence of the Nb gap in the

SIS' junctions. According to the modeling study of SIS' junctions (see Fig. 5.3), this means that the subgap conductances can not be described by the smeared BCS expression which introduces an intrinsic gaplessness, suggesting that the subgap conductance is of extrinsic origin.

6.2. Sample Preparation and Experimental Procedure

Polycrystalline samples of $Sr_{1-x}Nd_xCuO_2$ with x = 0.12 were provided by J. T. Markert at University of Texas - Austin. Samples were prepared from copper metal, high-purity (99.99%) powders of $SrCO_3$ and Nd_2O_3 (Markert, 1994). Pre-dried powders were mixed in stoichiometric proportions and pre-calcined in air (primarily to burn off the carbonate and obtain an intimate mixture) for several days at 900 °C with several intermediate grindings. At this point, no infinite-layer phase is observed in x-rays. For the high-pressure synthesis, the powder was sealed in platinum capsules (5 mm diameter and 5 mm long, with ~ 0.005" wall thickness). The samples were reacted in a commercial tungsten carbide piston-cylinder apparatus using a graphite furnace assembly at 25 kbar and temperatures in the range 950 °C to 1080 °C, typically for 2-3 h. The best superconducting samples were obtained for reaction temperatures near 1035 °C to 1065 °C, as measured by a chromel-alumel thermocouple in contact with the sample capsule. The samples were quenched to room temperature (initial rate of ~ 200 °C/s) before releasing the pressure. Approximately 0.10 to 0.20 g of material is extracted in each run, some of which is used for characterizations.

Most such samples are characterized by x-ray diffraction and all by SQUID magnetometry. X-ray diffraction patterns for this composition display clear peaks of the $Sr_{1-x}Nd_xCuO_2$ infinite-layer phase. But some impurity phases (~ 5-10%) often occur, most notably Sr_2CuO_3. High pressure synthesis typically involves some inherent reduction of the samples; it became apparent that samples reacted for less than 2 h or at too low a temperature were probably insufficiently reduced. While those reacted for more than 3 h or at too high a temperature were excessively reduced. After much effort, the optimal phase for bulk superconductivity is believed to exist for x ~ 0.10 - 0.12. Magnetic characterization was performed with both zero-field-cooled (screening) and field-cooled (Meissner) sweeps. The onset T_c is in the range 42-43 K and T_c midpoint ~ 35 K. The superconducting fraction at 10 K from screening (Meissner) data is $-4\pi\chi$ = 0.36 (0.24).

The polycrystalline pellets are broken to expose a fresh surface which is polished with various grades of diamond paper, the final one containing 3 μm diameter grit. The samples are then blown clean with dry N_2 gas. Electrical connections to the sample are made with Ag filled conductive paint. Both SIN and SIS' tunnel junctions have been fabricated using a mechanical point-contact technique with Au and Nb tips, respectively. All low-temperature measurements were done with the apparatus cooled by exchange gas to liquid ^{4}He. We waited about 5 h after transferring liquid ^{4}He for thermal stability so that stable junctions could be maintained. Raising the temperature above 4.2 K with a heater was possible, but

resulted in much poorer stability of the tunneling contact. An insulating surface prevented vacuum tunneling and the blunt tip was used to mechanically cleave or scrape the HTS surfaces at low temperature, leaving a thin barrier for elastic tunneling. The resistance of the resulting junctions could be varied by adjusting the force of the tip on the sample. The current-voltage characteristic I(V) was monitored while the tip was maneuvered to obtain an acceptable junction. First derivative data dI/dV were obtained using a Kelvin bridge with the usual lock-in techniques.

6.3. Experimental Results

A typical I-V and dI/dV vs. V characteristic is shown in Fig. 6.2 for an SIN junction on SNCO using a Au tip. The dI/dV curve displays a well-resolved gap feature, with nearly perfectly symmetric conductance peaks, but a non-zero value of the superconducting conductance at zero-bias, $\sigma_S(0)$. Analysis of the tunneling data requires the normalized conductance obtained by dividing the superconducting data by the normal state data, σ_n. This is done either by raising the temperature above T_c or by the preferable method of applying a magnetic field which exceeds the critical field. Neither approach is possible here as the critical field is much too large for our experimental setup and raising the temperature above T_c = 35 K always changed the tunnel contact. Instead, we estimated the normal state conductance by fitting a smooth curve through the high-bias data ($|V| > 20$ mV) which should approach the normal state data. The normal state curve obtained in this way is shown as the dashed line in Fig. 6.2. The resulting

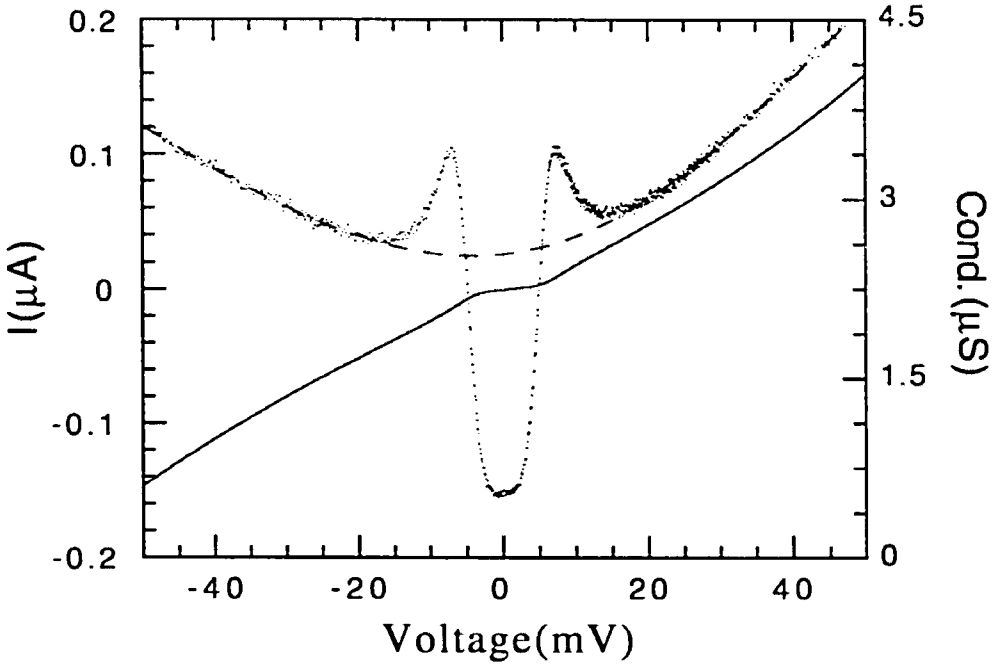

Fig. 6.2. Experimental I vs. V (solid line) and dI/dV vs. V (dots) for a typical point-contact SIN junction on $Sr_{1-x}Nd_xCuO_2$ using a Au tip. The normal state curve (dashed line) is obtained using a polynomial fit (4th order) to the high-bias data, |V| > 20 mV.

normalized conductance curve is shown as dots in Fig. 6.3. Note that the symmetric superconducting conductance peaks become slightly asymmetric after division by the asymmetric normal state curve. If the conductance data were due to purely elastic tunneling the superconducting data would display the asymmetry of the normal state background resulting in a symmetric normalized conductance. That we do not see such an effect is the first hint that another conductance channel is present. We will argue later that this channel is likely to be due to inelastic tunneling and may be responsible for the 20% value of the measured normalized conductance at zero bias $\sigma_S/\sigma_n(0)$.

In order to fit the normalized conductance data, we used a modified BCS density of states as in Eq. (5.1), first introduced by Dynes et al (1978) to account for quasiparticle lifetime effects in superconductors. It should be noted that in our case the use of the expression in Eq. (5.1) is one of convenience and the value of Γ may not have any physical significance for SNCO. The fit using Eq. (5.1) is shown as the solid line in Fig. 6.3 and leads to the parameters, Δ = 6.0 meV and Γ = 1.4 meV. Using the midpoint of the magnetic transition for T_c (35 K), we obtained $2\Delta/k_BT_c$ = 4.0, which indicates moderate coupling strength. Similar values for $2\Delta/k_BT_c$ were found on NCCO using the point-contact method (Huang *et al.*, 1990a) and penetration depth measurements (Wu *et al.*, 1993). Nearly identical gap values were found on ten different junctions made on two samples. It should be mentioned here that while our normalization procedure may be inaccurate, the magnitude of the gap was insensitive to the

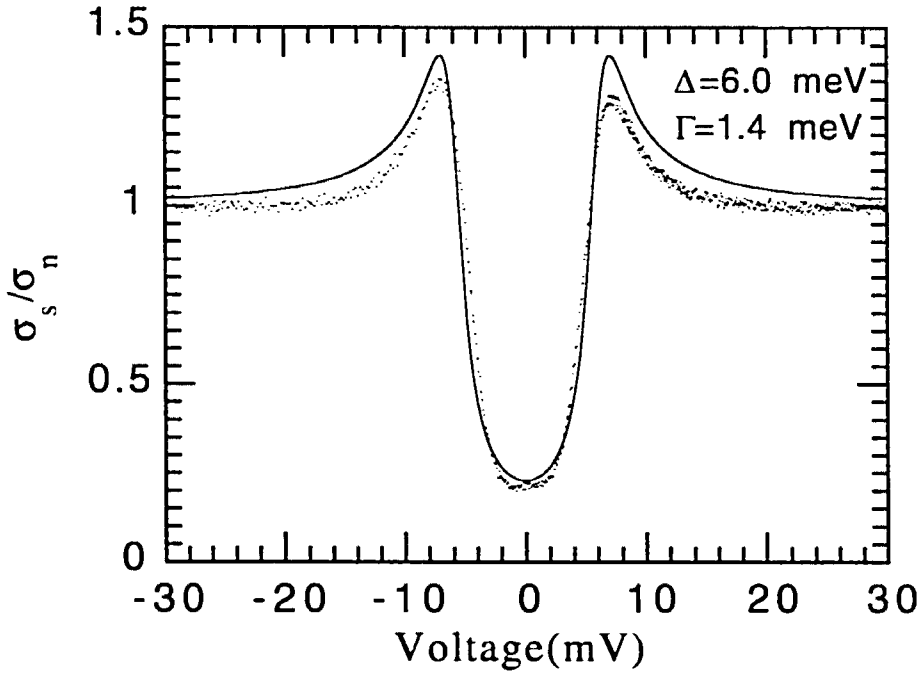

Fig. 6.3. Normalized tunneling conductance (dots), σ_S/σ_n, for the junction shown in Fig. 6.2. The fit (solid line) utilizes the smeared BCS DOS as discussed in the text with Δ and Γ values as indicated.

type of normal state curve used. For example, using a constant to normalize the data led to a poorer quality fit than shown in Fig. 6.3, but nevertheless the same gap value.

The tunneling data for the junction of Fig. 6.2 is shown out to a higher voltage range in Fig. 6.4 along with three other junctions made near the same spot on one SNCO sample. The other junctions were obtained by slightly raising the temperature to a maximum of 6 K using a thin-film strip heater and then lowering back to 4.2 K. The four junctions differ in resistance by roughly an order of magnitude, from ~ 200 kΩ to ~ 2 MΩ at 50 mV bias, indicating that the nature of the contact has changed considerably. This incredible sensitivity to temperature was not found on the point-contact tunneling studies of NCCO where a temperature rise of 20 K was possible with little change in junction resistance, allowing a measurement of the normal state σ_n (Huang *et al.*, 1990a). We do not know the origin of these large changes in SNCO, however, junction resistances on NCCO were typically in the range of a few kΩ and this might give a clue. The much higher resistances found on the SNCO samples may be due to a native surface layer that has a larger barrier height than found on NCCO. The tunneling conductance at zero-bias varies as $\exp(-cd\phi^{1/2})$ for an NIN contact where d is the barrier width, ϕ is the barrier height and c is a constant. Then the resistance ratio R'/R for two contacts with the same junction area but with different widths would be $\exp(c\phi^{1/2}(d'-d))$. Thus, the sensitivity of junction resistance to a change in barrier width, $\Delta d=d'-d$, depends exponentially on the barrier height and thus on the junction resistance itself. The higher

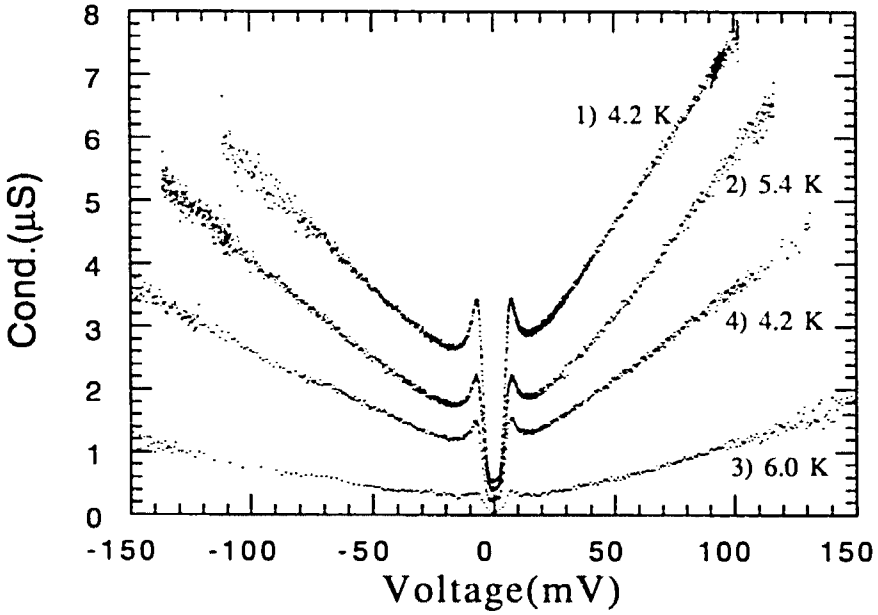

Fig. 6.4. Experimental superconducting tunneling conductances for four different junctions made on the same $Sr_{1-x}Nd_xCuO_2$ sample. Numbering of the junction sequence corresponds to raising and lowering of the temperature between 4.2 K and 6.0 K. The topmost curve is the same junction as shown in Fig. 6.2.

the resistance of a junction contact, the greater the sensitivity to a change in the barrier width. Therefore, even minor movements of the tip in a high resistance tunnel contact may lead to large changes in resistance.

The four junctions of Fig. 6.4 all show a sharp linear rise in conductance with bias voltage as has been observed in several cuprate superconductors (Hasegawa *et al.*, 1992a). Further insight can be found by normalizing all of the curves by a *constant* value given by the conductance of each junction at 6 mV bias and this is shown in Fig. 6.5a. Note that the gap region ($|V| < 20$ mV) curves of each junction lie on top of each other (Fig. 6.5b), leading to identical gap values, whereas the high-bias conductances display the same qualitative but not quantitative behavior. For positive bias voltages the junction conductances increase from ~ 1.5% per mV to ~ 2.5% per mV. These values are close to the limiting values found by Kirtley et al (1992) in Al/Al-oxide,Cr-oxide/Pb junctions where inelastic tunneling processes dominate the high-bias junction characteristics. An example of this behavior is shown in Fig. 6.6, where it should be noted that the inelastic channel (long dashed curve) becomes quite small for $|eV| < \Delta$. If we assume that the inelastic component is an additive conductance that decreases linearly with decreasing bias voltage, then the absence of any differences in the curves of Fig. 6.5b at low bias voltages, $|V| < 20$mV, is consistent with inelastic tunneling.

The general behavior of the superconducting tunneling conductances of the SNCO is surprisingly similar to that of other

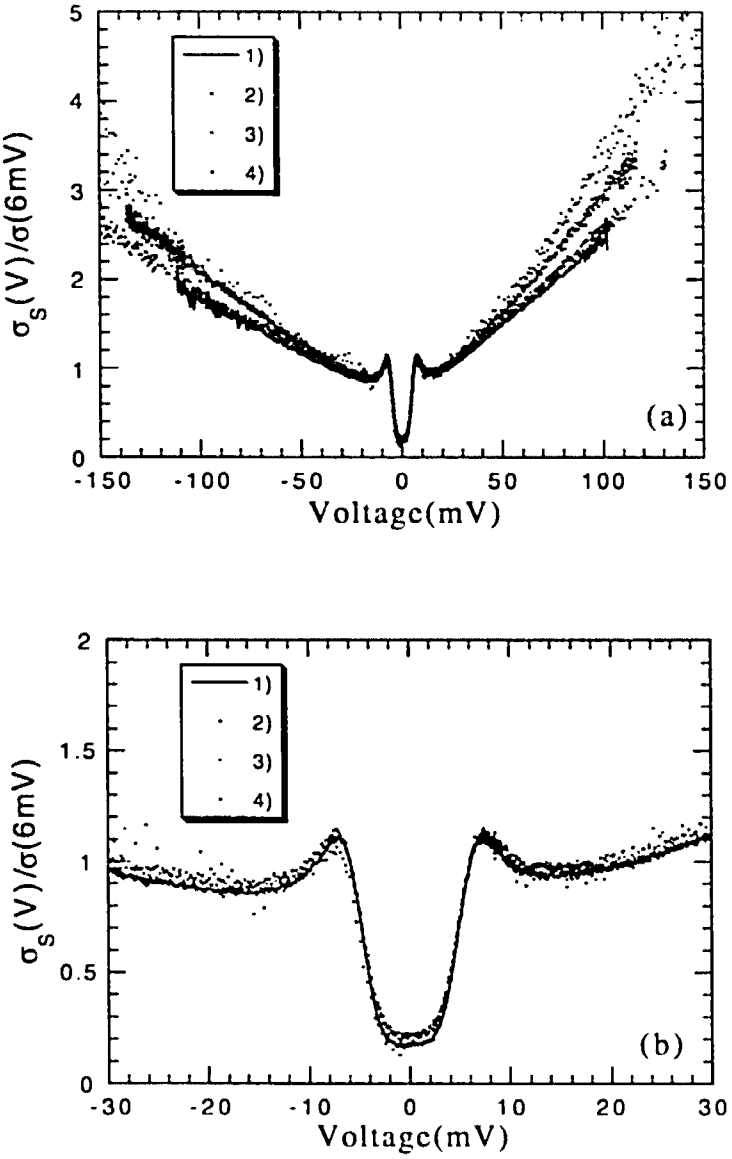

Fig. 6.5. (a) Superconducting tunneling conductances of the junctions shown in Fig. 6.4 normalized by the value of the conductance at V = 6 mV. The data are numbered according to the junction sequence shown in Fig. 6.4. (b) Expanded voltage scale demonstrating that the normalized conductances in the gap region lie on top of each other.

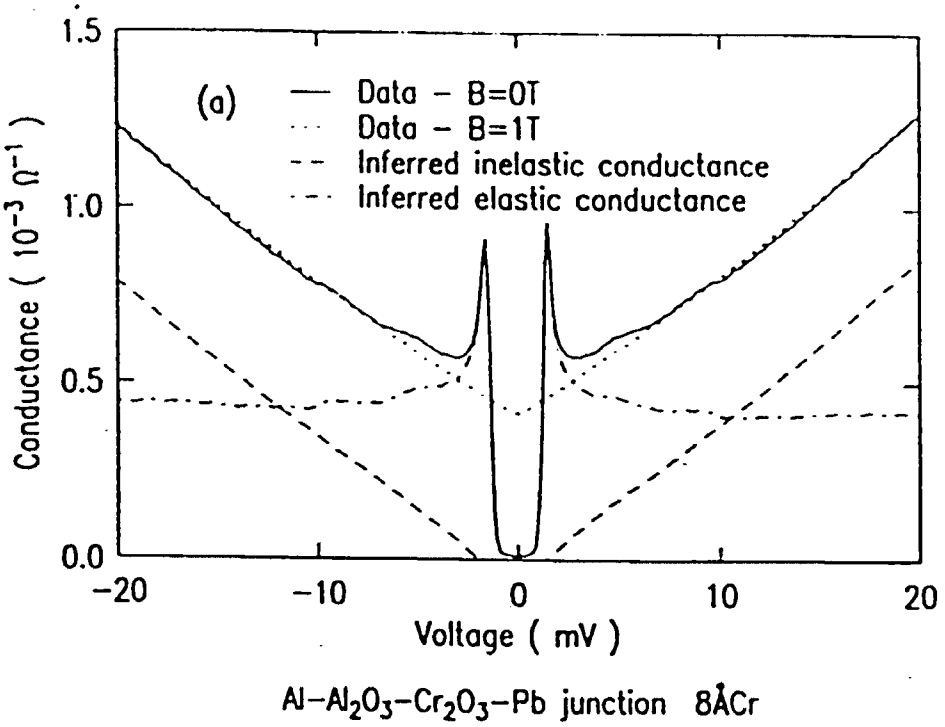

Fig. 6.6. Solid line is the superconducting tunneling conductance of a thin-film Al-Al_2O_3-Cr_2O_3-Pb junction (from Kirtley et al, 1992) showing the strong linear background conductance coming from spin fluctuations in the Cr oxide. The temperature is 0.5 K. The dotted curve is with a field of 1 T applied normal to the plane of the film to suppress the Pb superconductivity. The dashed curve is the inelastic component of the total conductance as inferred from a model based on a broad, flat continuum of states. The dot-dashed curve is the inferred elastic conductance obtained by subtraction of the inelastic term from the data.

electron-doped cuprates. In Fig. 6.7 is shown the tunneling conductances out to high-bias of four representative junctions on NCCO taken by Huang et al (1990a) using the point-contact tunneling apparatus. The junction resistances differ by roughly a factor of 10 (10^3-10^4 Ω) but the shapes of the σ(V) are the same. These include a nearly identical energy gap (Δ = 3.6 ± 0.1 meV) and a strong linearly increasing, asymmetric background conductance, such that the slope of the positive bias background is always slightly larger than that of the negative bias value. This weak asymmetry is also the same in each junction and is the same as found on the infinite-layer compound SNCO.

To check these apparent trends of the electron-doped cuprates further, we analyzed unpublished point-contact tunneling data by Huang et al (1992) on $Pr_{2-x}Th_xCuO_{4-y}$ (PTCO). Representative curves are shown in Figs. 6.8 and 6.9 for nine different junctions. The PTCO polycrystals are isoelectronic, sister compounds of the NCCO with nearly the same T_c ~ 22 K. Both the NCCO and PTCO electron-doped samples were obtained from the same group at the University of Maryland. The junction resistances shown in Figs. 6.8 and 6.9 differ by roughly a factor of 20 but again display similar behavior to that of the SNCO and NCCO compounds. A nearly identical gap value is found for each junction. An example of a normalized conductance and smeared BCS fit are shown in Fig. 6.10 taken from the highest conductance junction of Fig. 6.8. The gap value is Δ = 3.5 meV and this value was found (to within 0.1 meV) for more than twenty

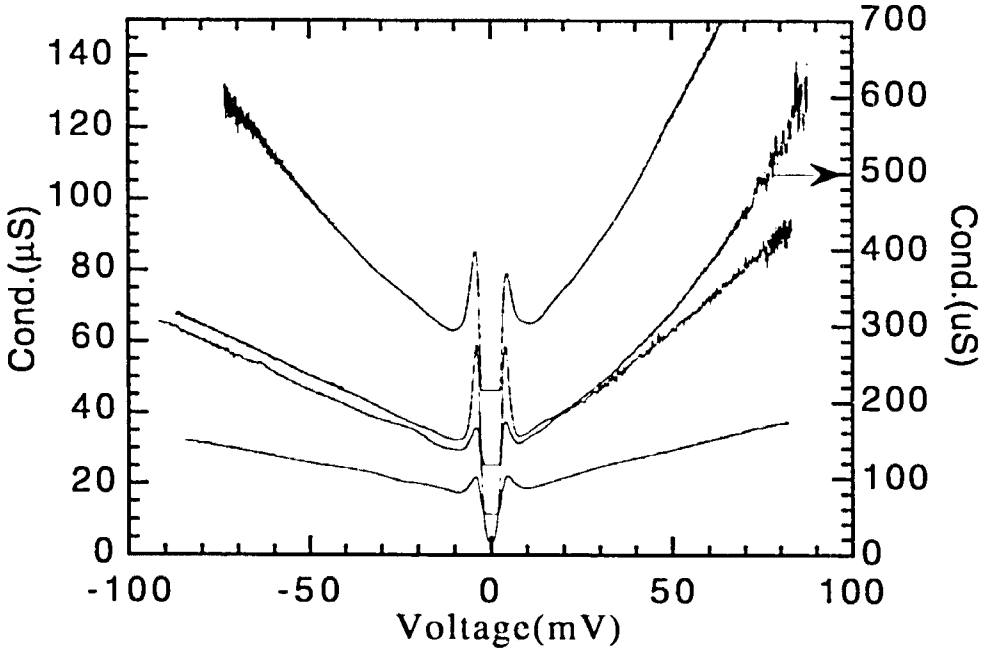

Fig. 6.7. Tunneling conductances of four point-contact junctions on $Nd_{2-x}Ce_xCuO_{4-y}$ taken by Huang *et al.* (1990a). Note the similarity in magnitude and shape of the asymmetric linear background to that of the $Sr_{1-x}Nd_xCuO_2$ shown in Figs. 6.4 and 6.5. The straight lines inside the gap are due to lock-in overload, because the junctions are balanced to maximize the sensitivity for phonon structures at high-bias voltage.

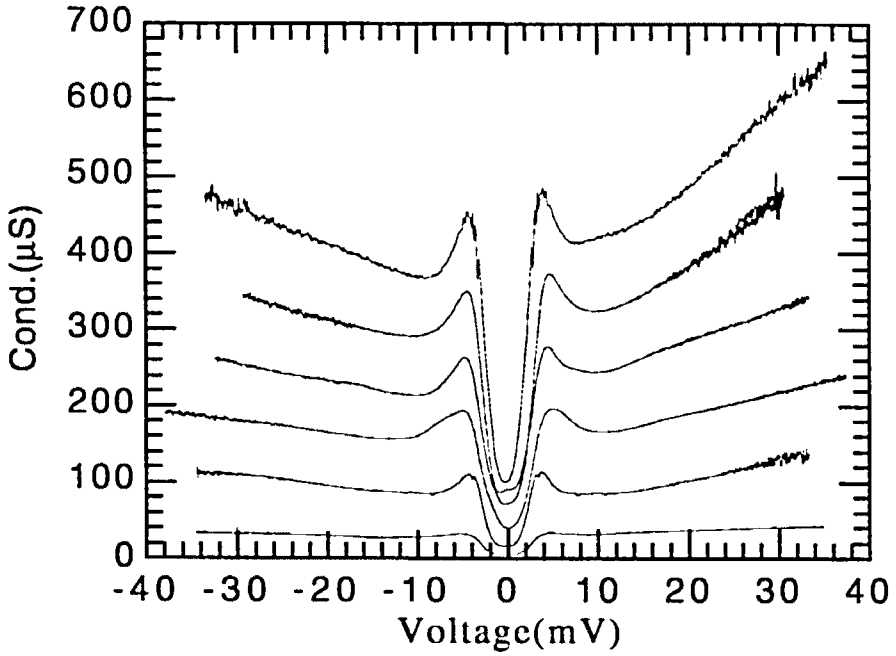

Fig. 6.8. Tunneling conductances of six different point-contact junctions on $Pr_{2-x}Th_xCuO_{4-y}$ from the unpublished data of Huang *et al.* (1992).

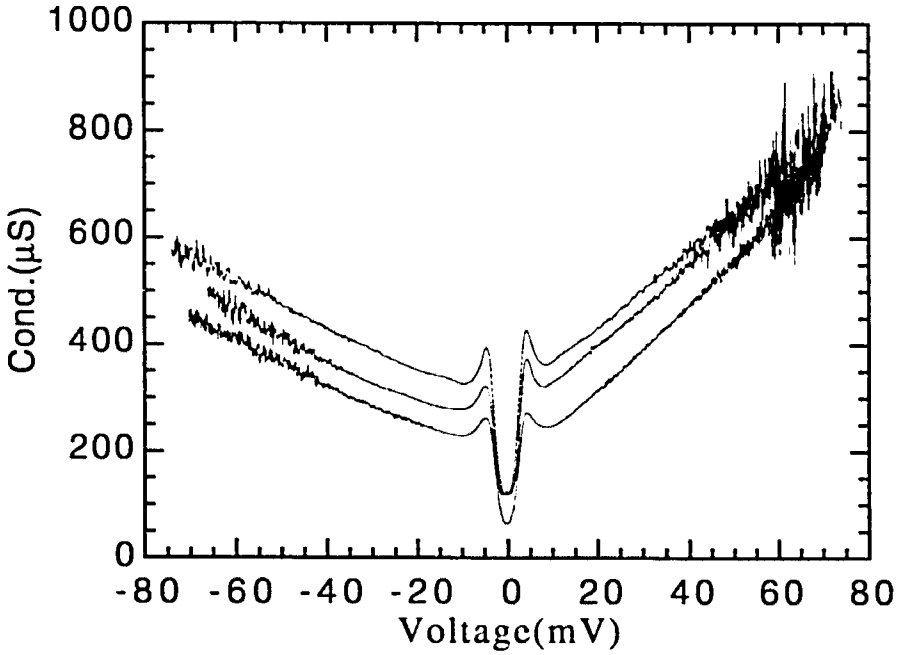

Fig. 6.9. Tunneling conductances of three point-contact junctions on $Pr_{2-x}Th_xCuO_{4-y}$ (from Huang *et al.*, 1992) taken out to higher bias voltages, demonstrating the asymmetric linear background conductance.

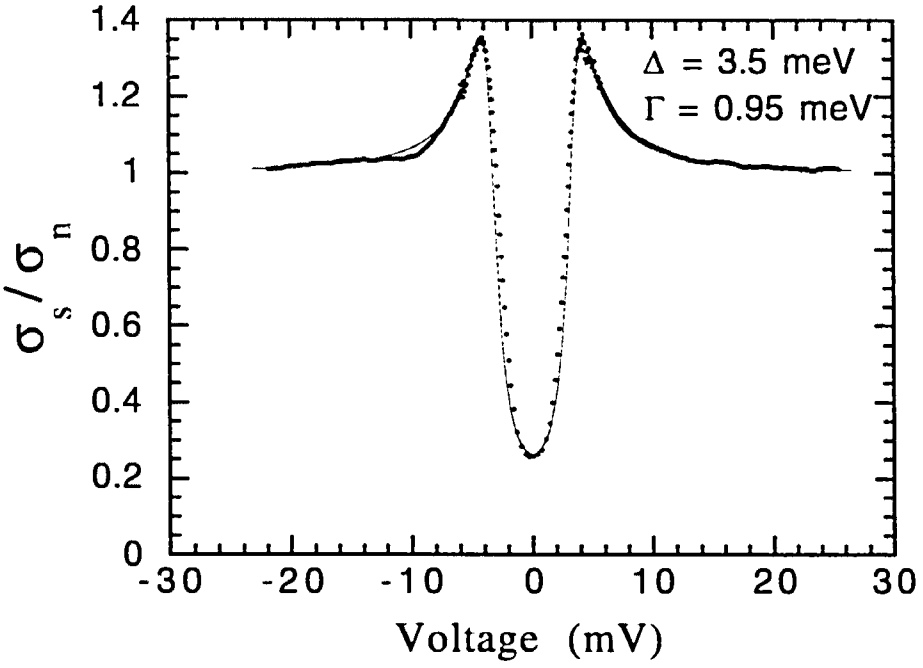

Fig. 6.10. Normalized experimental tunneling conductance (dots) of $Pr_{2-x}Th_xCuO_{4-y}$ obtained from the top curve of Fig. 6.8. The solid line is a fit using the smeared BCS DOS as discussed in the text with parameters Δ and Γ as indicated.

junctions taken at different locations on two different samples. The value of $2\Delta/k_BT_c = 3.7$, indicating moderate coupling strength.

The shape of the background conductance out to high-bias voltages is indicated in Fig. 6.9. A strong, linearly increasing conductance is found with a slope of ~ 2% per mV for positive bias which is always slightly larger than the slope for negative bias. This asymmetry is again the same as found on the other electron-doped cuprates. While the similarity of the tunneling conductances of the NCCO and PTCO compounds is encouraging from the perspective of reproducibility, it is also expected given the similarity in crystal structure, doping concentration and T_c in these materials. Both have a single CuO_2 layer per unit cell. However, the similarity to the infinite-layer cuprate, SNCO, is unexpected and suggests that there is something intrinsic about electron-doped cuprates that is producing the characteristic tunneling features: 1) consistent gap values, and 2) strong linear background conductances.

It should be noted that r.f. penetration depth measurements on NCCO by the Maryland group (Wu *et al.*, 1993) could be fit with BCS theory and a gap value of Δ = 3.6-3.8 meV, in excellent agreement with the point-contact tunneling data. These two sets of measurements, taken together, strongly point to an isotropic, s-wave gap parameter in NCCO. An isotropic gap would explain the consistency of the tunneling gap measurements. This is in contrast to tunneling measurements on $Bi_2Sr_2CaCu_2O_8$ for example, where a range of gap values (typically Δ = 10-30 meV) is reported from various tunneling measurements (Hasegawa *et al.*, 1992a). Such a

range of tunneling gap values in $Bi_2Sr_2CaCu_2O_8$ may be due in part to the apparent gap anisotropy in **k**-space found in photoemission experiments (Shen *et al.*, 1993; Ding *et al.*, 1994). Such measurements indicate that $\Delta(\mathbf{k})$ has a maximum along the ΓX direction of about 28 meV and a minimum close to 0 along the $\Gamma \overline{M}$ direction. A provocative conclusion from these data is that the other electron-doped cuprates, SNCO and PTCO are s-wave in a similar fashion to NCCO.

A nagging problem in the tunneling data of all the electron-doped cuprates is the presence of a substantial zero-bias conductance. The values of $\sigma_S/\sigma_n(0)$ range from a minimum of 15% for NCCO up to typically 25% for SNCO and PTCO. Such large values, if intrinsic, are not consistent with a simple isotropic, BCS gap. We have modeled the gap region conductance using the smeared BCS expression used by Dynes (Eq. 5.1) to describe inelastic quasiparticle scattering as found near T_c in conventional superconductors. Such a model introduces an intrinsic gaplessness which, if present, has a dramatic effect on SIS' junctions as indicated in the modeling study at the beginning of Chapter V. The modeling shows that for SIS' junctions with Nb as the counterelectrode, a strong Nb gap feature should be present in the data as a result of the gaplessness in the cuprate. To investigate this point we fabricated SIS' junctions on the infinite-layer SNCO samples using a Nb tip. An example is shown in Fig. 6.11 for a single junction at four temperatures (4.2 K, 4.8 K, 6.1 K and 7.0 K). Changing the temperature had little effect on the junction resistance in this case. Note that the conductance near zero-bias is

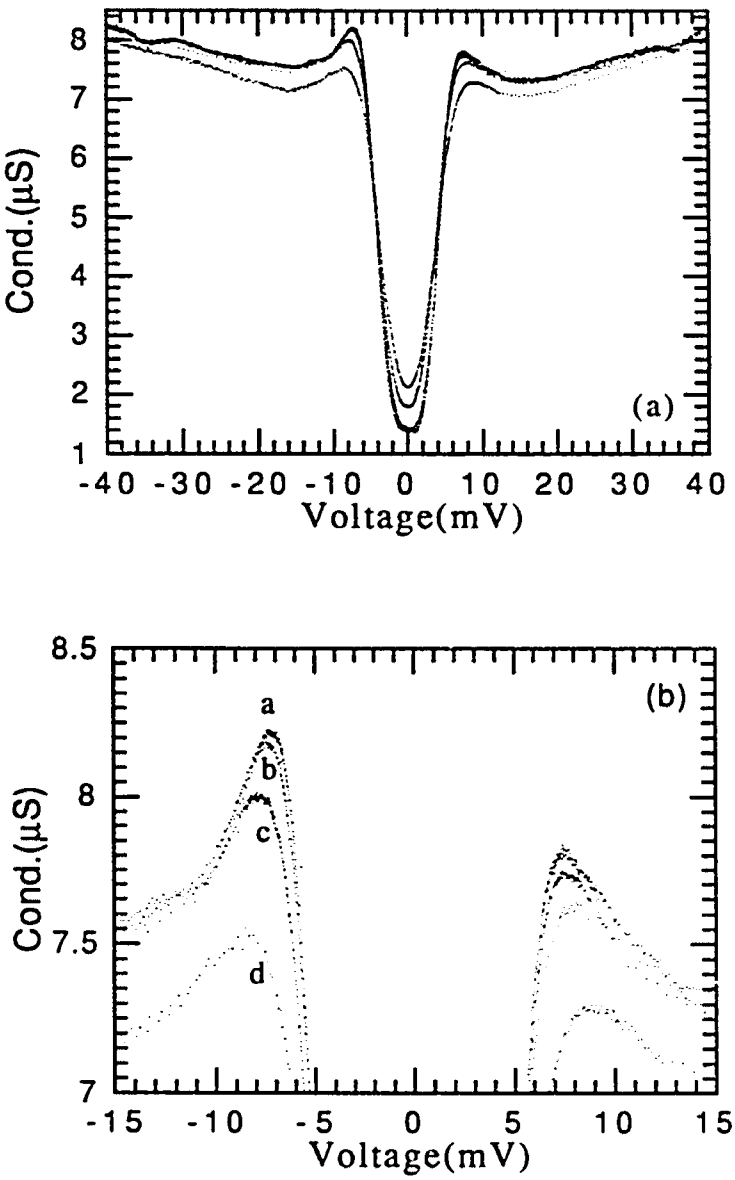

Fig. 6.11. (a) Conductance curves at temperatures from 4.2 K to 7.0 K for a SIS' tunnel junction on $Sr_{1-x}Nd_xCuO_2$ using a Nb tip. (b) Expanded x and y scale plot of the SIS' conductances at the following temperatures: a) 4.2 K, b) 4.8 K, c) 6.1 K, d) 7.0 K.

still approximately 25% of the expected normal state value and that there is no evidence of a Nb gap feature at any of the temperatures.

The data of Fig. 6.11b indicate a conductance peak near 7.5 mV at 4.2 K which decreases in magnitude and shifts to higher voltages as the temperature is increased. The SIS' modeling for this junction is shown in Fig. 6.12. Curve A assumes Δ = 6.0 meV and Γ/Δ = 0.2 for the SNCO and Δ = 1.5 meV and Γ/Δ = 0.01 for the Nb and T = 4.2 K. Comparison of curve A of Fig. 6.12 with the data at 4.2 K shows that the conductance peak location is reasonably consistent with the SIS' model but there are several major discrepancies. The peak heights of the model are much higher than the data but agreement here could be improved by increasing Γ for the SNCO. More importantly, the model shows a well-defined Nb gap feature and a very small zero-bias conductance, neither of which are observed in the data. Changing the modeling parameters to fit the 7.0 K data results in the curve B of Fig. 6.12. Here, the Nb gap has been reduced to 1.125 meV as would be expected at 7.0 K and Γ/Δ is 0.01, a value obtained from Dynes' work on Pb (Dynes *et al.*, 1978). The SNCO parameters have been fixed since we assume that the change in temperature does not affect this electrode with a T_c = 35 K. Curve B shows a reduced peak height but little shift in location. The Nb gap feature has been smeared out and a linear increase in conductance near zero-bias is evident.

The disagreement of the SIS' modeling study with the data on SNCO suggests that the smeared BCS DOS is not a correct picture to

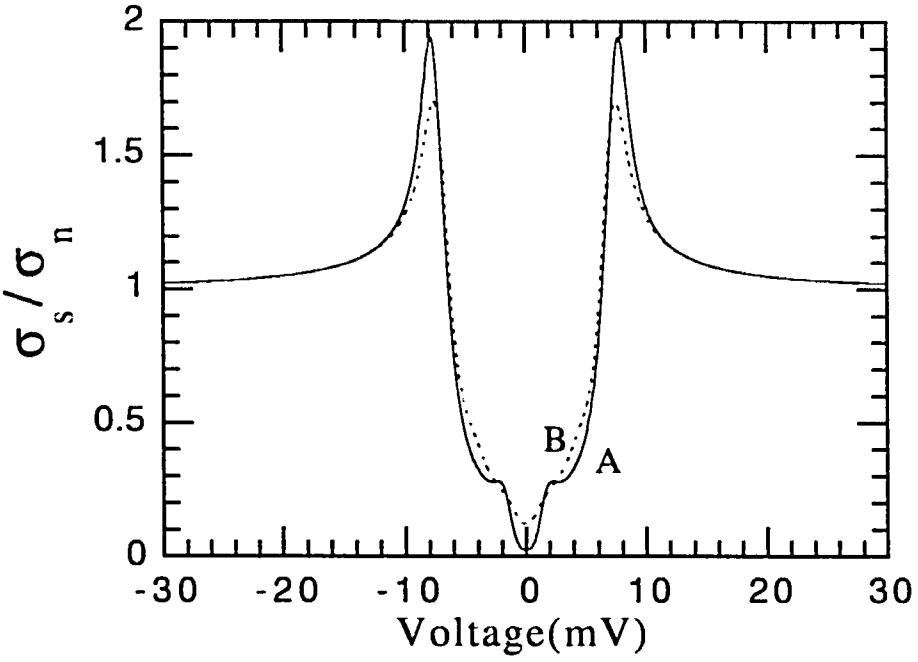

Fig. 6.12. Model calculation of the SIS' junction conductances. Curve A is at 4.2 K (solid line) and curve B is at 7.0 K (dashed line). In both calculations the $Sr_{1-x}Nd_xCuO_2$ parameters are fixed at Δ = 6.0 meV and Γ/Δ = 0.2. The values of the parameters for the Nb electrode are discussed in detail in the text.

analyze the gap region. A mechanism other than gaplessness is responsible for the zero-bias conductance found in SIN and SIS' junctions. One possibility is that inelastic tunneling is responsible. The Kirtley model shown in Fig. 6.6 indicates that inelastic tunneling is nearly zero for $|eV| < \Delta$, but this model assumes a temperature of 0.5 K to fit the experimental data. Thermal effects in inelastic tunneling are stronger than for elastic tunneling and tend to smear out the zero temperature features by ~ $5k_BT$ (Kirtley *et al.*, 1992). Thus, the inelastic contribution at 4.2 K to the subgap conductance may not be negligible. A detailed modeling of inelastic contributions to the subgap conductance at various temperatures is currently underway, but the results are not yet available for this thesis.

A number of important conclusions about the infinite-layer cuprate, SNCO, and other electron-doped cuprates have resulted from the point-contact tunneling data and can be summarized. First, reproducibility of the measured gap values seems to be the rule for electron-doped cuprates. We always obtain Δ values of 6.0 meV, 3.6 meV and 3.5 meV for SNCO, NCCO and PTCO, respectively. Such reproducibility is consistent with isotropic s-wave superconductivity as indicated in penetration depth measurements on NCCO (Wu *et al.*, 1993). Our tunneling study suggests that the electron-doped infinite-layer cuprates may be s-wave also. One might also expect variations in measured gap values to result from local variations in doping concentration either from surface exposure to air or from the bulk preparation itself. That we do not see such variations might be an indication that underdoping or overdoping of the superconducting

phase is not easily obtained. It has been suggested that NCCO for example is really a line compound (Hinks, private communication). In this case, the superconducting phase exists for a single value of doping concentration, making overdoping and underdoping impossible.

The observation of a similar linear background conductance in all of the electron-doped cuprates suggests a similar inelastic tunneling contribution from a broad continuum of states. Kirtley and Scalapino (1990) suggested that the continuum states was coming from spin fluctuations. Our tunneling study would suggest that the nature of the spin fluctuation spectrum would be similar in these electron-doped cuprates. What is more surprising is that no other type of background shape was observed. In $Bi_2Sr_2CaCu_2O_8$ and $Tl_2Ba_2CaCu_2O_x$ (Hasegawa *et al.*, 1992a), for example, the point-contact tunneling method yielded a variety of background shapes, from increasing with bias to decreasing with bias. A weakly decreasing background is the general feature of $Bi_2Sr_2CaCu_2O_8$ tunneling. The consistency of the tunneling background in electron-doped systems is not understood.

Finally, the origin of the ever present subgap conductance in all the electron-doped cuprates remains a mystery. However, our study seems to rule out gaplessness as a cause. The absence of the Nb gap feature in SIS' junctions strongly suggests an extrinsic origin to the subgap conductance. An extrinsic source would also explain why an apparently isotropic, s-wave superconductor yields such broadened BCS-like gap region characteristics. One possible source is the same

inelastic tunneling that gives rise to the linear background at high-bias. This has to be examined further both experimentally and theoretically. A simple experimental proposal would be to measure the tunneling conductance at very low temperatures (< 1 K) to observe if the subgap conductance disappears as it should for inelastic tunneling.

CHAPTER VII
Proximity Effect Tunnel Junctions

7.1. Introduction

Numerous methods have been tried to make reproducible and reliable tunnel junctions. Planar tunnel junctions which use a thin film for one or both electrodes are highly desirable to unambiguously reveal the properties of a superconducting state, and make superconducting electronics devices. These kinds of junctions have been widely used and are spectacularly successful for conventional superconductors. But preparing planar tunnel junctions for HTS is nontrivial because of the short coherence lengths and the difficulties of overcoming thick dead surface layers. One of the potential methods to overcome these difficulties is proximity effect tunneling. A thin proximity layer of well known properties such as gold *in-situ* deposited onto the superconductor may protect it from any contamination of the surface. This proximity layer might eliminate the naturally occurring, non-superconducting layer that has unknown properties and thickness. The proximity effect tunneling technique (Zasadzinski *et al.*, 1982) combined with the Arnold theory (Arnold, 1978) has been successfully applied to transition metals (Wolf and Arnold, 1982). These fundamental studies have led, in part, to the utilization of Al proximity layers in Nb-based superconducting devices. Numerous examples of Nb/Al bilayers for junction devices can be found in IEEE Trans. on Superconductivity **3**, Part III (1993). The McMillan (1968) model has been studied extensively in SN bilayer systems where an interfacial barrier layer

has been purposely introduced. Tunneling experiments on Au/Al-oxide/Al sandwiches (Gray, 1972), for example, have allowed an estimate of the electron-phonon coupling constant λ in Au. Such studies of Au backed by conventional superconductors are useful for comparisons with HTS results.

For HTS the most widely studied geometry to date has been the SNS junction, which indirectly probes the proximity effect through the Josephson current (Wolf, 1985). A more direct probe of the proximity effect is a measurement of the induced superconducting energy gap in the N layer displayed in the quasiparticle density of states (DOS). Three relevant experiments in the search for this energy gap are: 1) the photoemission (Dessau *et al.*, 1990) and 2) the point-contact tunneling study (Zasadzinski *et al.*, 1994) of cleaved $Bi_2Sr_2CaCu_2O_8$ (Bi-2212) crystals with Au overlayers, and 3) tunneling measurements (Gjis *et al.*, 1990) on mixed, preferential a- and c- type, oriented $YBa_2Cu_3O_{7-y}$ films with Ag overlayers. While the photoemission experiment showed no evidence of a induced gap in the Au, previous point-contact tunneling study on cleaved Bi-2212 crystals at Argonne (Zasadzinski *et al.*, 1994) consistently showed a gap-like feature which decreased in voltage in a monotonic fashion from an average value of approximately 10 meV to 5 meV for 200Å and 600 Å Au layers, respectively (see Fig. 7.1). Several junctions with 200 Å Au layers showed very low subgap conductances, compared to junctions formed directly on the Bi-2212 surfaces. In one junction, no conductance peaks were observed, and this is consistent with tunneling measurements on $YBa_2Cu_3O_{7-y}$ films with

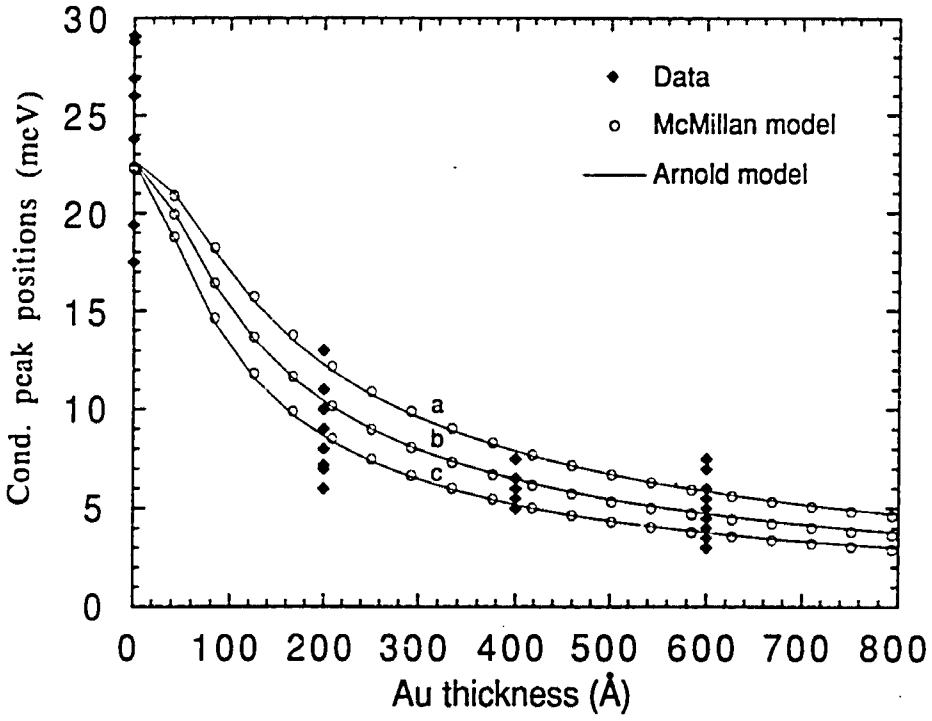

Fig. 7.1. Experimental conductance peak positions (solid diamonds) versus gold film thickness. The fit shown as solid lines (open circles) is from Arnold (McMillan) model of proximity effect tunneling (after Huang et al., unpublished).

Ag overlayers (Gjis *et al.*, 1990), which showed reduced energy gap but no conductance peaks.

Development of the point-contact proximity tunneling can be useful in its own right, but it can also give insight into the problems needed to be solved for possible thin film type proximity tunneling on HTS. As an extension of the point-contact tunneling method, proximity-effect tunneling was utilized to study interface properties on all-thin-film SN bilayers of Bi-2212/Au and some preliminary results are presented in this chapter. The SN bilayers were fabricated using laser ablation. The Au was deposited *in-situ*, but after cool-down of the Bi-2212 film. An indium tip is used to tunnel into the N side of the bilayer and indium-oxide presumably forms the tunnel barrier. We obtained junctions with much lower subgap resistances compared to tunneling directly into bulk superconductors. The reduced conductance peak positions indicate they are likely the counterelectrode-insulator-normal metal-superconductor (C-I-NS) type proximity tunnel junctions. In order to understand the experimental data quantitatively, we first give a review on proximity effect models.

7.2. Proximity Effect Models

There are two well-established proximity effect models, the Arnold (1978) and McMillan (1968) models, which deal with two extreme cases. As in Fig. 7.2, a proximity tunnel junction is composed of a counter electrode (C), being separated from a normal metal/superconductor (NS) sandwich by an insulating layer (I). This

is more simply referred to as a CINS junction. Both models can be applied to the same tunneling geometry pictured in Fig. 7.2, the difference being the transmission across the NS interface (no barrier: Arnold; tunneling barrier: McMillan). The Arnold model considers that the NS layers in the bilayer are in perfect electrical contact and provides an exact expression for the Green's function in both layers, through a solution of the boundary value problem. On the other hand, the McMillan tunneling model assumes that the layers are weakly coupled due to a thin barrier between N and S which allows a perturbation treatment. Both models assume the thickness d_N of the normal metal in the NS bilayer to be much less than the coherence length. While the dependence of the energy gap with Au thickness in Fig. 7.2 can be fit using both Arnold and McMillan models, the tunneling DOS can only be fit using the McMillan model with reasonable quantitative agreement (Zasadzinski *et al.*, 1994). The McMillan model will also be used later to fit our experimental data. Hence we focus here on the McMillan model.

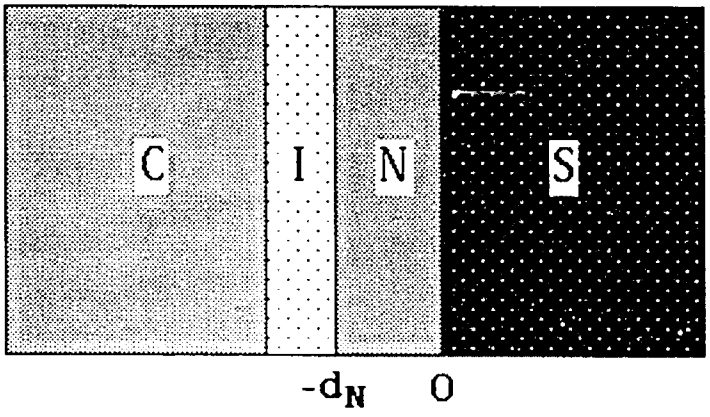

Fig. 7.2. Schematic view of a proximity tunneling junction.

The McMillan model treats the Hamiltonian

$$H = H_S + H_N + H_T \tag{7.1}$$

using the second-order, self-consistent perturbation theory, where H_S, H_N, and H_T are the Hamiltonians for the superconducting and normal layers, and the tunneling Hamiltonian, respectively. This calculation results in the simultaneous, nonlinear equations as follows:

$$\Delta_N(E) = \left(\Delta_{N^{ph}} + \frac{\Gamma_N \Delta_S(E)}{\left[\Delta^2_S(E) - E^2\right]^{1/2}} \right) \left(1 + \frac{\Gamma_N}{\left[\Delta^2_S(E) - E^2\right]^{1/2}} \right)^{-1} \tag{7.2}$$

$$\Delta_S(E) = \left(\Delta_{S^{ph}} + \frac{\Gamma_S \Delta_N(E)}{\left[\Delta^2_N(E) - E^2\right]^{1/2}} \right) \left(1 + \frac{\Gamma_S}{\left[\Delta^2_N(E) - E^2\right]^{1/2}} \right)^{-1} \tag{7.3}$$

The self-energies, $\Delta_N(E)$ and $\Delta_S(E)$ can be determined by solving these coupled equations. $\Delta_{S^{ph}}$ and $\Delta_{N^{ph}}$ are the BCS pair potentials. $\Gamma_{S,N}$ is defined as

$$\Gamma_{s,N} = \frac{\hbar v_f t^2}{2 d_{s,N}} \tag{7.4}$$

where v_f is the Fermi velocity, $d_{S,N}$ is the superconducting and normal metal thickness, respectively, and the transmission coefficient t^2 comes from the tunnel barrier at the interface and in general should be small, i.e. << 1. Once $\Delta_N(E)$ and $\Delta_S(E)$ are calculated, they can be substituted into

$$N_{S,N}(E) = Re\left\{\frac{E}{\sqrt{E^2 - \Delta^2_{S,N}(E)}}\right\} \qquad (7.5)$$

to determine the electronic DOS for the superconducting and normal layers. According to the tunneling theory, this electronic DOS is measured directly by placing a tunnel junction on one or the other side of the SN sandwich and measuring the normalized first derivative of the tunneling current versus voltage. In this chapter we assume the normal state electron density of states at the Fermi level N(0) = 1 for simplicity.

In our study, d_S was considered much larger than d_N, so that in this limit, $\Gamma_S \approx 0$. Also, Δ_{Nph} and Δ_{Sph} were considered equal to the bulk energy gap values for the normal and superconducting layers, respectively. At any measurable temperature, Δ_N^{bulk} is zero, therefore, Δ_{Nph} can be set to zero. In the case when $\Gamma_S = 0$ and $\Delta_{Nph} = 0$, the simultaneous equations (7.2) and (7.3) are decoupled, resulting in

$$\Delta_S(E) = \Delta_{Sph} \qquad (7.6)$$

$$\Delta_N(E) = \frac{\Gamma_N \Delta_{Sph}}{(\Delta^2_{Sph} - E^2)^{1/2} + \Gamma_N} \qquad (7.7)$$

The normal metal DOS can be calculated straightforward by substituting Eq. (7.7) in Eq. (7.5). Since the value of Δ_{Sph} needs to be close to the conventional energy gap value of the superconductor, Γ_N can be considered the only free parameter used to fit the data.

It is of interest to examine the qualitative features of the resulting tunneling conductance curves. Figure 7.3 displays the

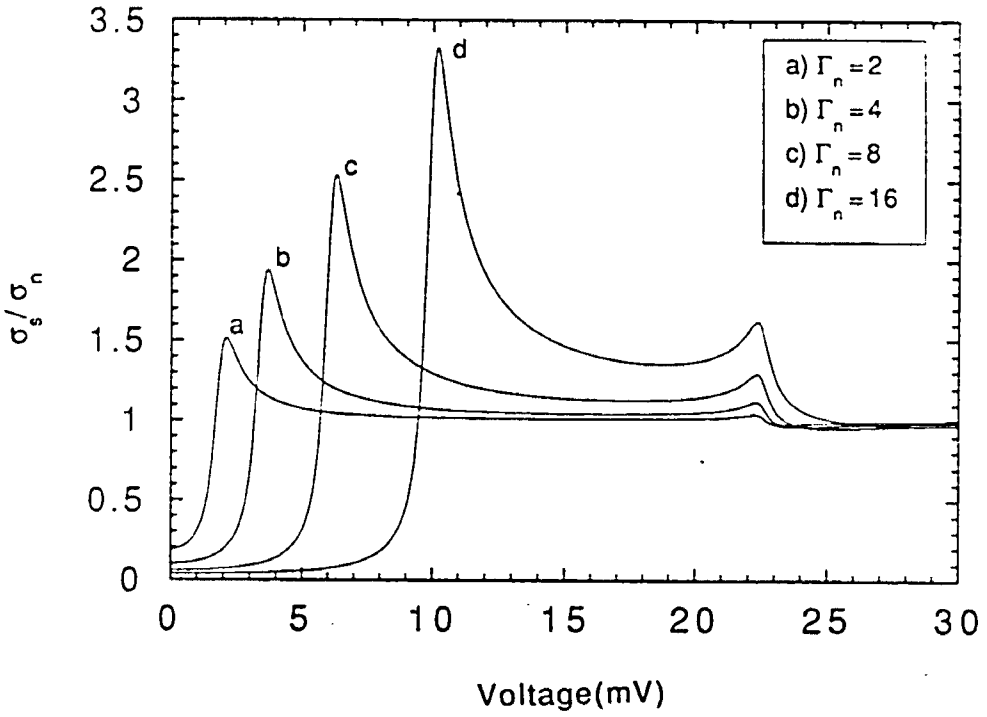

Fig. 7.3. Normalized conductances for a N-I-NS junction using the McMillan model density of states for the normal metal of the NS sandwich, with $\Delta_{Nph} = 0$ and $\Delta_{Sph} = 22.5$ meV. Thermal smearing at T = 4.2 K is accounted for by introducing a smearing parameter $\Gamma = k_B T = 0.36$ meV.

normalized conductance for a N-I-NS junction using the McMillan model DOS for the normal metal of the NS sandwich with $\Delta_{Nph} = 0$, and $\Delta_{Sph} = 22.5$ meV, an average experimental superconducting gap value for Bi-2212. Thermal smearing at T = 4.2 K is accounted for by introducing a smearing parameter $\Gamma = k_B T = 0.36$ meV in Eq. (5.1). The values of Γ_N are varied, since Γ_N is essentially the only free parameter. At low energies, $E << \Delta_{Sph}$, a peak at Ω_N, the induced energy gap in the normal metal, can be observed, as well as some structure at Δ_{Sph} for $E \approx \Delta_{Sph}$. As the thickness of the normal metal decreases, Γ_N increases, and the positions of these innermost peaks get pushed out toward Δ_{Sph}, while also increasing in magnitude (a feature of the BCS DOS). In the limit as $d_N \rightarrow 0$, the McMillan model density of states will appear like the BCS DOS curve for the superconductor alone, possessing a single peak at Δ_{Sph}. This is an intuitive result, since as d_N gets smaller and smaller, the normal metal layer has less and less of an effect in the NS sandwich.

In our experimental study, the normal metal is thin relative to the superconductor and the transmission coefficient is small, such that $\Gamma_S << \Gamma_N << \Delta_{Sph}$. Then the self-energy for the normal metal is approximately

$$\Delta_N(E) = \Delta_{Nph} + \Gamma_N \tag{7.8}$$

at low energies, $E << \Delta_{Sph}$. The DOS in N is then BCS-like

$$N_N(E) \approx Re\left[\frac{E}{\sqrt{E^2 - \Omega^2_N}}\right] \tag{7.9}$$

at low energies, with the energy gap

$$\Omega_N = \frac{\Gamma_N}{1+\Gamma_N/\Delta_S}. \qquad (7.10)$$

and has a little anomaly for $E \approx \Delta_{Sph}$. Then $\Omega_N \approx \Gamma_N$ ($\Gamma_N << \Delta_S$) can be considered the induced proximity energy gap in the normal metal by the superconductor. This is evident as in Fig. 7.3a. Hence we may use a BCS DOS to fit our data and refer the BCS energy gap Δ as the induced proximity energy gap $\Omega_N \approx \Gamma_N$ when $\Gamma_N << \Delta_S$.

7.3. Experimental Results and Discussions

Point-contact tunneling was carried out on all thin film Bi-2212/Au bilayers with Au thickness ~ 400 Å. An indium tip was used to tunnel into the N side of the bilayer as a counterelectrode. Indium is softer than gold or niobium and contact can be made without damage to the gold film if care is taken. The indium tip was etched in nitric acid before mounting to the tunneling apparatus. The barrier in the junction is believed to be indium oxide.

Low-temperature measurements were done by cooling with exchange gas to liquid ^{4}He. The current-voltage characteristic I(V) and derivative dI/dV were obtained using a bridge circuit with the usual lock-in techniques. The procedure was first tried by Huang *et al.* (unpublished) on Nb/Au bilayers (d_N = 300 Å) with success. A clean energy gap was observed at 1.4 meV, reduced from the bulk Nb value of 1.55 meV, and this result was consistent with previous proximity effect studies of Nb (Wolf and Arnold, 1982). Furthermore, the high-bias d^2V/dI^2 showed evidence of Au phonon structure (Huang *et al.*, unpublished), proving that the tunneling was

not just through pinholes or punch-throughs in the Au layer. Then Huang and Zasadzinski (Zasadzinski *et al.*, 1994) studied single crystal Bi-2212 with a Au overlayer using this point-contact method. They observed a broadened, BCS-like DOS with a large gap parameter, decreasing from an average value of approximately 10 meV to 5 meV (Fig. 7.1), for Au thicknesses of 200 Å and 600 Å, respectively.

We report here preliminary results on point-contact tunneling into all thin film Bi-2212/Au bilayers with Au thickness ~ 400 Å. Figure 7.4a shows the experimental result on one junction. X-ray diffraction showed mainly 2212 phase for the underlying superconductor and resistivity measurement revealed a T_c of 70 K, reduced from T_c ~ 96 K of the bulk material. This junction shows clear and well-defined gap features and the reduced conductance peak positions Ω_N indicate it is likely the CINS type proximity tunnel junctions. The value of Ω_N ~ 4 meV is consistent with that (~ 5-8 meV in Fig. 7.1) found on single crystal Bi-2212/Au bilayers with the same Au thickness of 400 Å but a higher T_c. The fact that Ω_N is much reduced from bulk value Δ_S (see Fig. 7.3a) may also be the reason that we did not see the weak feature at Δ_S. While we do not understand the origin for the reduced height or absence of the conductance peaks in Fig. 7.4b, this is very similar to previous proximity tunneling results (Fig. 7.4c) on single crystal Bi-2212/Au obtained with the same apparatus (Zasadzinski *et al.*, 1994). The absence of the conductance peaks is also observed by Gjis (Gjis *et al.*, 1990) on mixed a- and c-oriented $YBa_2Cu_3O_{7-y}$ films. It is very

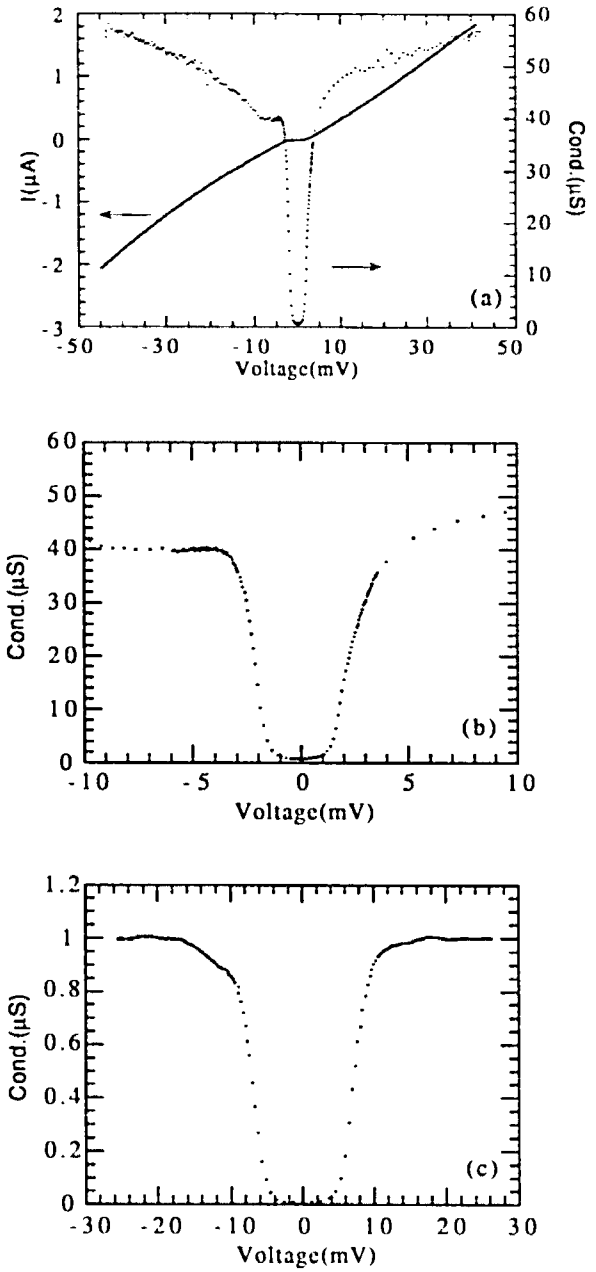

Fig. 7.4. (a) Experimental I(V) characteristics (solid line) and conductances (dots) for a proximity effect junction on all-thin-film $Bi_2Sr_2CaCu_2O_8$/Au bilayer with an In tip. (b) Expanded x-scale plot of the junction in (a), showing the gap region data. (c) Experimental conductances for a proximity effect junction on single crystal $Bi_2Sr_2CaCu_2O_8$/Au with an In tip (from Zasadzinski *et al.*, 1994). Notice the similarity of (b) and (c).

encouraging to note the flat, near-zero conductance at zero bias. Note the zero-bias conductance is lower than the best value of ~ 15% (Hasegawa *et al.*, 1992a) found in the bare Bi-2212 crystals (d_N = 0).

In some cases, very high quality junctions were observed as shown in Fig. 7.5 with Au thickness ~ 400 Å. Resistivity measurements showed a low T_c ~ 30 K for the underlying superconducting film. While x-ray diffraction data displayed mainly Bi-2212 phase, we suspect that there is a substantial contribution from Bi-2201 which is often an impurity phase in 2212 films. The junction in Fig. 7.5 shows very high conductance peaks and clear gap difference peaks. As a first approximation, the tunneling conductance was fit using BCS density of states, including thermal smearing (Eq. 5.3) with Δ_{In} = 0.35 meV and Γ_{In}/Δ_{In} = 1%. The fit in Fig. 7.5b shown as solid line provides values of Δ = 0.85 meV and Γ/Δ = 7%. The small smearing parameter is compatible to the lowest value found on $HgBa_2CuO_{4+x}$ (Chen *et al.*, 1994&1995). Note the observation (and fitting) of the difference peak structure (Δ_1-Δ_2) in Fig. 7.5b, however the BCS gap Δ was quite small (~ 1 meV). The small gap appears to be due to a combination of proximity effect and low value of T_c ~ 30 K.

As is mentioned earlier, we may interpret the BCS energy gap Δ as proximity induced energy gap $\Omega_N \approx \Gamma_N$ ($\Gamma_N << \Delta_S$) within the McMillan model. To see whether a quantitative agreement can be obtained, we tried to compare a DOS of the McMillan model using Eqs. (7.5) and (7.7) with the BCS DOS used in the fitting of Fig. 7.5b. In order to obtain the best agreement we had to smear the theoretical

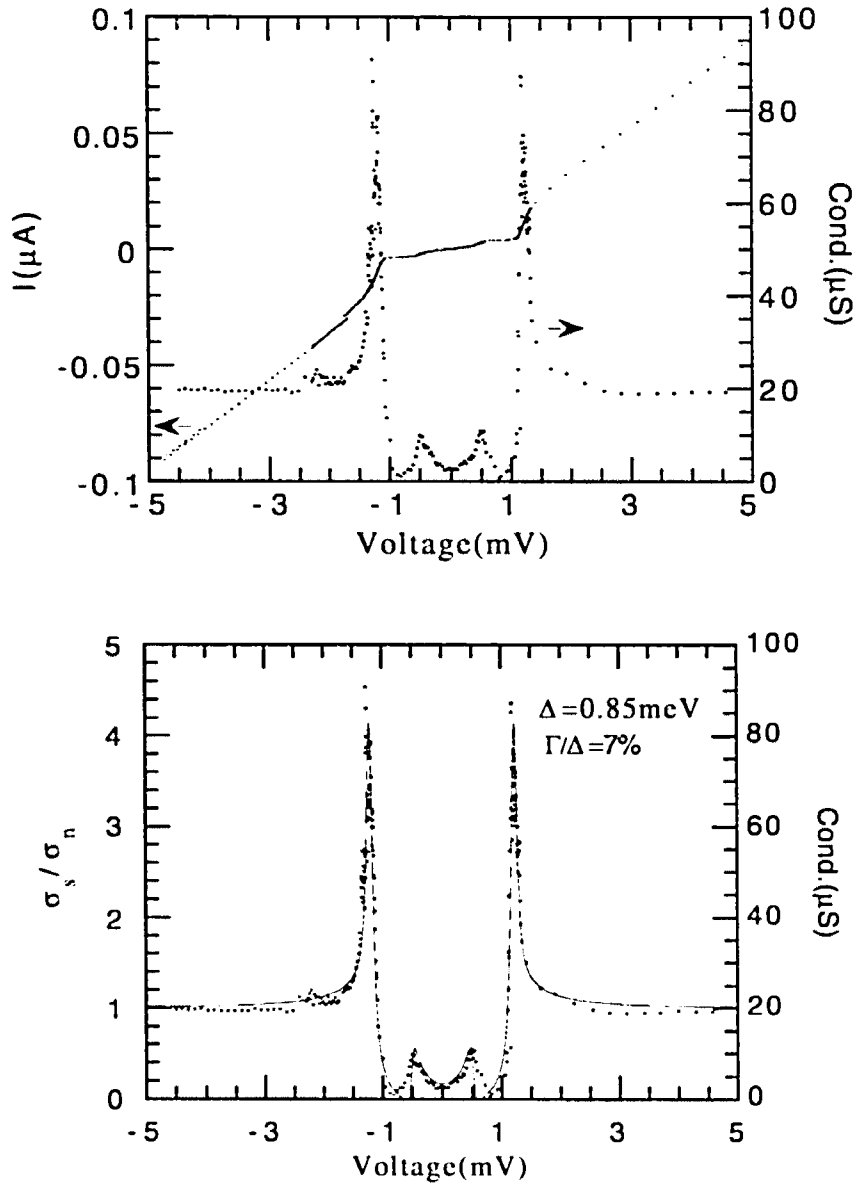

Fig. 7.5. (a) Experimental I(V) characteristic and conductance for a proximity effect junction on all-thin-film $Bi_2Sr_2CaCu_2O_8$/Au bilayer with an In tip. The measurement is taken at T = 2.5 K. (b) The solid line is a fit to the experimental conductance (dots), using BCS gaps, Δ = 0.85 meV and Δ_{In} = 0.35 meV.

BCS DOS (Eq. 7.5) by introducing a small parameter Γ, in analogy to Eq. (5.1). We are not certain about the origin of the additional smearing of experimental data, but this is a common feature found in tunneling studies of HTS. Note that the agreement of DOS from both models (see Fig. 7.6a) is very good. It indicates that we may use the DOS of the McMillan model for SN bilayer and convolute it with the DOS of In tip in Eq. (5.2) to generate the same fit as in Fig. 7.5b. Thus, the fit with The McMillan model is excellent, including the gap difference peaks. It is important to point out that according to the McMillan model, the conductance peak position $\Omega_N \approx \Gamma_N$ when $\Gamma_N << \Delta_S$ and is no longer sensitive to the bulk superconductor energy gap Δ_S (Fig. 7.6b). We used Δ_S = 22.5 meV, an average gap value for bulk Bi-2212, for the fitting. Based on the value of Γ_N which gives the best fit, the transmission coefficient is calculated from Eq. (7.4): t^2 = 0.074. The rather small value of t^2 justifies the use of the McMillan model. The low subgap conductances and high conductance peaks indicate that a proximity effect approach may have potential for junction devices. Although in some cases, the usable gap is much reduced.

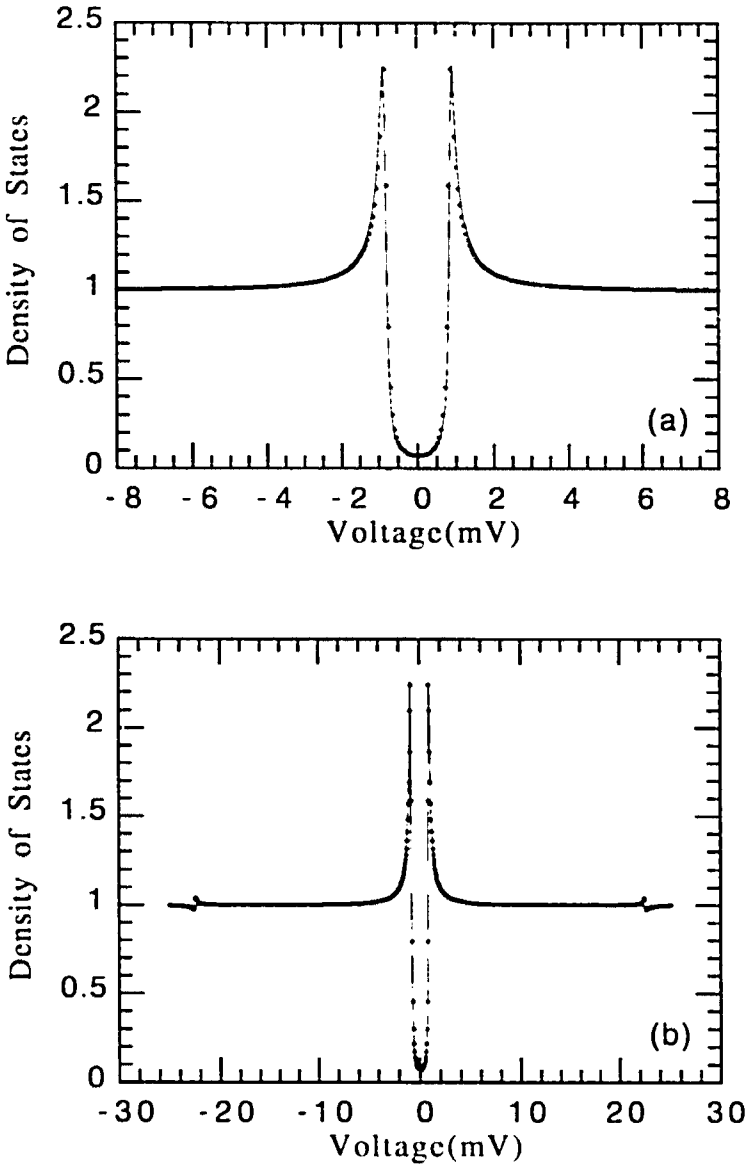

Fig. 7.6. (a) Comparison of a McMillan density of states (Δ_S = 22.5 meV, Γ_N = 0.85 meV, and Γ/Γ_N = 7%), shown as dots, with a BCS density of states (Δ = 0.85 meV and Γ/Δ = 7%), shown as solid lines. (b) Same density of states taken out to high-bias voltage, showing the weak feature at Δ_S = 22.5 meV for the McMillan model.

CHAPTER VIII
SUMMARY

Tunneling measurements have been an important probe of high-temperature superconductors (HTS), providing a direct measure of the superconducting energy gap and giving insight into the quasiparticle density of states. Because of the short coherence length and the dead surface layer of HTS, most tunneling measurements for HTS have been of the point-contact type. We used this method to fabricate tunnel junctions on cuprate HTS materials: $HgBa_2CuO_{4+x}$ and the infinite-layer compound $Sr_{1-x}Nd_xCuO_2$.

$HgBa_2CuO_{4+x}$ is of particular interest because of its simple structure and unusual high T_c of 97 K for a compound with only one CuO_2 layer per unit cell. Both superconductor-insulator-normal metal (SIN) and superconductor-insulator-superconductor (SIS) junctions have been studied using Au and Nb tips, respectively and consistent results are obtained. The data exhibit low and flat subgap conductances and are fit using a BCS density of states with a weak smearing parameter, Γ, and energy gap, Δ, is determined. The ratio Γ/Δ is typically in the range of 5%-7%, making this the lowest, reproducible value found on any cuprate superconductor. Typical gap parameter values are Δ = 13-16 meV. The data are more compatible with an s-wave pairing state, but d-wave cannot be ruled out due to the possibility of directional tunneling (Kouznetsov and Coffey, preprint). The high quality junctions indicate that

$HgBa_2CuO_{4+x}$ may be a suitable candidate for quasiparticle-based junction devices such as mixers.

The point-contact tunneling study on the infinite-layer compound $Sr_{1-x}Nd_xCuO_2$ showed that this electron-doped cuprate behaves like other electron-doped cuprates, such as $Nd_{2-x}Ce_xCuO_{4-y}$ and $Pr_{2-x}Th_xCuO_{4-y}$. First, reproducibility of the measured gap values seems to be the rule for electron-doped cuprates. We always obtain Δ values of 6.0 meV, 3.6 meV, and 3.5 meV for $Sr_{1-x}Nd_xCuO_2$, $Nd_{2-x}Ce_xCuO_{4-y}$, and $Pr_{2-x}Th_xCuO_{4-y}$, respectively. Such reproducibility is consistent with isotropic s-wave superconductivity as indicated in penetration depth measurements on $Nd_{2-x}Ce_xCuO_{4-y}$ (Wu *et al.*, 1993). Our tunneling study suggests that the electron-doped infinite-layer cuprates would be an interesting choice for future penetration depth measurements.

Secondly, the observation of a similar linear background conductance in all of the electron-doped cuprates suggests a similar inelastic tunneling contribution from a broad continuum of states. If spin fluctuations (Kirtley and Scalapino, 1990) are the cause, then our tunneling study suggests that the nature of the spin fluctuation spectrum would be similar in the electron-doped cuprates. Neutron scattering measurements would shed light on this issue.

Finally, the absence of the Nb gap feature in SIS' junctions strongly suggests an extrinsic origin to the subgap conductance. An extrinsic source would also explain why an apparently isotropic, s-wave superconductor yields such broadened BCS-like gap region

characteristics. Our modeling study seems to rule out gaplessness as a cause. One possible source is the same inelastic tunneling that gives rise to the linear background at high-bias. This has to be examined further both experimentally and theoretically. A simple experimental proposal would be to measure the tunneling conductance at very low temperatures (< 1 K) to observe if the subgap conductance disappears as it should for inelastic tunneling.

As an extension of the above method, proximity-effect tunneling was utilized to study *in-situ* deposited metal/superconductor bilayers. The hope was that the overlayer would prevent insulating layers from forming on top of the HTS surface. All-thin-film bilayers of $Bi_2Sr_2CaCu_2O_8$/Au were fabricated using laser ablation. An In tip was used to tunnel into the N side of the bilayer and successful junctions were obtained. The results are preliminary, but some junctions displayed very low subgap conductances, improved over junctions formed directly on the $Bi_2Sr_2CaCu_2O_8$ surface. This is consistent with previous results on single crystal $Bi_2Sr_2CaCu_2O_8$ with Au overlayers (Zasadzinski *et al.*, 1994). In a few cases, very high quality junctions were obtained. Agreement with the McMillan model has been found in detailed fits, including both conductance peaks and gap difference features. The low subgap conductances and high conductance peaks indicate that a proximity effect approach may have potential for junction devices. A future approach might be to incorporate the proximity effect method with $HgBa_2CuO_{4+x}$ films.

REFERENCES

J. G. Adler and J. E. Jackson, Rev. Sci. Instr. **37**, 1049 (1966).

P. B. Allen, in *Dynamical Properties of Solids 3*, edited by G. K. Horton and A. A. Maradudin (North-Holland, New York, 1980).

P. W. Anderson, J. Phys. Chem. Solids **11**, 26 (1959).

P. W. Anderson, in *Proc. of the VIIth Int. Conf. on Low Temp. Physics*, edited by G. M. Graham and A. C. H. Hallett (University of Toronto Press, Toronto, 1961).

G. B. Arnold, Phys. Rev. B **18**, 1076 (1978).

J. Bardeen, L. N. Cooper, and J. R. Schrieffer, Phys. Rev. **106**, 162 (1957).

S. E. Barrett, D. J. Durand, C. H. Pennington, C. P. Slichter, T. A. Friedmann, J. P. Rice, and D. M. Ginsberg, Phys. Rev. B **41**, 6283 (1990).

J. G. Bednorz and K. A. Müller, Z. Phys. B **64**, 189 (1986).

G. E. Blonder and M. Tinkham, Phys. Rev. B **27**, 112 (1983).

N. N. Bogoliubov, V. V. Tolmachev, and D. V. Shirkov, *A New Method in the Theory of Superconductivity*, (Academy of Science, Moscow. Consultant Bureau, New York, 1959).

J. Chen, J. F. Zasadzinski, K. E. Gray, J. L. Wagner, and D. G. Hinks, Phys. Rev. B, **49**, 3683 (1994).

J. Chen, J. F. Zasadzinski, K. E. Gray, J. L. Wagner, D. G. Hinks, K. Kouznetsov, and L. Coffey, IEEE Trans. Appl. Superconductivity **5**, 1502 (1995).

O. Chmaissem, Q. Huang, S. N. Putilin, M. Marezio, and A. Santoro, Physica C **212**, 259 (1993).

C. W. Chu, L. Gao, F. Chen, Z. J. Huang, R. L. Meng, and Y. Y. Xue, Nature (London) **365**, 323 (1993).

L. N. Cooper, Phys. Rev. **104**, 1189 (1956).

B. J. Dalrymple and D. E. Prober, J. of Low Temp. Phys. **56**, 545 (1984).

D. I. Decker, D. E. Mapother, and R. W. Shaw, Phys. Rev. **112**, 1888, (1958).

D. S. Dessau, B. O. Wells, Z.-X. Shen, W. E. Spicer, A. J. Arko, R. S. List, C. G. Olson, C. B. Eom, D. B. Mitzi, A. Kapitulnik, and T. H. Geballe, Appl. Phys. Lett. **57**, 1152 (1990).

H. Ding, J. C. Campuzano, K. Gofron, C. Gu, R. Liu, B. W. Veal, G. Jennings, Phys. Rev. B **50**, 1333 (1994).

D. H. Douglass Jr.and L. M. Falicov, in *Progress in Low Temperature Physics IV*, edited by C. J. Gorter (North Holland, Amsterdam, 1964).

R. C. Dynes and J. M. Rowell, Phys. Rev. B **11**, 1884 (1975).

R. C. Dynes, V. Narayanamurti, and J. P. Garno, Phys. Rev. Lett. **41**, 1509 (1978).

H. L. Edwards, J. T. Markert, A. L. de Lozanne, Phys. Rev. Lett. **69**, 2967 (1992).

G. M. Eliashberg, Soviet Phys. JETP **11**, 696 (1960).

G. M. Eliashberg, Zh. Eksp. Teor. Fiz. **38**, 966 (1960).

D. Esteve, J. M. Martinis, C. Urbina, M. H. Devoret, G. Collin, P. Monod, M. Ribault, and A. Revcolevschi, Europhys. Lett. **3**, 1237 (1987).

D. K. Finnemore, D. E. Mapother, and R. W. Shaw, Phys. Rev. **118**, 127 (1960).

H. Frohlich, Proc. Roy. Soc. A **215**, 291 (1952).

L. Gao, Z. J. Huang, R. L. Meng, G. Lin, F. Chen, L. Beauvais, Y. Y. Xue, and C. W. Chu, Physica C **213**, 261 (1993).

J. Geerk, M. Gurvitch, D. B. McWhan, and J. M. Rowell, Physica B+C **109&110**, 1775 (1982).

I. Giaever and K. Megerle, Phys. Rev. **4**, 1101 (1961).

D. M. Ginsberg in *Physical Properties in High Temperature Superconductors IV*, edited by D. M. Ginsberg (World Scientific, Singapore, 1994).

M. A. M. Gjis, D. Scholten, Th. van Rooy, and A. M. Gerrits, Appl. Phys. Lett. **57**, 2600 (1990).

C. E. Gough, M. S. Colclough, E. M. Forgan, R. G. Jordan, M. Keene, C. M. Muirhead, A. I. M. Rae, N. Thomas, J. S. Abell, and S. Sutton, Nature (London) **326**, 855 (1987).

K. E. Gray, Phys. Rev. Lett. **28**, 959 (1972).

K. E. Gray, M. E. Hawley and E. R. Moog, in *Novel Mechanisms of Superconductivity*, edited by S. A. Wolf and V. Z. Kresin (Plenum, New York, 1987)

K. E. Gray, Mod. Phys. Lett. B **2**, 1125 (1988).

H. Hasegawa, H. Suzuki, S. Yaegashi, H. Takagi, K. Kishio, S. Uchida, K. Kitazawa, and K. Fueki, Jpn. J. Appl. Phys. **28**, L179 (1989).

T. Hasegawa, H. Ikuta, and K. Kitazawa in *Physical Properties of High Temperature Superconductors III*, edited by D. M. Ginsberg (World Scientific Publishing, Singapore, 1992a).

T. Hasegawa, M. Nantoh, A. Takagi, H. Ikuta, M. Kawasaki, H. Koinuma and K. Kitazawa, J. Phys. Chem. Solids **53**, 1643 (1992b).

M. E. Hawley, K. E. Gray, B. D. Terris, H. H. Wang, K. D. Carlson, and J. M. Williams, Phys. Rev. Lett. **57**, 629 (1986).

M. E. Hawley, K. E. Gray, D. W. Capone II, and D. G. Hinks, Phys. Rev. B **35**, 7224 (1987).

H. F. Hess, R. B. Robinson, R. C. Dynes, J. M. Valles Jr., and J. V. Waszczak, Phys. Rev. Lett. **62**, 214 (1989).

H. F. Hess, Physica (Amsterdam) **169B**, 422 (1991).

H. F. Hess, C. A. Murray, and J. V. Waszczak, Phys. Rev. Lett. **69**, 2138 (1992).

D. G. Hinks, D. R. Richards, B. Dabrowski, D. T. Marx, and A. W. Mitchell, Nature (London) **335**, 419 (1988).

D. G. Hinks, private communication.

C. J. Hou, R. L. Fink, C. Hilbert, and H. Kroger, Appl. Phys. Lett. **60**, 1262 (1992).

Q. Hu and P. L. Richards, in *Superconducting Devices*, edited by S. T. Ruggiero and D. A. Rudman (Academic, San Diego, 1990).

Q. Huang, J. F. Zasadzinski, K. E. Gray, J. Z. Liu and H. Claus, Phys. Rev. B **40**, 9366 (1989a).

Q. Huang, J. F. Zasadzinski, K. E. Gray, E. D. Bukowski and D. M. Ginsberg, Physica C **161**, 141 (1989b).

Q. Huang, J. F. Zasadzinski, N. Tralshawala, K. E. Gray, D. G. Hinks, J. L. Peng, and R. L. Greene, Nature (London) **347**, 369 (1990a).

Q. Huang, J. F. Zasadzinski, and K.E. Gray, Phys. Rev. B **42**, 7953 (1990b).

Q. Huang, J. F. Zasadzinski, K.E. Gray, D. R. Richards, and D. G. Hinks, Appl. Phys. Lett. **57**, 2356 (1990c).

Q. Huang, J. F. Zasadzinski, K. E. Gray, unpublished.

Q. Huang, J. F. Zasadzinski, and K. E. Gray, APS March meeting abstract, Indianapolis, IN (1992).

Z. J. Huang, R. L. Meng, X. D. Qiu, Y. Y. Sun, J. Kulik, Y. Y. Xue, and C. W. Chu, Physica C **217**, 1 (1993).

Z. G. Khim, D. M. Burnell, and E. L. Wolf, Solid State Commun. **39**, 159 (1981).

D. H. Kim, K. E. Gray, R. T. Kampwirth, J. C. Smith, D. S. Richardson, T. J. Marks, J. H. Kang, J. Talvacchio, M. Eddy, Physica C **177**, 431 (1991).

J. R. Kirtley and D. J. Scalapino, Phys. Rev. Lett. **65**, 798 (1990).

J. R. Kirtley, S. Washburn, D. J. Scalapino, Phys. Rev. B **45**, 336 (1992).

C. Kittel, *Introduction to Solid State Physics*, (John Wiley & Sons, Inc, 6th ed. 1986).

K. Kouznetsov, L. Coffey, and J. F. Zasadzinski, Appl. Superconductivity **2**, 735 (1994).

K. Kouznetsov and L. Coffey, preprint.

A. Kussmaul, E. S. Hellman, E. H. Hartford Jr., and P. M. Tedrow, Appl. Phys. Lett. **63**, 2824 (1993).

D. Mandrus, L. Forro, D. Koller, and L. Mihaly, Nature (London) **351**, 460 (1991).

J. T. Markert, private communication.

W. L. McMillan, Phys. Rev. **175**, 537 (1968).

W. L. McMillan and J. M. Rowell, Phys. Rev. Lett. **14**, 108 (1965).

W. L. McMillan and J. M. Rowell, in *Superconductivity*, edited by R. D. Parks (Marcel Dekker, New York, 1969).

P. Mendels and H. Alloul, Physica C **156**, 355 (1988).

J. Moreland and J. W. Ekin, J. Appl. Phys. **58**, 3888 (1985).

H. Kamerlingh Onnes, Akad. van Wetenschappen (Amsterdam) **14**, 113 (1911).

M. Paranthaman, J.R. Thompson, Y.R. Sun, and J. Brynestad, Physica C **213**, 271 (1993).

M. Paranthaman, J.R. Thompson, Y.R. Sun, J. Brynestad and D. M. Kroeger, unpublished.

A. N. Pargellis, F. Sharifi, R. C. Dynes, B. Miller, E. S. Hellman, J. M. Rosamilia, and E. H. Hartford, Jr., Appl. Phys. Lett. **58**, 95 (1991).

D. E. Prober, M. R. Beasley, and R. E. Schwall, Phys. Rev. B **15**, 5245 (1977).

S. N. Putilin, E. V. Antipov, O. Chmaissem and M. Marezio, Nature (London) **362**, 226 (1993).

J. S. Rogers, Rev. Sci. Instr. **41**, 1184 (1970).

J. M. Rowell and L. Kopf, Phys. Rev. A **137**, 907 (1965).

A. Schilling, M. Cantoni, J. D. Guo and H. R. Ott, Nature (London) **363**, 56 (1993).

J. R. Schrieffer, *Theory of Superconductivity*, (W. A. Benjamin, Inc., New York, 1964).

R. B. Schwarz, P. J. Yvon, and D. Coffey, in *Studies of High Temperature Superconductors 8*, edited by A. Narlikar (Nova Science Publishers, New York, 1991).

Z.-X. Shen *et al.*, Phys. Rev. Lett. **70**, 1553 (1993).

T. Siegrist, S. M. Zahurak, D. W. Murphy, and R. S. Roth, Nature (London) **334**, 231 (1988).

M. G. Smith, A. Manthiram, J. Zhou, J. B. Goodenough, and J. T. Markert, Nature (London) **351**, 549 (1991).

A. G. Sun, D. A. Gajewski, M. B. Maple, and R. C. Dynes, Phys. Rev. Lett. **72**, 2267 (1994).

M. Takigawa, P. C. Hammel, R. H. Heffner, and Z. Fisk, Phys. Rev. B **39**, 7371 (1989).

M. Tanaka, T. Takahashi, H. Katayama-Yoshida, S. Yamazaki, M. Fujinami, Y. Okabe, W. Mizutani, M. Ono, and K. Kajimura, Nature London) **339**, 691 (1989).

M. Tinkham, *Introduction to Superconductivity*, (McGraw-Hill Press, New York, 1975).

N. Tralshawala, J. F. Zasadzinski, L. Coffey and Q. Huang, Phys. Rev. B **44**, 2102 (1991).

N. Tralshawala, J. F. Zasadzinski, L. Coffey, W. Gai, M. Romalis, Q. Huang, R. Vaglio, and K. E. Gray, Phys. Rev. B **51**, 3812 (1995).

J. R. Tucker and M. J. Feldman, Rev. Mod. Phys.**57**,1055 (1985).

A. Umezawa, W. Zhang, A. Gurevich, Y. Feng, E. E. Hellstrom and D. C. Larbalestier, Nature (London) **364**, 129 (1993).

J. L. Wagner, P. G. Radaelli, D. G. Hinks, J. D. Jorgenson, J. F. Mitchell, B. Dabrowski, G. S. Knapp, and M. A. Beno, Physica C **210**, 447 (1993).

U. Welp, G. W. Crabtree, J. L. Wagner, D. G. Hinks, P. G. Radaelli, J. D. Jorgensen and J. F. Mitchell, Appl. Phys. Lett. **63**, 693 (1993).

E. L. Wolf, J. F. Zasadzinski, J. W. Osmun, and G. B. Arnold, J. Low Temp. Phys. **40**, 19 (1980).

E. L. Wolf and G. B. Arnold, Phys. Report **91**, 31-102 (1982).

E. L. Wolf, *Principles of Electron Tunneling Spectroscopy*, (Oxford University Press, New York, 1985).

D. H. Wu, J. Mao, S. N. Mao, J. L. Peng, X. X. Xi, T. Venkatesan, R. L. Greene, and S. M. Anlage, Phys. Rev. Lett. **70**, 85 (1993).

P. Wzietek, D. Kongeter, P. Auban, D. Jerome, J. M. Bassat, J. P. Coutures, B. Dubois, and P. Odier, Europhys. Lett. **8**, 363 (1989).

J. F. Zasadzinski, D. M. Burnell, and E. L. Wolf, Phys. Rev. B **25**, 1622 (1982).

J. F. Zasadzinski, N. Tralshawala, D. G. Hinks, B. Dabrowski, A. W. Mitchell, and D. R. Richards, Physica C **158**, 519 (1989).

J. F. Zasadzinski, N. Tralshawala, P. Romano, Q. Huang, J. Chen, K. E. Gray, J. Phys. Chem. Solids **53**, 1635 (1992).

J. F. Zasadzinski, J. Chen, K. E. Gray, and D. G. Hinks, in *Proc. of the Int. Conf. on Millimeter and Submillimeter Waves and Applications*, edited by M. N. Afsar (SPIE, 1994).

J. F. Zasadzinski, M. V. Romalis, Q. Huang, K. E. Gray, and G. B. Arnold, unpublished.

R. Zasadzinski, K. G. Vandervoort, and G. W. Crabtree, unpublished.